

COORDINATION OF MITOCHONDRIAL DNA HOMEOSTASIS WITH CELL GROWTH

Dissertation

at the Faculty of Biology of the Ludwig-Maximilians-Universität München

for the award of the degree

“Doctor rerum naturalium”



Anika Vanessa Seel

from Berlin, Germany

March 2022

This dissertation was prepared under the supervision of Dr. Kurt M. Schmöller at the Institute of Functional Epigenetics, at the Helmholtz Zentrum München, the German Research Center for Environmental Health.

First examiner: Prof. Dr. Christof Osman

Second examiner: Prof. Dr. Ralf Jungmann

Day of submission: March 29, 2022

Day of oral examination: October 12, 2022

Affidavit

I hereby declare, that the submitted thesis entitled 'Coordination of mitochondrial DNA homeostasis with cell growth' is my own work.

I have only used the sources indicated and have not made unauthorized use of services of a third party. Where the work of others has been quoted or reproduced, the source is always given.

I further declare that the submitted thesis or parts thereof have not been presented as part of an examination degree to any other university.

München, 29.03.2022

Anika Seel

Parts of this work were published in:

Seel, A., Padovani, F., Finster, A., Mayer, M., Bureik, D., Osman, C., Klecker, T., Schmoller, K. M. (2021). Regulation with cell size ensures mitochondrial DNA homeostasis during cell growth. BioRxiv, DOI: <https://doi.org/10.1101/2021.12.03.471050>

Table of Contents

AFFIDAVIT	I
TABLE OF CONTENTS	III
LIST OF FIGURES	VI
ABSTRACT	VII
ZUSAMMENFASSUNG	IX
1. INTRODUCTION	1
1.1. What is a mitochondrion?	2
1.2. Mitochondrial origin and evolution of the mitochondrial genome	3
1.3. Mitochondrial functions - a brief overview	4
1.4. mtDNA structure and organization in <i>S. cerevisiae</i>	6
1.4.1. mtDNA structure of <i>S. cerevisiae</i>	6
1.4.2. mtDNA organization and stabilization	7
1.4.3. Mitochondrial DNA replication in <i>S. cerevisiae</i>	8
1.5. Mitochondrial network dynamics and mtDNA quality control	12
1.6. Regulation of mtDNA maintenance	13
1.6.1. Importance of mtDNA copy number homeostasis	13
1.6.2. mtDNA factors important for the homeostasis of mtDNA copy number	13
1.6.3. Mitochondrial replication during cell cycle.....	14
1.6.4. Allometric scaling of metabolism, mitochondrial mass and nucleoids.....	15
1.7. Cell size as a regulator for organelles and subcellular structures	16
1.8. Aim of this study	17
2. MATERIALS AND METHODS	19
2.1. Chemicals and Consumables	19
2.2. Devices.....	20
2.3. Kits.....	20
2.4. Strains	20
2.5. Enzymes.....	26
2.6. Plasmids.....	26
2.7. Oligonucleotides.....	27
2.8. Buffer and Media.....	28
2.9. Cell cultivation	31
2.9.1. Cultivation of wild-type and <i>Whi5</i> -inducible <i>S. cerevisiae</i> strains	31
2.9.2. Cultivation for induction of G1 arrest in <i>S. cerevisiae</i>	31
2.9.3. Cultivation of the hormone-inducible <i>Mip1-mCitrine (ASY40-1)</i>	32

Table of Contents

2.9.4.	Cultivation of <i>E. coli</i>	33
2.9.5.	Transformation of <i>E. coli</i> and plasmid isolation	33
2.9.6.	Transformation of <i>S. cerevisiae</i>	33
2.10.	Cloning, DNA purification and DNA analysis.....	34
2.10.1.	Polymerase chain reaction (PCR) and purification	34
2.10.2.	Agarose gel electrophoresis.....	34
2.10.3.	Digestion with restriction enzymes.....	35
2.10.4.	Ligation of DNA fragments	35
2.10.5.	Sequencing.....	35
2.11.	Molecular biological methods with yeast	36
2.11.1.	Gene deletion in yeast.....	36
2.11.2.	Generation of mtDNA microscopy strains.....	36
2.11.3.	Integration of additional gene copies	36
2.11.4.	Insertion of chromosomal C-terminal protein tags and modification of terminator sequences	37
2.11.5.	Modification of promoter sequences	37
2.11.6.	Genomic DNA extraction and RNase A digestion	37
2.11.7.	Quantitative DNA PCR and analysis.....	38
2.11.8.	Cell volume measurements.....	40
2.11.9.	Extraction of total RNA from yeast.....	41
2.11.10.	cDNA synthesis and quantitative reverse transcription PCR (RT-qPCR).....	42
2.12.	Microscopy and image analysis.....	42
2.12.1.	Live-cell imaging by confocal microscopy.....	42
2.12.2.	Cell segmentation.....	43
2.12.3.	Nucleoid counting and network volume calculation.....	43
2.12.4.	Mip1-mCitrine fluorescence intensity measurements.....	45
2.12.5.	Electron Microscopy	45
2.13.	Flow Cytometry	46
2.14.	Statistical analysis.....	48
3.	RESULTS	49
3.1.	mtDNA copy number increases with cell volume modulated by nutrients	49
3.2.	mtDNA copy number increases with cell volume during G1 arrest.....	51
3.3.	Number of nucleoids increases with cell volume and is modulated by nutrients.....	53
3.4.	Mitochondrial network increases independent of mtDNA	55
3.5.	Mitochondrial diameter stays constant with increasing cell volume.....	57
3.6.	Amount of mtDNA maintenance factors increases with cell size	59
3.7.	mtDNA copy number in Mip1-mCitrine strain is slightly affected by <i>ADH1</i> terminator variants	63

Table of Contents

3.8. Reducing the expression of mtDNA maintenance factors leads to altered mtDNA copy numbers.....	64
3.8.1. Mip1 and Abf2 are limiting for mtDNA maintenance.....	64
3.8.2. Reduction of Mrx6 expression increases mtDNA copy number.....	66
3.8.3. Double hemizygote <i>MIP1/ABF2</i> shows a stronger decrease of mtDNA copy number.....	67
3.9. Overexpression of Mip1-mCitrine shows limited mtDNA increase.....	69
3.10. Expression of <i>ABF2</i> and <i>MIP1</i> from histone promoters increases mtDNA copy number.....	71
3.11. Mip1 and Abf2 together can upregulate mtDNA copy number.....	74
4. DISCUSSION.....	76
4.1. Cell volume regulates mitochondrial biogenesis.....	76
4.2. mtDNA copy number maintenance during cell growth relies on increased expression of mtDNA maintenance factors.....	77
4.3. The synergy of Mip1 and Abf2 protein homeostasis regulates mtDNA copy number.....	78
4.4. mtDNA copy number is modulated by additional mechanisms.....	81
4.4.1. mtDNA copy number can be regulated by quality control mechanisms.....	81
4.4.2. mtDNA copy number is modulated by nutrients.....	82
4.5. Further experimental validation of the proposed model is required.....	84
4.6. Regulation of mtDNA copy number with cell size is likely conserved across eukaryotes.....	85
BIBLIOGRAPHY.....	87
LIST OF ABBREVIATIONS.....	XI
ACKNOWLEDGEMENT - DANKSAGUNG.....	XV

List of Figures

Figure 1.1: Simplified representation of the mitochondrial morphology.....	2
Figure 1.2: Schematic depiction of oxidative phosphorylation in budding yeast	5
Figure 1.3: Schematic depiction of circular mtDNA.....	6
Figure 1.4: Graphic depiction of a mitochondrial nucleoid.	7
Figure 1.5: Possible mechanism for mtDNA replication in budding yeast	11
Figure 2.1: Growth test of wild-type, Mip1-mCitrine and Mip1-mCitrine+HI-Mip1-mCitrine ...	32
Figure 2.2: qPCR calibration standard curves.....	40
Figure 2.3: Comparison of mitochondrial network volume calculated by Python routine and MitoGraph.....	44
Figure 2.4: Comparison of flow cytometry side scatter and forward scatter measurements with Coulter counter measurements	47
Figure 3.1: mtDNA copy number increases with cell volume.....	50
Figure 3.2: mtDNA copy number increases with cell volume during G1 arrest	52
Figure 3.3: Number of nucleoids and the mitochondrial network volume increase with cell volume	54
Figure 3.4: Mitochondrial network volume increases with cell volume independent of mtDNA	56
Figure 3.5: Mitochondrial diameter stays constant with increasing cell volume but is modulated by nutrients.....	58
Figure 3.6: Abundance of mtDNA maintenance factors increases with cell volume	60
Figure 3.7: Protein concentrations of Mip1-mCitrine and Abf2-mCitrine increase with cell volume	62
Figure 3.8. Increase of mtDNA copy number by mCitrine tagged Mip1 is not influenced by the terminator sequence	64
Figure 3.9: Identification of mtDNA limiting factors using hemizygous deletion mutants	65
Figure 3.10: <i>mrx6</i> deletion increases mtDNA copy number	67
Figure 3.11: mtDNA copy number depends on concentrations of Mip1 and Abf2.	68
Figure 3.12: Impact of Mip1 concentration on mtDNA copy number is limited.....	70
Figure 3.13: Histone promoter leads to overexpression of Mip1 and Abf2 causing increased mtDNA copy numbers.....	72
Figure 3.14: Histone promoter leads to overexpression of Abf2 causing increased mtDNA copy numbers.....	73
Figure 3.15: Higher concentrations of MIP1 and ABF2 increase mtDNA alone and together	75
Figure 4.1: Mathematical model to represent the impact of replication and degradation on mtDNA	79
Figure 4.2: Illustration of mtDNA copy number homeostasis during cell growth by the limiting-machinery mechanism.....	85

Abstract

During cell growth, the size of the cells can vary significantly. To ensure that the balance between growth and division is maintained, metabolic activity must be adjusted. In this context, mitochondria play a crucial role. As the powerhouse of the cell, mitochondria are the main organelles that, among other things, convert carbon sources into energy that can be utilized by the cell. This requires mitochondrial DNA, which encodes the main components of the electron transport chain and is present in multiple copies. This copy number must be adjusted during cell growth. However, the molecular mechanism underlying the coordination of mtDNA homeostasis with cell size is unclear.

This study investigated mtDNA homeostasis in different cell sizes using budding yeast. It shows that mtDNA copy number and mitochondrial nucleoids increase linearly with cell size, both in asynchronously cycling populations and during G1 arrest. Combining live-cell imaging and qPCR, it was demonstrated that the quantitative dependence of nucleoids and mtDNA copy number on cell volume depends on the carbon source. Respiring cells, in which mtDNA is essential, have more mtDNA copies and nucleoids than fermenting cells, in which mtDNA is not essential. However, it should be emphasized that even under conditions when mtDNA is not essential, the dependence on cell volume remains. A similar increase was also observed for the mitochondrial network. Interestingly, RT-qPCR and flow cytometry revealed an increase of mtDNA maintenance factors with cell size, suggesting a coupling to global protein expression. Thus, the increase of mtDNA copy number is likely due to an increased abundance of the replication machinery. To identify factors with a dose-dependent effect on mtDNA maintenance, the expression of proteins involved in mitochondrial replication was modified. By generating hemizygous diploid strains, the concentration of mtDNA maintenance factors was reduced. Thereby, the mtDNA polymerase Mip1 and the packaging factor Abf2 were identified as limiting factors controlling mtDNA levels. The opposite experiment, i.e., overexpression of these factors, also demonstrated dosage-dependence of the mtDNA from these two factors. In particular, Mip1 and Abf2 together affect mtDNA synergistically, suggesting that the mtDNA copy number depends on several limiting factors.

The data and theoretical considerations generated in this study show that the mtDNA copy number is cell volume-dependent and its regulation is achieved by nuclear-encoded limiting factors, which are as well expressed cell volume-dependent. Thus, coupling global protein expression to cell volume provides a robust mechanism that ensures constant mtDNA concentrations during cell growth, independent of cell cycle regulation. Because the increase in protein levels during cell growth is largely conserved in eukaryotes, this mechanism may also achieve mtDNA homeostasis in growing cells in other eukaryotes.

Zusammenfassung

Während des Zellwachstums kann die Größe der Zellen erheblich schwanken. Um das Gleichgewicht zwischen Wachstum und Teilung aufrechtzuerhalten, muss die Stoffwechselaktivität angepasst werden. In diesem Zusammenhang spielen die Mitochondrien eine entscheidende Rolle. Als Kraftwerk der Zelle sind die Mitochondrien die Hauptorganellen, die unter anderem Kohlenstoffquellen in Energie umwandeln, die von der Zelle verwertet werden kann. Dazu ist die mitochondriale DNA (mtDNA) erforderlich, die für die Hauptbestandteile der Elektronentransportkette kodiert und in mehreren Kopien vorhanden ist. Diese Kopienzahl muss während des Zellwachstums angepasst werden. Der molekulare Mechanismus, der der Koordination der mtDNA-Homöostase mit der Zellgröße zugrunde liegt, ist jedoch unklar.

In dieser Studie wurde die mtDNA-Homöostase in verschiedenen Zellgrößen mit Hilfe der Bäckerhefe *S. cerevisiae* untersucht. Hier wurde gezeigt, dass die mtDNA-Kopienzahl und die mitochondrialen Nukleotide linear mit der Zellgröße zunehmen, sowohl in asynchron zyklischen Populationen als auch während des G1-Arrestes. Durch die Kombination von Live-Cell Imaging und qPCR konnte gezeigt werden, dass die quantitative Abhängigkeit der Nukleotide und der mtDNA-Kopienzahl vom Zellvolumen von der Kohlenstoffquelle abhängt. Atmende Zellen, in denen mtDNA essentiell ist, haben mehr mtDNA-Kopien und Nukleotide als fermentierende Zellen, in denen mtDNA nicht essentiell ist. Es ist jedoch zu betonen, dass auch unter Bedingungen, unter denen mtDNA nicht essentiell ist, die Abhängigkeit vom Zellvolumen bestehen bleibt. Ein ähnlicher Anstieg wurde auch für das mitochondriale Netzwerk beobachtet. Interessanterweise zeigten RT-qPCR und Durchflusszytometrie Daten einen Anstieg der mtDNA-Erhaltungsfaktoren mit der Zellgröße, was auf eine Kopplung an die globale Proteinexpression hindeutet. Somit ist die Zunahme der mtDNA-Kopienzahl wahrscheinlich auf eine erhöhte Menge der Replikationsmaschinerie zurückzuführen. Um Faktoren mit einer dosisabhängigen Wirkung auf die mtDNA-Erhaltung zu identifizieren, wurde die Expression von Proteinen, die an der mitochondrialen Replikation beteiligt sind, verändert. Durch die Erzeugung hemizygoter diploider Stämme wurde die Konzentration der mtDNA-Erhaltungsfaktoren reduziert. Dabei wurden die mtDNA-Polymerase Mip1 und der Verpackungsfaktor Abf2 als limitierende Faktoren identifiziert, die den mtDNA-Spiegel kontrollieren. Das gegenteilige Experiment, d. h. die Überexpression dieser Faktoren, zeigte ebenfalls die Dosisabhängigkeit der mtDNA von diesen beiden Faktoren. Insbesondere wirken sich Mip1 und Abf2 zusammen synergistisch auf die mtDNA aus, was darauf hindeutet, dass die mtDNA-Kopienzahl von mehreren limitierenden Faktoren abhängt.

Die in dieser Studie gewonnenen Daten und theoretischen Überlegungen zeigen, dass die mtDNA-Kopienzahl zellvolumenabhängig ist und ihre Regulierung durch kernkodierte

limitierende Faktoren erfolgt, die ebenfalls zellvolumenabhängig exprimiert werden. Die Kopplung der globalen Proteinexpression an das Zellvolumen stellt somit einen robusten Mechanismus dar, der während des Zellwachstums konstante mtDNA-Konzentrationen gewährleistet, unabhängig von der Zellzyklusregulation. Da der Anstieg der Proteinkonzentrationen während des Zellwachstums in Eukaryonten weitgehend konserviert ist, könnte dieser Mechanismus auch in anderen Eukaryonten für eine mtDNA-Homöostase in wachsenden Zellen sorgen.

Error! Use the Home tab to apply Überschrift 1 to the text that you want to appear here.

1. Introduction

Energy is what keeps all metabolically active cells alive. During catabolism, the supplied energy sources are broken down into their individual parts and energy is saved in form of ATP. During anabolism the biological building blocks and the saved energy are used for cell growth. Depending on the energy source, there are different processes for energy conversion in eukaryotic cells. Carbon sources are first converted in the cytoplasm during glycolysis and then metabolized in the mitochondria, where the main part of ATP is generated by oxidative phosphorylation (Nolfi-Donagan et al. 2020).

Depending on the cell type, cells have different tasks. Thus, every cell type and species harbors their specific amount of mitochondrial network and mitochondrial DNA (mtDNA). Human oocytes for example contain ~100,000 mtDNA molecules (Chen et al. 1995), whereas lung cells comprise 5,000 - 20,000 mtDNA copies per cell (D'Erchia et al. 2015). What exactly sets the mitochondrial concentration and mtDNA copy number within a cell has not been elucidated so far. However, the regulation of mitochondrial biogenesis is important to ensure that sufficient energy can be produced to maintain cellular function. To dissect the question which mechanisms set mitochondrial mass and mtDNA content, the unicellular model organism *Saccharomyces cerevisiae*, also termed budding yeast, was used in this study. In general, much of today's knowledge comes from the study of yeast mitochondria, which is not surprising considering the several advantages of budding yeast (Altmann et al., 2007). Many pathways of mitochondrial biogenesis and mtDNA replication are conserved from lower to higher eukaryotes resulting in significant similarities between human and yeast mtDNA replication (Shadel, 1999). Especially, the simpler regulatory architecture in yeast facilitates the study of fundamental molecular processes. One striking advantage of budding yeast is its good fermenting capacity, which allows yeast to grow without mtDNA. This allows studying strains in which genes that are critical for mtDNA maintenance have been deleted. In contrast, mammalian cells without mtDNA are not viable. Another advantage of yeast is a new system that was developed to visualize mtDNA in living cells (Osman et al. 2015). For this purpose, mtDNA was genetically manipulated to provide binding sites for the LacI protein which is tagged with a fluorophore. This allows the visualization of nucleoids in living cells. Thus, budding yeast is an ideal model organism for answering fundamental questions of mitochondrial biology, including questions regarding mtDNA.

As already described, mtDNA copy number varies between cell types and species, but within a given species or cell type, mtDNA copy number is reproducibly constant. What regulates mtDNA copy number during cell growth and thus ensures that all cells have similar mtDNA copy numbers is yet unknown. An exclusive coupling of the mtDNA replication or biosynthesis

Error! Use the Home tab to apply Überschrift 1 to the text that you want to appear here.

of the mitochondrial network to a specific cell cycle phase has neither been found for yeast nor for human cells. However, recent studies suggest that cell volume may be an important regulator of mtDNA and network volume (Rafelski et al. 2012, Jajoo et al. 2016). Therefore, this study uses budding yeast to investigate how the mtDNA copy number and the mitochondrial network are coupled to cell volume and what is responsible for this coupling.

1.1. What is a mitochondrion?

Mitochondria are found in nearly all eukaryotic cells, always with quite similar functionality, which is mainly the supply of energy. However, depending on the cell type, mitochondria differ in abundance and shape. In yeast, the mitochondrial structure resembles a network which permeates the whole cell, whereas in liver tissue the mitochondria are rather in a spherical shape (Scalettar et al. 1991, Brandt et al. 2017). Mitochondria are double membrane bound organelles, which consist of an outer membrane surrounding an inner membrane, thereby separating the intermembrane space from the mitochondrial matrix (Fig. 1.1).

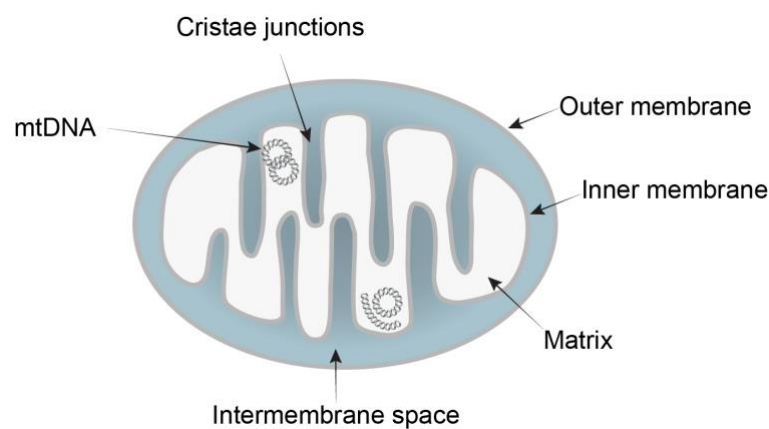


Figure 1.1: Simplified representation of the mitochondrial morphology. Mitochondria consist of an outer membrane that envelops the inner membrane, thereby generating an intermembrane space. Within the mitochondrial network, in the mitochondrial matrix, several copies of mtDNA are equally distributed. Cristae structures are inner membrane folds which, among others, provide space for the subunits of the electron transport chain.

The outer membrane is non-specifically permeable to proteins of 5000 kDa or less (Lemasters 2007). In contrast, the inner mitochondrial membrane is impermeable such that not even the small hydrogen ion can pass (Lemasters 2007). Thus, metabolites need to be transferred with the help of transporters and exchangers. In addition, the inner membrane forms folds called cristae structures, which, among other things, provide space for the subunits of the electron transport chain. In contrast to other organelles in mammalian cells or budding yeast,

Error! Use the Home tab to apply Überschrift 1 to the text that you want to appear here.

mitochondria are semi-autonomous organelles, meaning they have their own DNA (Nass and Nass 1963), which is replicated, transcribed and translated in the mitochondrial matrix. However, replication of mtDNA depends also on nuclear-encoded proteins.

1.2. Mitochondrial origin and evolution of the mitochondrial genome

According to the endosymbiosis theory, mitochondria most likely originated from an alphaproteobacterium which was integrated into an archaeal-derived host cell (Wang and Wu 2015), resulting in an eukaryotic precursor cell. Since then, the endosymbiont became specialized as an aerobically respiring organelle, generating ATP from carbohydrates. This transition from an endosymbiont to a fully functional mitochondrial ancestor required many adaptations as for example the ability to import or export proteins, retargeting of proteins to mitochondria and endosymbiotic gene transfer to the nucleus (Roger et al. 2017).

The reduction in mitochondrial genome size occurred largely through the loss of unnecessary or redundant genes and only a small number of genes was transferred to the nuclear host genome. Of the about 1000 mitochondrial protein-encoding genes in human cells (400 in yeast) only 16.3% of the proteins for yeast and 12.6% for humans come from alphaproteobacterial (Gabaldón and Huynen 2007). According to estimates, of about 1000-8000 genes only 0.5-1.2% are retained in mitochondria (Burger et al. 2013). Human mtDNA retained 13 (Anderson et al. 1981) and budding yeast retained 8 protein-encoding genes (Foury et al. 1998) and several transfer RNA (tRNA) and ribosomal RNAs (rRNA). Of the 8 proteins encoded by the mtDNA, 7 proteins are subunits of the electron transport chain and one encodes a ribosomal protein. In budding yeast these proteins are cytochrome c oxidase subunits I, II and III (*COX1*, *COX2* and *COX3*), ATP synthase subunits 6, 8 and 9 (*ATP6*, *ATP8* and *ATP9*), apocytochrome b (*COB*) and a ribosomal protein (*VAR1*) (Foury et al. 1998). Some of these genes are highly conserved across many species as those encode subunits for the electron transport chain.

The question why some genes are kept in the mitochondrial compartment is highly discussed and two hypotheses attempt to explain it. The Co-location for Redox Regulation (CoRR) hypothesis (Allen 1992, 2015) states that retention of distinct mitochondrial genes can give a fitness advantage as reaction to environmental changes can occur much faster. Sensing the redox state of mitochondria and allowing an immediate transcription of ETC genes can prevent reactive oxygen species (ROS) damage and can be the decisive advantage to retain these genes in the organelle.

A second explanation gives the hydrophobicity hypothesis, which argues that the retained mitochondrial genes encode large hydrophobic proteins which cannot be synthesized in the

Error! Use the Home tab to apply Überschrift 1 to the text that you want to appear here.

cytosol. Additionally, studies in human cells have shown that when those mitochondrial genes are nuclear expressed, the proteins are transported to the endoplasmic reticulum (ER) (Björkholm et al. 2017). So, simply the mislocalization of mitochondrial proteins when nuclear expressed could be an evolutionary obstruction for the nuclear gene transfer.

1.3. Mitochondrial functions - a brief overview

The main mitochondrial task is the oxidation of substrates including carbohydrates, fats, and proteins, thereby generating adenosine triphosphate (ATP) from adenosine diphosphate (ADP) (Nolfi-Donagan et al., 2020). The catabolism of mitochondrial substrates leads to the formation of acetyl-CoA which is metabolized by the citric acid cycle (Fig. 1.2). Here, the electron donors, nicotinamide adenine dinucleotide (NADH) and flavin adenine dinucleotide (FADH₂) are generated and passed to the electron transport chain (ETC) (Saraste, 1999). The ETC is located in the inner mitochondrial membrane and, in mammalian cells, consists of five multi subunit enzyme complexes and two electron carriers, cytochrome c and ubiquinone. Interestingly, budding yeast is missing complex I which is compensated by two types of NADH dehydrogenases (de Vries and Marres 1987). In budding yeast, some subunits of the ATP synthase (ATP synthase subunits 6, 8 and 9), apocytochrome b, and cytochrome c oxidase subunits I, II and III are encoded by the mtDNA (Foury et al. 1998). The remaining subunits are nuclear encoded and transported to the mitochondria.

The basic principle of how ATP is generated by the ETC is mainly conserved from yeast to mammalian cells. The electrons of the electron donors (NADH, FADH₂ in mammalian cells, NADH and succinate in budding yeast) are transferred to the complexes of the ETC and passed through the electron transport chain. This electron flow is an exergonic process which is coupled to the translocation of protons (H⁺) from the matrix across the inner membrane into the intermembrane space. This leads to the generation of an electrochemical gradient between the intermembrane space and the matrix also known as mitochondrial membrane potential. This membrane potential is used by the ATP synthase (Complex V) which is located in the inner membrane. The reflux of protons through the ATP synthase complex provides the energy to synthesize ATP from ADP .

Error! Use the Home tab to apply Überschrift 1 to the text that you want to appear here.

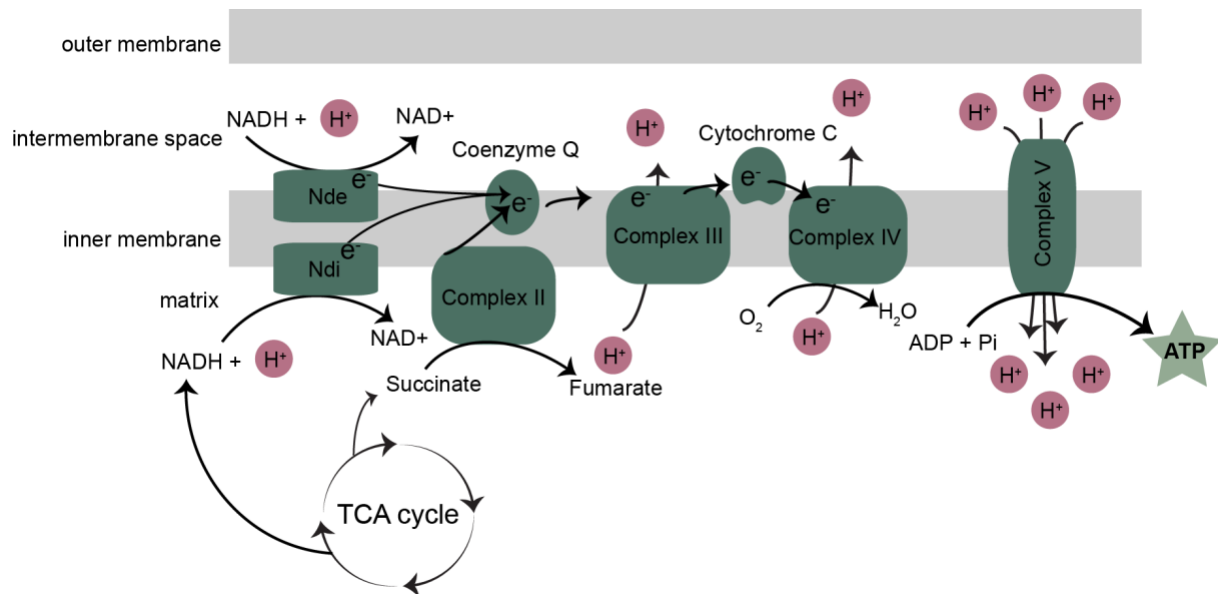


Figure 1.2: Schematic depiction of oxidative phosphorylation in budding yeast (adapted from Sharma et al. 2011). The electron carriers NADH+H⁺ and succinate are generated during the tricarboxylic acid cycle (TCA) by reduction of their precursors. The electron carriers are oxidized by either the NADH dehydrogenases or complex II of the electron transport chain. Electrons are transferred from NADH dehydrogenases or complex II to coenzyme Q and passed through the electron transport chain. This delivers complex III and complex IV the energy to transport protons from the matrix to the intermembrane space, thereby generating an electrochemical gradient. The ATP-synthase, displayed as complex V, uses the energy provided by the reflux of the protons to generate ATP.

Besides respiration and ATP generation, the ETC also produces reactive oxygen species (ROS) such as hydrogen peroxide (H₂O₂) and the superoxide anion radical (O₂^{•-}). They are used as key redox signaling agents involved in several signal transduction pathways, thereby stimulating cell proliferation (Sauer et al. 2001, Nolfi-Donagan et al. 2020). Additionally, it is hypothesized that ROS stimulates activity of transcription factors and induces mtDNA replication.

Cellular metabolism can adapt to environmental changes, such as the nutrient availability (Visser et al. 1995). The availability of a certain nutrient can repress pathways needed for the utilization of other nutrients. In budding yeast, glucose for example leads to the downregulation of several metabolic pathways important for the utilization of other carbon sources, also known as glucose repression. Here, among other things, the transcription of genes required for the utilization of alternative carbon sources, gluconeogenesis and respiration is repressed. Glucose repression also downregulates mtDNA abundance (Bleeg et al. 1972). One of the proteins involved in glucose repression is the transcription factor Mig1. At high glucose concentrations, it directly binds to carbon source responsive elements. At low glucose concentrations, Mig1 is inhibited by the Snf1 complex by phosphorylation (Carlson, 1999). However, also during glucose repression mitochondria remain essential as they contribute to

Error! Use the Home tab to apply Überschrift 1 to the text that you want to appear here.

the biosynthesis of amino acids, heme groups and iron-sulfur clusters or the synthesis of phospholipids for membrane biogenesis. Altogether, mitochondria are especially important for respiration at low levels of glucose.

1.4. mtDNA structure and organization in *S. cerevisiae*

1.4.1. mtDNA structure of *S. cerevisiae*

The complete mtDNA sequence of *S. cerevisiae* was first published in 1998 and contains ~86 kb (Foury et al., 1998) (Fig. 1.3). It encodes three subunits of the ATP synthase complex (Atp6, Atp8, and Atp9), apocytochrome b (Cob), three subunits of cytochrome c oxidase (Cox1, Cox2, and Cox3), and a ribosomal protein (rps3/VAR1). In addition, the mtDNA contains small and large rRNAs, an RNA component of mitochondrial RNase P, and 24 tRNAs. Coding regions consist of approximately 30% GC and the intergenic regions are separated in yeast by long AT-rich stretches (de Zamaroczy and Bernardi 1986). In contrast to mammalian mtDNA genes, yeast coding regions include introns. The yeast mitochondrial genome contains eight replication origin-like (ori) elements (Tzagoloff and Myers 1986). mtDNA is present in three forms which are linear filaments, open and closed circles (Shapiro et al. 1968). Its conformation has been further studied and the majority of mtDNA is present in linear filaments, named concatemers, of heterogenous sizes (Maleszka et al. 1991). The functionality of the different conformations is not completely understood, however, it is likely related to mtDNA replication. In addition, DNA strands of mtDNA are distinguished into a heavy strand and a light strand (Berk and Clayton 1974).

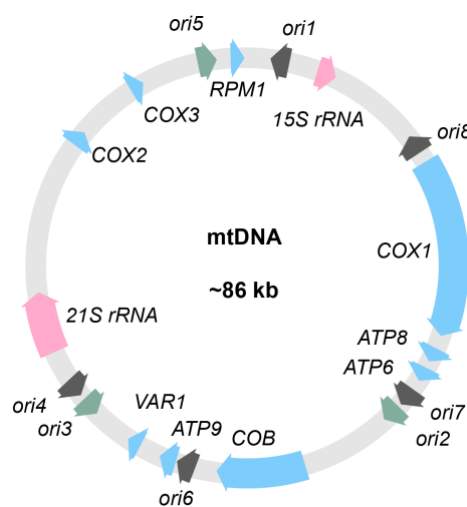


Figure 1.3: Schematic depiction of circular mtDNA (adapted from Wolters et al. 2015). mtDNA encodes 8 protein-encoding genes and several tRNAs and rRNAs. Of the 8 proteins encoded by the mtDNA, 7 proteins are subunits of the electron transport chain and one encodes a ribosomal protein. In budding yeast these subunits are cytochrome c oxidase subunits I, II and III (COX1, COX2 and COX3),

Error! Use the Home tab to apply Überschrift 1 to the text that you want to appear here.

ATP synthase subunits 6, 8 and 9 (*ATP6*, *ATP8* and *ATP9*), apocytochrome b (*COB*) and a ribosomal protein (*VAR1*) (Foury et al. 1998).

1.4.2. mtDNA organization and stabilization

mtDNA molecules are organized in nucleoprotein complexes (Fig. 1.4), in budding yeast and higher eukaryotes (Williamson and Fennell 1975, Kukat et al. 2011). Nucleoids consist of several mitochondrial binding proteins and, depending on the growth condition, of ~1-2 mtDNA copies (Miyakawa et al. 2004, Kukat et al. 2011). In budding yeast, the nucleoids are positioned throughout the mitochondrial network and are evenly spaced in a distance of 800 nm on average (Osman et al. 2015). It is also speculated that nucleoids are anchored at the inner membrane, to ensure the evenly distribution and thereby controlled inheritance of the mitochondrial genome (Rickwood et al. 1981, Nunnari et al. 1997, Cho et al. 1998).

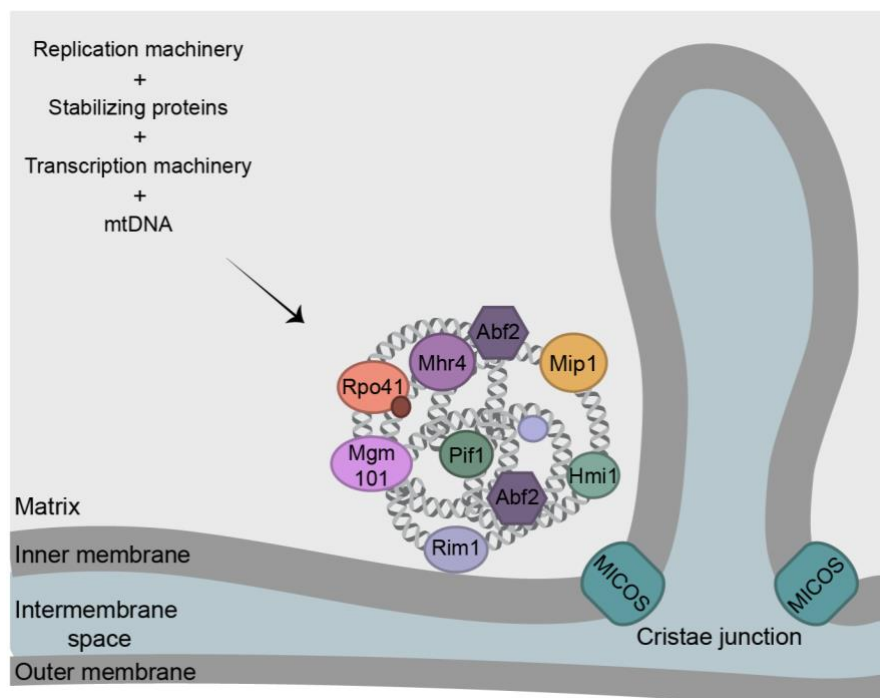


Figure 1.4: Graphic depiction of a mitochondrial nucleoid. mtDNA is organized in nucleoprotein complexes composed of 1-2 mtDNA copies and DNA binding proteins. The indicated proteins represent a selection of replication, transcription and stabilization factors. Selected replication factors shown here are the mtDNA polymerase Mip1, the packaging factor Abf2, the RNA polymerase Rpo41 and the single-strand binding protein Rim1. Many of these proteins also exhibit a dual function in, for example, stabilization or mRNA synthesis during mtDNA transcription.

The key component of nucleoids and the main factor for mtDNA packaging is the HMG-protein Abf2 in yeast (Zelenaya-Troitskaya et al. 1995) and in human its homolog TFAM (Ekstrand et al. 2004). The functionality of both proteins is partly conserved. Both proteins are abundant enough to fully cover and stabilize the mtDNA (Kukat et al. 2015). In addition, mtDNA shows a dose-dependent effect on the concentrations of both proteins. However, TFAM also functions

Error! Use the Home tab to apply Überschrift 1 to the text that you want to appear here.

as transcription factor, a function that Abf2 does not share (Farge and Falkenberg 2019). In yeast, Abf2 introduces with the help of a DNA topoisomerase, negative supercoils into the circular mtDNA and wraps mtDNA (Diffley and Stillman 1992). In contrast, atomic force microscopy showed that linear DNA is rather loosely packaged and also only weakly bound by Abf2, most likely allowing the enzymes to access mtDNA regulatory sites (Brewer et al. 2003). If Abf2 is missing, the cells very quickly lose their mitochondrial genome resulting in so called ρ^0 or petite cells when grown on glucose (fermentable) (Diffley and Stillman 1991). However, as long as the yeast cells are cultivated under selective pressure on medium with glycerol (non-fermentable), cells maintain their mtDNA (Diffley and Stillman 1991). In *abf2* Δ cells, the mitochondrial nucleoids are not compactly packaged and show rather a diffused structure (Newman 1996). In contrast, moderate overexpression of Abf2 by 2-3-fold leads to an increase of mtDNA copy number, indicating a function of Abf2 in mtDNA copy number control (Zelenaya-Troitskaya et al. 1998). Strong overexpression on the contrary leads to the complete loss of mtDNA. Abf2 not only stabilizes mtDNA but it is also supposed to function in mtDNA recombination, thereby potentially facilitating mtDNA replication (MacAlpine et al. 1998). Besides Abf2, several other proteins have been identified to be part of a nucleoid (Chen and Butow 2005, Miyakawa 2017). In general, all proteins involved in mtDNA stabilization, replication and transcription are part of nucleoid complexes. Especially Hmi1, a helicase was found to stabilize linear mtDNA in budding yeast (Sedman et al. 2000).

1.4.3. Mitochondrial DNA replication in *S. cerevisiae*

Nuclear DNA (nDNA) replication is very well investigated. nDNA is present in form of chromosomes which are replicated during S phase of the cell cycle. In contrast to nDNA replication, very little is known about the mtDNA replication in yeast and mammals. In budding yeast genes for a mitochondrial-specific primase, a ribonuclease H or a topoisomerase are not found, which are usually needed for conventional leading and lagging strand synthesis (Stodola and Burgers 2017). Nevertheless, some proteins, as the nuclear topoisomerase I, seem to have a dual function in mitochondria and the nucleus. Additionally, mtDNA was found to be linear or circular in yeast (Maleszka et al. 1991, Bendich 1996), which impedes the drawing of an analogy to already known DNA replication mechanisms. Therefore, the exact mtDNA replication mechanism is still debated.

In several eukaryotic species there is evidence for the rolling-circle replication model (RCR) such as in *C. elegans* (Lewis et al. 2015), higher plants (Backert et al. 1996) and in budding yeast (Maleszka et al. 1991). The fact that in budding yeast, circular mtDNA molecules are forming lariats and that linear fragments of heterogenous size are existing led to the hypothesis that replication occurs by RCR (Maleszka et al. 1991). However, the exact order of events by

Error! Use the Home tab to apply Überschrift 1 to the text that you want to appear here.

which RCR proceeds, and if this is the only possibility of mtDNA replication remains unclear for all of the organisms.

How mtDNA replication is initiated is dependent on the organism and for budding yeast two possible models have emerged over the past decades. The first one is the RNA-polymerase priming or transcription-dependent mtDNA replication model (Fig. 1.5) (Sanchez-Sandoval et al. 2015). Here, the RNA-polymerase Rpo41 primes the origins of replication. Rpo41 specificity is determined by the mitochondrial transcription factor Mtf1, which stabilizes the Rpo41-promoter complex (Lisowsky and Michaelis 1989, Yang et al. 2015). However, Rpo41 was shown to be not essential for mtDNA maintenance (Fangman et al. 1990), suggesting that there is most likely an additional Rpo41 independent mechanism.

The recombination-dependent rolling-circle replication model (RDR) became more popular in the past years. Again, for budding yeast the exact molecular mechanism has not been fully elucidated, however, many single results were assembled giving a rough picture. RDR postulates that a double-strand break is initiated most likely at ori5, a GC-rich sequence identified as origin of replication possibly with the help of the endonuclease Ntg1 (Ling et al. 2007). Here, ROS is suggested to be a possible activator of Ntg1 (Hori et al. 2009). Thereby a linear double-stranded DNA is formed, also termed concatemer (Maleszka et al. 1991, Bendich 1996). At such a concatemer a free 3' end is generated with the help of the 5'-3' exonuclease Din7 (Ling et al. 2013), allowing homologous priming with other mtDNA concatemers which are used as priming templates (Ling and Yoshida 2020). Recombination of both ends is assumed to be mediated by Mhr1, a mitochondrial recombinase and Mgm101. Mhr1 was found to be essential for mtDNA recombination and DSB repair (Ling et al. 1995), and is thought to pair linear single-stranded DNA with homologous circular double-stranded DNA (Ling 2002). Mgm101 was shown to have a very similar function. It likely participates in mtDNA recombination by catalyzing the annealing of ssDNA bound by the single strand binding protein, Rim1 (Zuo et al. 2002, Mbantenkhu et al. 2011) with a pre-existing single-stranded circular DNA (Chen and Clark-Walker 2018). Rim1 itself has been shown to interact with Pif1, one out of three helicases located in the mitochondrial matrix (Ramanagoudr-Bhojappa et al. 2013), which may unwind mtDNA structure. Additionally, a second helicase Hmi1 was shown to be involved in concatemer stabilization (Sedman et al. 2005). This allows mtDNA replication by the mtDNA polymerase Mip1 (Genga et al. 1986) which was shown to interact with and is potentially recruited by Mgm101 (Meeusen and Nunnari 2003). Mip1 is the only mtDNA polymerase and its deletion leads to the complete loss of mtDNA. Other than the human mitochondrial polymerase PolG, the yeast mitochondrial polymerase Mip1 is missing the accessory subunit which increases the processivity of the polymerase (Lucas 2004). However, Mip1 still is a highly processive polymerase which exhibits an C-terminal extension, essential for polymerase activity (Viikov et al. 2012). While replicating, the exonuclease activity

Error! Use the Home tab to apply Überschrift 1 to the text that you want to appear here.

of Mip1 is responsible for extrinsic proofreading, ensuring correct synthesis of mtDNA (Foury and Vanderstraeten 1992). While in mammalian cells mtDNA replication is terminated at the 3' end of a D-loop (Jemt et al. 2015), information about yeast replication termination is missing. After termination, the resulting circular mtDNA and concatemers are most likely either involved in priming or performing intermolecular recombination.

In summary, several factors have been identified and molecular mechanisms proposed, but many questions remain. For example, the relative contribution of the Rpo41-dependent or the RDR mechanism is unknown, as are the driving parameters that trigger mtDNA replication. And a particularly important question for this study is: How does a cell limit mtDNA replication in order to maintain approximately constant concentrations of mtDNA?

Error! Use the Home tab to apply Überschrift 1 to the text that you want to appear here.

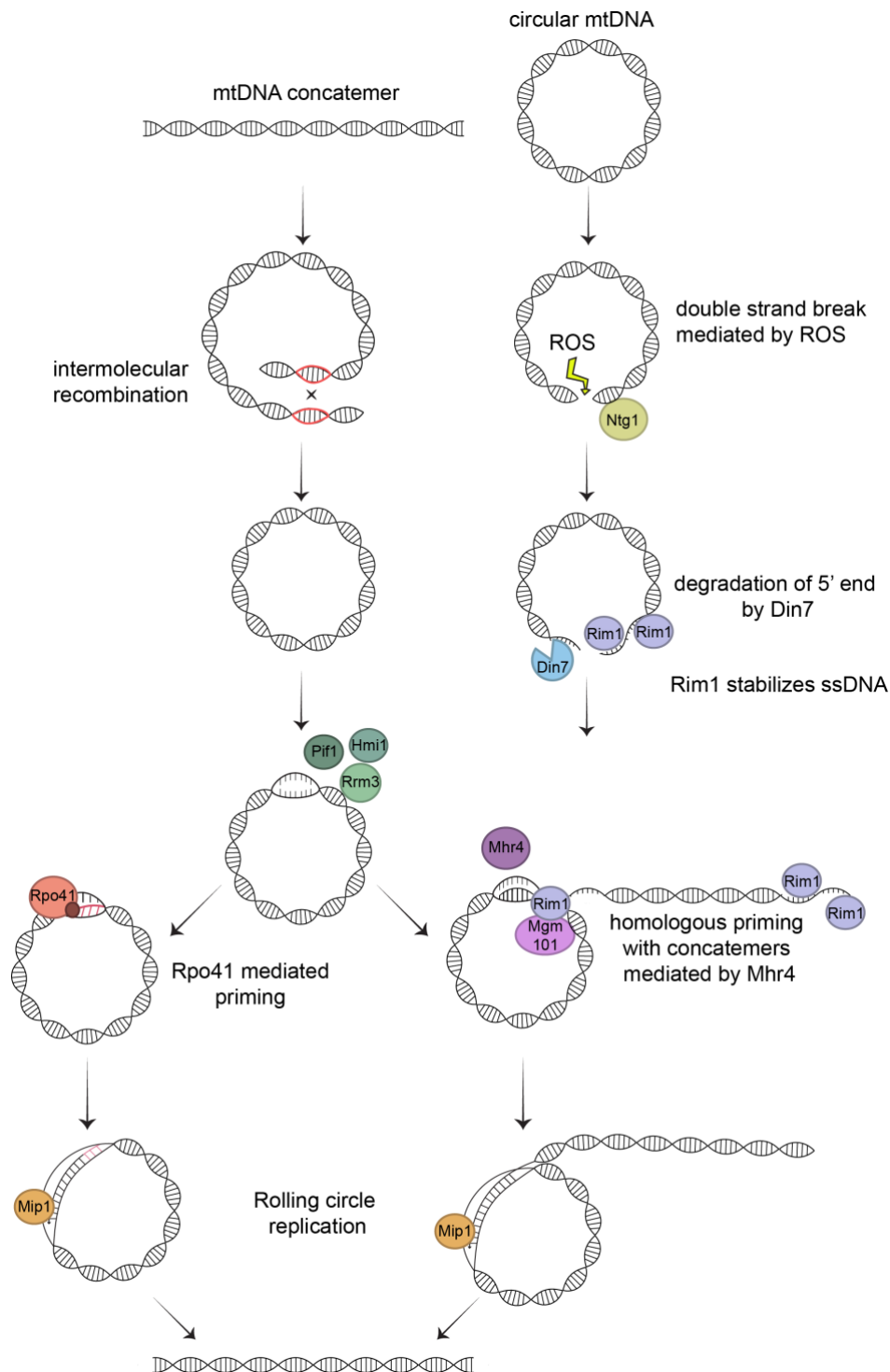


Figure 1.5: Possible mechanism for mtDNA replication in budding yeast. mtDNA copies exist as linear and circular molecules. mtDNA replication starts from a specific origin. There, double stranded mtDNA is separated by mitochondrial helicases and forms a lariat-structure, allowing the replication machinery to assess the origin of replication. Two possible mechanisms for replication initiation are proposed. Either the RNA polymerase Rpo41 together with its specificity factor Mtf1 primes mtDNA, or linear mtDNA molecules are self-priming other mtDNA molecules. This homologous priming is facilitated by Mhr4, Mgm101 and stabilized by Rim1. So far as this is known, both initiation processes result in rolling-circle mtDNA polymerization facilitated by Mip1.

Error! Use the Home tab to apply Überschrift 1 to the text that you want to appear here.

1.5. Mitochondrial network dynamics and mtDNA quality control

Mitochondrial morphology is highly dynamic and regulated by fission and fusion. Fusion of mitochondrial compartments seems to be important for the exchange of mitochondrial metabolites, proteins and mtDNA (Ono et al. 2001). At least two studies in mouse have shown that mtDNA stability relies the protein stoichiometry which is likely established by fusion. For example, fusion-defective cells show a misdistribution of mtDNA maintenance factors between the different mitochondrial compartments (Chen et al. 2010). This is in agreement with a recent study, where the composition of the protein components of the mtDNA replication machinery was shown to be altered in fusion-defective cells, leading to altered mtDNA replication and mtDNA nucleoid distribution (Ramos et al. 2019). Both studies are outlining the importance of fusion, which propagates a balance of mtDNA maintenance factors to stabilize mtDNA. However, how exactly fusion contributes to a proper stoichiometry of mtDNA maintenance factors and thereby correct mtDNA copy numbers is not clear. In contrast to fusion, fission divides mitochondria into new units and thereby enables selective degradation of mitochondrial compartments (Youle and van der Bliek, 2012). Thus, fission and fusion contribute to mitochondrial quality control and ensure mtDNA inheritance (Nunnari et al. 1997).

The importance of mitochondrial quality control is based on the maintenance of cellular processes. As already described, cells contain several mtDNA copies and often some of the copies are damaged due to ROS (Doudican et al. 2005) or faulty replication (Stumpf et al. 2010) resulting in a mix of correct and mutated mtDNA, also known as heteroplasmy. To prevent accumulation of mutant mtDNA, mechanisms to detect and remove faulty mtDNA copies have been evolved, which involve the mitochondrial network morphology. Cristae junctions arise when inner and outer mitochondrial membranes come in close proximity, whereby mitochondrial contact sites emerge, which are stabilized by the mitochondrial contact sites (MICOS) complex (Harner et al. 2011). Recently, it was shown that these cristae structures are required for mtDNA quality control in budding yeast (Jakubke et al. 2021). mtDNA and their encoded proteins are expected to have only a spatially limited influence, and so faulty proteins only influence mitochondrial functionality in close proximity (Busch et al., 2014). This spatially limited reduction in functionality is potentially detected by a specific mechanism involving cristae structures and leading to a selective degradation of mutated mtDNA (Jakubke et al. 2021). If cristae structures are also needed to ensure stable mtDNA copy numbers is unknown, however, due to their function in quality control it is feasible.

Error! Use the Home tab to apply Überschrift 1 to the text that you want to appear here.

1.6. Regulation of mtDNA maintenance

1.6.1. Importance of mtDNA copy number homeostasis

The correct amount of mtDNA copy number is of high importance for proper cellular function, as it encodes essential subunits for oxidative phosphorylation. Therefore, variations in mtDNA copy number often come with mitochondrial dysfunction with reduced oxidative phosphorylation (Nicolson 2014). Surprisingly, for yeast and other single-cell organisms little is known about the impact of mtDNA copy number variations on metabolic activities, whereas for higher eukaryotes several studies exist. In human, for example, several diseases have been associated with a reduced mtDNA copy number such as breast cancer, type 2 diabetes and liver disease (Clay Montier et al., 2009). Mutations in genes involved in mtDNA integrity can lead to primary mitochondrial disease and to a reduction or depletion of mtDNA. Additionally, severeness of the pathogenic m.3243A>G mitochondrial disease can be influenced by mtDNA copy number (Grady et al. 2018). Whether these diseases become phenotypic upstream or downstream of mtDNA copy number reduction is not clear so far.

In *Drosophila*, it has been shown that manipulation of mtDNA copy number in zygotes by using endonuclease perturbs embryonic development (Bahhir et al. 2019). Moreover, reducing mtDNA copy number in embryonic mice leads to an epigenetic alteration of hepatic lipolytic genes leading to abnormal lipid accumulation in adult mice (Wang et al. 2021). Both studies show a disease pattern that is directly caused by a low number of mtDNA copies and highlights the importance of mtDNA copy number regulation. So far, several factors have been described to be responsible for mtDNA copy number maintenance.

1.6.2. mtDNA factors important for the homeostasis of mtDNA copy number

The mechanism behind mtDNA copy number regulation is widely unknown, however, several factors have been identified to be important for mtDNA copy number maintenance. Especially modulating concentrations of mtDNA replication factors was shown to have an impact on mtDNA copy number. In budding yeast, an upregulation of the mtDNA-packaging factor Abf2 leads to an increase of mtDNA (Zelenaya-Troitskaya et al. 1998). Similar observations were made for mouse embryos where TFAM, the Abf2 homolog, is a major regulatory factor for mtDNA copy number (Hance et al. 2005, Filograna et al. 2019). In addition, the yeast mtDNA polymerase Mip1 is important for the homeostasis of mtDNA. It has been shown that mutations in the protein can lead to altered mtDNA copy numbers (Stumpf et al. 2010). Mutation of the C-terminal extension of the yeast mtDNA polymerase Mip1 also affected the processivity of

Error! Use the Home tab to apply Überschrift 1 to the text that you want to appear here.

Mip1 (Viikov et al. 2012). Moreover, in mouse cells the helicase TWINKLE (missing in yeast) was found to regulate mtDNA copy number (Tynismaa et al. 2004).

Besides the replication machinery, in yeast very recently the protein Mrx6, which is associated with the mitochondrial ribosome, was described to be involved in mtDNA copy number regulation (Göke et al. 2020). It forms a complex with the Lon protease Pim1, Pet20 and Mam33 and is essential for complex formation. The *MRX6* deletion mutant shows an increase in mtDNA copy number by 1.5-2-fold (Göke et al. 2020). By combining both results, it was hypothesized that Pim1 degrades mitochondrial proteins important for mtDNA replication. The substrate specificity of Pim1 might be determined by Mrx6, thereby regulating the degradation of mtDNA copy number regulating proteins (Göke et al. 2020).

All these studies indicate the importance of a balance between mtDNA maintenance factors, to maintain a stable cell-type-dependent mtDNA copy number. However, it is still not clear what the basic mechanism is that regulates these factors and mtDNA copy number.

1.6.3. Mitochondrial replication during cell cycle

The question, whether mitochondrial network biogenesis and mtDNA replication are coupled to the cell cycle has been studied frequently in the past. Neither for yeast nor for human cells a coupling of mitochondrial biogenesis and mtDNA replication to a specific cell cycle phase has been found. In unsynchronized HeLa cells, for example, mitochondrial growth and the cell cycle were shown to be uncoupled (Posakony et al. 1977). Also in yeast, mtDNA replication has been shown to continue in a number of cell cycle mutants independently of nDNA synthesis (Newlon and Fangman 1975). Thus, in fact, mtDNA replication occurs throughout the cell cycle. In addition, there is no limitation of replication to a specific site in the network. Instead, mtDNA replication occurs evenly distributed throughout the network in human cells (Magnusson 2003). However, whether modulation of mtDNA synthesis occurs during specific cell cycle phases is yet unclear. In particular, links between cell cycle and mtDNA synthesis have been found in synchronized cells. For example, in synchronized human HeLa cells, mtDNA replication appears to be coordinated with nuclear DNA synthesis (Chatre and Ricchetti, 2013). Others found that mitochondrial mass increases during S phase, but the increase in mtDNA was not significant in HeLa cells (Lee et al. 2007). mtDNA replication might also occur throughout the cell cycle, with peaks of activation at different cell cycle phases in synchronized (Pica-Mattoccia and Attardi 1972) and unsynchronized HeLa cells (Sasaki et al. 2017). They showed that the activity of mtDNA replication approximately doubles in S phase compared to G1 phase (Sasaki et al., 2017).

Error! Use the Home tab to apply Überschrift 1 to the text that you want to appear here.

Although it is not yet clear whether there are modulations of mtDNA synthesis during specific cell cycle phases, it is clear that mtDNA synthesis occurs throughout the cell cycle. The question that remains is, if it is not the cell cycle that regulates mtDNA replication, then what is responsible for keeping the mtDNA copy number stable during cell growth?

1.6.4. Allometric scaling of metabolism, mitochondrial mass and nucleoids

Even though there is no clear evidence for a coupling of mtDNA replication with cell cycle in yeast and human, metabolism and cell proliferation are closely wired. This is, among others, essential to ensure the cellular functionality through all stages of cell growth, as during cell cycle cells usually vary in cell size. In budding yeast specifically, cell sizes can vary more than two-fold during cell cycle. To ensure that sufficient energy and building blocks are supplied during each of these growth phases, the amount of energy and of building blocks must be adjusted, to keep concentrations on an acceptable level.

Indeed, on the organismal level, the metabolic rate i.e., the energy transformation within an organism, increases with total mass (West et al. 2002). In addition, the metabolic rate increases in sub-linear proportion to mass (Bertalanffy 1934). While the metabolic rate has been extensively studied on the organismal level, only few studies address the question how mitochondrial functionality is maintained on the cellular level. One of those rare studies has shown that in Jurkat and *Drosophila* cells the membrane potential scales non-linearly with cell size and does not depend on cell cycle (Miettinen and Björklund 2016). The membrane potential sets the rate of ATP production and thus the higher the membrane potential, the more energy can be generated. However, in cells bigger than the average population, mitochondrial functionality declines.

In contrast, mitochondrial content scales linearly with cell volume in Jurkat, HeLa and budding yeast cells (Kitami et al. 2012, Posakony et al. 1977, Miettinen and Björklund 2016, Rafelski et al. 2012). This suggests that mtDNA might also scale with cell volume. Indeed, the number of nucleoids increases with the length of the mitochondrial network (Osman et al. 2015), and studies in fission yeast have shown that the number of nucleoids increases in proportion to cell volume (Jajoo et al. 2016). This leads to the suggestion that cell size is potentially the key regulator of mitochondrial content and mtDNA homeostasis.

Error! Use the Home tab to apply Überschrift 1 to the text that you want to appear here.

1.7. Cell size as a regulator for organelles and subcellular structures

Not only mitochondrial volume increases with cell volume. Also for other organelles and subcellular structures, a linear increase in organelle volume with cell volume was observed (Chan and Marshall 2010). For example, evidence was found that the size of the nucleus (Jorgensen et al. 2007), centrosomes (Decker et al. 2011), vacuoles (Chan et al. 2016), mitotic spindle (Hara and Kimura 2009) and nucleolus (Weber and Brangwynne 2015) increases with cell volume. Besides organelles, also subcellular structures such as the contractile ring in budding yeast are regulated by cell size (Kukhtevich et al. 2020). The underlying mechanisms regulating the increase of these organelles and subcellular structures with cell growth are largely unknown. However, a feasible hypothesis that arose is the limiting-pool mechanism (Goehring and Hyman 2012). It states that the availability of specific components in the cytoplasm limits the synthesis of the respective organelle, thereby controlling its size. Thus, in larger cells the pool of factors must increase compared to smaller cells, to ensure organelle growth. Indeed, several studies indicate that the nuclei size increases as soon as more limiting components are available (Gurdon et al. 1976). Similar observations were made for the centrosome size in *C. elegans*, where the concentration of one specific biogenesis factor acts limiting on the centrosome size (Decker et al. 2011). Fittingly, it was discovered in *Xenopus* eggs that the length of the spindle depends on the cytoplasmic volume, likely due to limiting components whose quantity increases with cytoplasmic volume (Good et al. 2013, Hazel et al. 2013).

The limiting component mechanism is also supported by the fact that in larger cells biosynthesis increases, meaning that larger cells have proportionally more total protein (Newman et al. 2006) and RNA (Zhurinsky et al. 2010). Thereby more building blocks which are needed to produce the organelles, such as membrane subunits, proteins or enzymes, are provided in larger cells. In an enzyme-catalyzed reaction, the rate of product formation is a function of substrate concentration (Michaelis-Menten kinetics). Thus, the growth rate of the subcellular structures depends directly on the concentration of the respective subunits. In addition, also the catalysts of the reaction can limit a reaction, suggesting that enzymes and other proteins that contribute to biogenesis are potential limiting factors. This mechanism could also apply to mtDNA synthesis. Increased amounts of biosynthesis factors and other building blocks such as dNTPs could lead to more mtDNA in larger cells. However, whether mitochondrial maintenance factors indeed increase with cell volume has not yet been investigated. Thus, a major question is whether the mtDNA copy number is controlled by a limiting machinery.

Error! Use the Home tab to apply Überschrift 1 to the text that you want to appear here.

1.8. Aim of this study

How mtDNA copy number is regulated during cell growth, ensuring that all cells have similar mtDNA copy numbers, remains unknown. Although mitochondrial biogenesis might be modulated in certain cell cycle phases, a specific coupling of mtDNA replication and biosynthesis of the network to the cell cycle was neither found for yeast nor human cells. Therefore, it is not yet clear how cells ensure the right amount of mtDNA during cell growth. However, recent studies suggest that cell volume may be an important regulator of mitochondrial biosynthesis. For example, the mitochondrial network volume in budding yeast (Rafelski et al. 2012) and the number of nucleoids in fission yeast (Jajoo et al. 2016) were found to increase linearly with cell size. Such an increase in mitochondrial content was also observed for human Jurkat cells (Miettinen and Björklund 2016). Thus, the question arises, which role the cell volume plays in the regulation of mtDNA copy number and network volume.

In combination with previous work showing that RNA and protein levels increase globally with cell volume (Wu et al. 2010, Marguerat and Bähler 2012, Padovan-Merhar et al. 2015), one could speculate that a higher amount of biogenesis factors could lead to more mtDNA and network. The coupling of mitochondrial homeostasis factors to cell volume could be a possible explanation for the increase in mitochondrial network volume and nucleoid number, as more protein amount potentially leads to more synthesis. Thus, in this study it is hypothesized that mtDNA homeostasis is regulated by a cell volume-dependent limiting machinery.

This hypothesis gives rise to three sub-objectives, which will be investigated with the help of the model organism *S. cerevisiae*. First, it must be determined whether and how the mtDNA is coupled to the cell volume. For this purpose, the influence of cell volume on mitochondrial network volume, mtDNA copy number and nucleoids will be investigated, by DNA-qPCR and live-cell imaging. Second, it has to be investigated how the amount of mitochondrial maintenance factors is coupled to the cell volume and thus global transcription and translation. For this purpose, selected factors will be tested by RT-qPCR and flow cytometry. Third, it will be examined, whether mtDNA is dependent on the concentration of mitochondrial homeostasis factors. For this purpose, the concentration of several factors will be manipulated and the influence on the mtDNA is detected by DNA-qPCR

Overall, this study will give mechanistic insight into mtDNA homeostasis and will shed light on the question, whether and how mtDNA is coupled to protein expression and thus to cell volume.

Error! Use the Home tab to apply Überschrift 1 to the text that you want to appear here.

2. Materials and Methods

2.1. Chemicals and Consumables

Table 2.1: Chemicals and consumables used in this study, sorted alphabetically.

Chemicals or consumables	Supplier
Sodium hydroxide (NaOH)	Thermo Fisher Scientific, Waltham, USA
β -estradiol	Sigma-Aldrich, St. Louis, USA
Acidic phenol	Sigma-Aldrich, St. Louis, USA
Agarose SERVA Wide Range	Serva Electrophoresis, Heidelberg, Germany
Amino acids	Sigma-Aldrich, St. Louis, USA
Ammonium sulfate	Schubert & Weiß Omnilab, München, Germany
Ampicillin	Roth, Karlsruhe, Germany
Chlorophorm	Thermo Fisher Scientific, Waltham, USA
Nourseothricin (clonNAT)	Jena Bioscience GmbH, Jena Germany
Concanavalin A TYPE IV	Sigma-Aldrich, St. Louis, USA
Coverslips (24 x 50 mm)	Gerhard Menzel GmbH, Braunschweig, Germany
D(+) Glucose	Sigma-Aldrich, St. Louis, USA
Difco Agar, granulated	Schubert & Weiß Omnilab, München, Germany
EDTA	Sigma-Aldrich, St. Louis, USA
Ethanol	Sigma-Aldrich, St. Louis, USA
Glycerol	Th. Greyer, Renningen, Germany
Kanamycin	Roth, Karlsruhe, Germany
LB Broth (Lennox)	Sigma-Aldrich, St. Louis, USA
LB-Agar (Lennox)	Sigma-Aldrich, St. Louis, USA
Lithium acetate dihydrate	Schubert & Weiß Omnilab, München, Germany
Sodium chloride (NaCl),5M	Promega, Madison, USA
Polyethylene glycol, (PEG), BIOXTRA	Sigma-Aldrich, St. Louis, USA
Peptone, BD Bacto™	Biozol, Eching, Germany
Phenol/ Chloroform/ Isoamyl alcohol (25:24:1)	Thermo Fisher Scientific, Waltham, USA
Microscope slides	Gerhard Menzel GmbH, Braunschweig, Germany
Sybr® Safe DNA Gel Stain	Invitrogen, Thermo Fisher Scientific, Waltham, USA
Tris acetate	Sigma-Aldrich, St. Louis, USA
Tris/HCl	Sigma-Aldrich, St. Louis, USA

Error! Use the Home tab to apply Überschrift 1 to the text that you want to appear here.

Yeast extract, BD Bacto™	Biozol, Eching, Germany
Yeast nitrogen base	Schubert & Weiß Omnilab, München, Germany
µ-Slide 8 Well, ibi-Treat	ibidi, Gräfelfing, Germany
Isoton II Diluent	Beckman Coulter, Krefeld, Germany
LightCycler 480 Multiwell Plate 96	Roche, Basel, Switzerland

2.2. Devices

Table 2.2: Devices used in this study.

Device	Supplier
Zeiss LSM 800 microscope	Zeiss Germany, Oberkochen, Germany
Mini-BeadBeater 24, 230V	BioSpec Products, Oklahoma, USA
NanoDrop OneC	Thermo Fisher Scientific, Waltham, USA
Z2 Coulter Particle Count and Size Analyzer	Beckman Coulter, Krefeld, Deutschland
LightCycler® 96	Roche, Basel, Switzerland
U:Genius3 Transilluminator	Syngene, Bengaluru, Karnataka, India
CytoFlex S Flow Cytometer	Beckman Coulter, Krefeld, Deutschland
Ecotron shaking incubator	Infors HT, Bottmingen, Switzerland

2.3. Kits

Table 2.3. Kits used in this study.

Kit	Supplier/Source
High-capacity cDNA Reverse Transcription Kit with RNase Inhibitor	Life Technologies, Carlsbad, California, USA
NucleoSpin Gel and PCR Clean-up	Macherey-Nagel, Düren, Germany
NucleoSpin Plasmid	Macherey-Nagel, Düren, Germany
YeaStar RNA Kit	Zymo Research, Freiburg, Germany

2.4. Strains

Table 2.4: List of Strains used in this study. All strains are derived from W303 background.

Name	Genotype	Description	Origin	Figure
ASY004-1	<i>Mat α; ADE2, ABF2-linker-mCitrine-ADH1term(long)-CglaTRP1</i>	<i>ABF2-mCitrine-ADH1term</i>	This study	3.7b,d,f

Error! Use the Home tab to apply Überschrift 1 to the text that you want to appear here.

		(KCE001-2) in MMY116-2c		
ASY006-1	<i>Mat a</i> ; ADE2, MIP1-linker- <i>mCitrine-ADH1term(long)-CglaTRP1</i>	<i>MIP1-mCitrine-ADH1term</i> (KCE001-2) in MMY116-2c	This study	2.1; 3.7a,c,e,g; 3.8; 3.12
ASY007-2	<i>Mat a</i> ; ADE2, MIP1-linker- <i>mCitrine:CglaTRP1</i> , <i>whi5Δ::kanMX6-LexApr-WHI5-ADH1term-LEU2</i> , <i>his3::LexA-ER-AD-TF-HIS3</i>	<i>MIP1-mCitrine-ADH1term</i> (KCE001-2) in MS63-1	This study	3.7c
ASY013-1	<i>Mat a</i> ; <i>mt-LacO</i> , ADE2, TRP1, <i>whi5Δ::KlacURA3</i> , <i>LexApr-WHI5-ADH1term-LEU2</i> , <i>his3::LexA-ER-LBD-HIS3</i> , <i>Pcup1-Su9-2xNEON-LacI-Pgk1-Su9-mKate2-KanMX4</i>	Haploid microscopy strain (ASE001-5), <i>Whi5</i> -inducible (<i>whi5Δ</i> with pPP2960, KSE113-1, FRP880)	This study	2.3; 3.3; 3.4
ASY015-1	<i>Mat a/a</i> ; <i>mt-LacO</i> , ADE2/ADE2, , <i>Δwhi5::KlacURA3/WHI5</i> , <i>LexApr-WHI5-ADH1term-LEU2</i> , <i>his3::LexA-ER-LBD-HIS3</i> , <i>Pcup1-Su9-2xNEON-LacI-Pgk1-Su9-mKate2-KanMX4</i>	Diploid microscopy stain (ASE001-5 in yCO381) crossed with <i>Whi5</i> -inducible (<i>whi5Δ</i> with pPP2960, KSE113-1, FRP880)	This study	2.3; 3,3
ASY020-1	<i>Mat a/a</i> ; ADE2/ADE2, URA3/ <i>ura3</i> , <i>leu2/LEU2</i>	Diploid WT	This study	3.1; 3.9; 3.10; 3.11
ASY023-1	<i>Mat a/a</i> ; ADE2/ADE2, <i>ura3-1/URA3</i> , <i>whi5Δ::kanMX6-LexApr-WHI5-ADH1term-LEU2/WHI5</i> , <i>his3::LexA-ER-AD-TF-HIS3/his3-11,15</i>	Diploid <i>Whi5</i> -inducible strain (URA3 in MMY116-2c, crossed with MS63)	This study	3.1; 3.11b-e
ASY024-1	<i>Mat a/a</i> ; ADE2/ADE2, <i>leu2-3/LEU2</i> , <i>ura3-1/URA3</i> , <i>mip1::CgalTRP1/MIP1</i>	Hemizygous <i>MIP1</i> strain (ASY20 with pPP2960)	This study	3.9; 3.11
ASY025-1	<i>Mat a/a</i> ; ADE2/ADE2, <i>ura3-1/URA3</i> , <i>whi5Δ::kanMX6-LexApr-WHI5-ADH1term-LEU2/WHI5</i> , <i>his3::LexA-ER-AD-TF-HIS3/his3-11,15</i> , <i>mip1::CgalTRP1/MIP1</i>	Hemizygous <i>MIP1</i> strain, <i>Whi5</i> -inducible, (ASY23 with pPP2960)	This study	3.11b-e
ASY033-1	<i>Mat a/a</i> ; ADE2/ADE2, <i>leu2-3/LEU2</i> , URA3/ <i>ura3-1</i> , <i>pif1::TRP1/PIF1</i>	Hemizygous <i>PIF1</i> strain (ASY20 with pPP2960)	This study	3.9

Error! Use the Home tab to apply Überschrift 1 to the text that you want to appear here.

ASY034-1	<i>Mat a/a; ADE2/ADE2, leu2-3/LEU2, URA3/ura3-1, rad53::TRP1/RAD53</i>	Hemizygous <i>RAD53</i> strain (ASY20 with pPPP2960)	This study	3.9
ASY035-1	<i>Mat a/a; ADE2/ADE2, leu2-3/LEU2, URA3/ura3-1, rrm3::TRP1/RRM3</i>	Hemizygous <i>RRM3</i> strain (ASY20 with pPPP2960)	This study	3.9
ASY039-1	<i>Mat a/a; ADE2, Δwhi5::KlacURA3, hiWHI5:LEU2, LexA-ER-LBD:HIS3, Pcup1-Su9-2xNEON-Lacl--Pgk1-Su9-mKate2:KanMX4, TRP1, mip1::clonNAT</i>	<i>mip1Δ</i> microscopy strain (ASY13-1 with pCA13)	This study	3.4
ASY040-1	<i>Mat a; ADE2, mip1-linker-mCitrine:CglaTRP1::LEU2, his3::LexA-ER-AD-TF-HIS3, ura3::LexApr-Mip1-mCitr-Cyc1term-URA3</i>	Hormone-Inducible (HI)-Mip1	This study	3.12
ASY041-1	<i>Mat a/a; ADE2/ADE2, leu2-3/LEU2, URA3/ura3-1, mrx6::TRP1/MRX6</i>	Hemizygous <i>MRX6</i> strain (ASY20 with pPPP2960)	This study	3.10a-b
ASY042-1	<i>Mat a/a; ADE2/ADE2, leu2-3/LEU2, URA3/ura3-1, sue1::TRP1/SUE1</i>	Hemizygous <i>SUE1</i> strain (ASY20 with pPPP2960)	This study	3.10a-b
ASY043-1	<i>Mat a/a; ADE2/ADE2, leu2-3/LEU2, URA3/ura3-1, pet20::TRP1/PET20</i>	Hemizygous <i>PET20</i> strain (ASY20 with pPPP2960)	This study	3.10a-b
ASY044-1	<i>Mat a; ADE2, mrx6::CgalTRP1</i>	Haploid <i>MRX6</i> deletion (MMY116-2c with pPPP2960)	This study	3.10c
ASY045-1	<i>Mat a; ADE2, whi5Δ::kanMX6-LexApr-WHI5-ADH1term-LEU2, his3::LexA-ER-AD-TF-HIS3, mrx6::CgalTRP1</i>	Haploid <i>Whi5</i> -inducible strain with <i>MRX6</i> deletion (MS63-1 with pPPP2960)	This study	3.10c
ASY046-1	<i>Mat a/a; ADE2/ADE2, leu2-3/LEU2, ura3-1/URA3, mip1::CgalTRP1/MIP1, abf2::clonNAT/ABF2</i>	Double hemizygous <i>MIP1 ABF2</i> strain (with pCA13)	This study	3.11
ASY049-2	<i>Mat a/a; whi5Δ::kanMX6-LexApr-WHI5-ADH1term-LEU2, his3::LexA-ER-AD-TF-</i>	Double hemizygous	This study	3.11b-e

Error! Use the Home tab to apply Überschrift 1 to the text that you want to appear here.

	<i>HIS3, mip1::CgalTRP1/MIP1, abf2::clonNAT/ABF2</i>	<i>MIP1 ABF2</i> strain; Whi5-inducible		
ASY051-2	<i>Mat α; ADE2, ura3::URA3/ABF2</i>	Haploid WT with additional copy of <i>ABF2</i> (ASE003-1 in MMY116-2c)	This study	3.15
ASY052-5	<i>Mat a; ADE2, whi5Δ::kanMX6-LexApr-WHI5-ADH1term-LEU2, his3::LexA-ER-AD-TF-HIS3, ura3::URA3/ABF2</i>	Haploid Whi5-inducible strain with additional copy of <i>ABF2</i> (ASE003-1 in MS63-1)	This study	3.15c-f
ASY057-3	<i>Mat α; ADE2, trp1::TRP1/MIP1</i>	Haploid WT with additional copy of <i>MIP1</i> (ASE002-2 in MMY116-2c)	This study	3.15
ASY058-1	<i>Mat a; ADE2, whi5Δ::kanMX6-LexApr-WHI5-ADH1term-LEU2, his3::LexA-ER-AD-TF-HIS3, trp1::TRP1/MIP1</i>	Haploid Whi5-inducible strain with additional copy of <i>MIP1</i> (ASE002-2 in MS63-1)	This study	3.15c-f
ASY059-2	<i>Mat α; ADE2, ura3::URA3/ABF2, trp1::TRP1/MIP1</i>	Haploid WT with additional <i>ABF2</i> and <i>MIP1</i> copies (ASE002-2 in ASY51-2)	This study	3.15
ASY060-1	<i>Mat a; ADE2, whi5Δ::kanMX6-LexApr-WHI5-ADH1term-LEU2, his3::LexA-ER-AD-TF-HIS3, ura3::URA3/ABF2, trp1::TRP1/MIP1</i>	Haploid Whi5-inducible strain with additional copies of <i>ABF2</i> and <i>MIP1</i> (ASE002-2 in ASY52-5)	This study	3.15c-f
JE611-c	<i>Mat α, cln1Δ, cln2Δ, cln3::leu2, lexOPr-Cln1-Leu2, ADE2, his3::cyc1-Pr-lexO TF-his3, TRP, URA</i>	Cln1-inducible strain	Jennifer Ewald, Skotheim lab	3.2
KCY005-1	<i>Mat α/a; ADE2/ADE2, whi5Δ::CglaTRP1/whi5Δ::kanMX6-LexApr-WHI5-ADH1term-LEU2, his3/his3::LexA-ERAD-TF-HIS3</i>	Diploid Whi5-inducible strain	Kora-Lee Claude, Schmoller lab	2.4
KSY244-1	<i>Mat α/a; ADE2/ADE2, leu2-3/LEU2, URA3/ura3-1, abf2::TRP1/ABF2</i>	Hemizygous <i>ABF2</i> strain (ASY20 with pPP2960)	This study	3.9, 3.11

Error! Use the Home tab to apply Überschrift 1 to the text that you want to appear here.

KSY245-1	<i>Mat α/a; ADE2/ADE2, ura3-1/URA3, whi5Δ::kanMX6-LexApr-WHI5-ADH1term-LEU2/WHI5, his3::LexA-ER-AD-TF-HIS3/his3-11,15, abf2::CgalTRP1/ABF2</i>	Hemizygous <i>ABF2</i> strain; Whi5-inducible (ASY23 with pPP2960)	This study	3.11b-e
KSY246-1	<i>Mat α/a; ADE2/ADE2, leu2-3/LEU2, URA3/ura3-1, hmi1::TRP1/HMI1</i>	Hemizygous <i>HMI1</i> strain (ASY20 with pPP2960)	This study	3.9
KSY251-1	<i>Mat α; ADE2, MIP1-linker-mCitrine- ADH1term-CglaTRP1, his3::LexA-ER-LBD-HIS3</i>	Control strain (FRP880 in ASY006-1)	This study	3.12d-e
KSY252-1	<i>Mat α; ADE2, MIP1-linker-mCitrine- ADH1term-CglaTRP1, his3::LexA-ER-LBD-HIS3; lexAprCterm-Mip1-mCitrine</i>	KSE177-6 (BstBI) in KSY251-1, <i>URA3</i> locus	This study	2.1
KSY253-1	<i>Mat α/a; ADE2/ADE2, leu2-3/LEU2, URA3/ura3-1, rpo41::TRP1/RPO41</i>	Hemizygous <i>RPO41</i> strain (ASY20 with pPP2960)	This study	3.9
KSY254-1	<i>Mat α/a; ADE2/ADE2, leu2-3/LEU2, URA3/ura3-1, mtf1::TRP1/MTF1</i>	Hemizygous <i>MTF1</i> strain (ASY20 with pPP2960)	This study	3.9
KSY255-1	<i>Mat α/a; ADE2/ADE2, leu2-3/LEU2, URA3/ura3-1, mhr1::TRP1/MHR1</i>	Hemizygous <i>MHR1</i> strain (ASY20 with pPP2960)	This study	3.9
KSY256-1	<i>Mat α/a; ADE2/ADE2, leu2-3/LEU2, URA3/ura3-1, mgm101::TRP1/MGM101</i>	Hemizygous <i>MGM101</i> strain (ASY20 with pPP2960)	This study	3.9
KSY257-1	<i>Mat α/a; ADE2/ADE2, leu2-3/LEU2, URA3/ura3-1, rim1::TRP1/RIM1</i>	Hemizygous <i>RIM1</i> strain (ASY20 with pPP2960)	This study	3.9
KSY299-1,2	<i>Mat α; ADE2, mip1::Mip1-Adh1term(short)-cglaTRP1</i>	Mip1- <i>Adh1term</i> (short) (from KCE001-2) in MMY116-2C	This study	3.8
KSY300-1,2	<i>Mat α; ADE2, mip1::Mip1-Adh1term(long)-cglaTRP1</i>	<i>MIP1-ADH1term</i> (long) (from KCE001-2) in MMY116-2C	This study	3.8

Error! Use the Home tab to apply Überschrift 1 to the text that you want to appear here.

KSY301-1,2	<i>Mat a; ADE2, mip1::Mip1-mCitr-Mip1term-cglaTRP1</i>	<i>MIP1-mCitrine-MIP1term</i> (from KSE181-2) in MMY116-2C	This study	3.8
KSY302-4	<i>Mat a; ADE2, whi5::kanMX6-LexApr-WHI5-ADH1term-LEU2, his3::LexA-ER-AD-TF-HIS3, abf2::CglaTRP1-Htb1pr-Abf2</i>	<i>HTB1pr-ABF2</i> (from KSE166-4) in MS63-1	This study	3.13
KSY303-1	<i>Mat a; ADE2, whi5::kanMX6-LexApr-WHI5-ADH1term-LEU2, his3::LexA-ER-AD-TF-HIS3, mip1::klacURA3-Htb1pr-Mip1</i>	<i>HTB1pr-MIP1</i> (from KSE183-1) in MS63-1	This study	3.13
KSY304-1	<i>Mat a; ADE2, whi5::kanMX6-LexApr-WHI5-ADH1term-LEU2, his3::LexA-ER-AD-TF-HIS3, abf2::CglaTRP1-Htb1pr-Abf2, mip1::klacURA3-Htb1pr-Mip1</i>	<i>HTB1pr-MIP1</i> (from KSE183-1) in KSY302-4	This study	3.13
KSY313-1	<i>Mat a; ADE2, whi5::kanMX6-LexApr-WHI5-ADH1term-LEU2, his3::LexA-ER-AD-TF-HIS3, abf2::CglaTRP1-Htb2pr-Abf2</i>	<i>HTB2pr-ABF2</i> (from KSE167-4) in MS63-1	This study	3.14
KSY314-4	<i>Mat a; ADE2, whi5::kanMX6-LexApr-WHI5-ADH1term-LEU2, his3::LexA-ER-AD-TF-HIS3, abf2::CglaTRP1-Htb1pr-Abf2-Adh1term-URA3</i>	<i>ABF2-ADH1term</i> (from KSE174-1) in KSY302-4	This study	3.14
KSY315-4	<i>Mat a; ADE2, whi5::kanMX6-LexApr-WHI5-ADH1term-LEU2, his3::LexA-ER-AD-TF-HIS3, abf2::CglaTRP1-Htb2pr-Abf2-Adh1term-URA3</i>	<i>ABF2-ADH1term</i> (from KSE174-1) in KSY313-1	This study	3.13
MMY116-2c	<i>Mat a; ADE2</i>	Haploid WT strain	Skotheim lab stock	2.1; 3.1; 3.5; 3.7c-f; 3.8; 3.10c; 3.12; 3.13; 3.14; 3.15
MS63-1	<i>Mat a; ADE2, whi5Δ::kanMX6-LexApr-WHI5-ADH1term-LEU2, his3::LexA-ER-AD-TF-HIS3</i>	Haploid Whi5-inducible strain	Matthew Swaffer, Skotheim lab	2.4; 3.1; 3.5; 3.6; 3.7c, 3.10c; 3.13; 3.14; 3.15c-f

Error! Use the Home tab to apply Überschrift 1 to the text that you want to appear here.

2.5. Enzymes

Table 2.5: Enzymes used in this study.

Enzyme	Supplier/Source
Alkaline phosphatase (CIP)	New England Biolabs GmbH, Frankfurt a.M., Germany
DNase I	Life Technologies, Carlsbad, California, USA
Phusion polymerase	Lab stock
Q5 polymerase	New England Biolabs GmbH, Frankfurt a.M., Germany
Restriction Enzymes	New England Biolabs GmbH, Frankfurt a.M., Germany
RNase A	Sigma-Aldrich, St. Louis, USA
T4 DNA Ligase	Thermo Fischer Scientific (Schwerte/Germany)

2.6. Plasmids

Table 2.6: List of plasmids used for transformation.

Plasmid	Description	Origin
ASE001-5	HO-homology-CuPr-SU9-2xmNeon-Lacl	This study
ASE002-2	<i>MIP1pr-MIP1-MIP1term</i> in pRS404	This study
ASE003-1	<i>ABF2pr-ABF2-ABF2term</i> in pRS406	This study
KSY177-6	<i>lexAprCterm-Mip1-mCitrine</i> in FRP793	Kurt Schmoller, this study
FRP880	<i>PACT1(-1-520)-LexA-ER-haB112-TCYC1</i>	Ottoz et al., 2014
KSE113-1	<i>LexApr-WHI5-ADH1term-LEU2</i>	Kurt Schmoller Lab

Table 2.7: List of plasmids used as templates for PCR-transformation. Sequences of interest were amplified with overlaps of the target locus.

Plasmid	Description	Origin
KCE001-2	<i>linker-mCitrine-Adh1term-CglaTRP1</i> in pPP2960	Kora-Lee Claude, Schmoller Lab
KSE166-4	full <i>HTB1</i> promoter in pPP2960	Kurt Schmoller, this study
KSE167-4	full <i>HTB2</i> promoter in pPP2960	Kurt Schmoller, this study
KSE174-1	<i>ADH1term-URA3</i> in pRS406	Kurt Schmoller, this study
KSE181-2	<i>ADH1term::MIP1term</i> in KCE001-2	Kurt Schmoller, this study
KSE183-1	<i>HTB1</i> promoter in pPP2961	Kurt Schmoller, this study

Error! Use the Home tab to apply Überschrift 1 to the text that you want to appear here.

Table 2.8: Plasmids used as PCR knock-out templates. The knock-out templates pPP2960, pPP2961 and pPP3129 were used to prevent homologous recombination with endogenous marker sequences.

Name	Description	Origin
pPP2960/ pFA6a-Cgla <i>TRP1</i>	knock-out template with <i>C. glabrata</i> <i>TRP1</i> gene	Peter Pryciak Lab
pPP2961/ pFA6a-Klac <i>URA3</i>	knock-out template with <i>K. lactis</i> <i>URA3</i> gene	Peter Pryciak Lab
pPP3129/ pFA6a-Cgla <i>LEU2</i>	knock-out template with <i>C. glabrata</i> <i>LEU2</i> gene	Peter Pryciak Lab
pCA13	plasmid with <i>natMX</i> gene	Jan Skotheim Lab

2.7. Oligonucleotides

Table 2.9: qPCR primers used in this study. All primers were ordered from Sigma-Aldrich.

Gene	qPCR primer direction	qPCR primer sequence (5'-3')
<i>ABF2</i>	forward	AACCAGCAGGACCCTTCATT
	reverse	AGTTGAGAGGGTAGCGAGCA
<i>ACT1</i>	forward	CACCCTGTTCTTTTGA CTGA
	reverse	CGTAGAAGGCTGGAACGTTG
<i>COX2</i>	forward	GTTGATGCTACTCCTGGTAGATT
	reverse	TTGCATGACCTGTCCCACAC
<i>COX3</i>	forward	TTGAAGCTGTACAACCTACC
	reverse	CCTGCGATTAAGGCATGATG
<i>MIP1</i>	forward	CCATCACAAGCAAGAACGGC
	reverse	GTCCCTTTCCAGCTCAACCA
<i>MRX6</i>	forward	CATCCGACGTGGTGCTCTTA
	reverse	TCTCATCTCTCCCTCCACCC
<i>MTF1</i>	forward	TTGCTAATGTGACGGGGGAG
	reverse	CTGTTGTGCTTGGCATCCAT
<i>PIM1</i>	forward	ACCCTACATTGGCGCTTTCA
	reverse	AGTGCCCGTCTTTTCGTCTT
<i>RDN18</i>	forward	AACTCACCAGGTCCAGACACAATAAGG
	reverse	AAGGTCTCGTTCGTTATCGCAATTAAGC
<i>RPO41</i>	forward	TCTGGGTAGAACACCGTGGA
	reverse	TTCGTCTTGTGCACCTGGAA

Error! Use the Home tab to apply Überschrift 1 to the text that you want to appear here.

2.8. Buffer and Media

Table 2.10: Buffer used in this study. All buffers were stored at room temperature.

Buffer	Composition
1 M TE/Lithium acetate	1 M Lithium acetate 10 mM Tris/HCl 1 mM EDTA
0.1 M TE/Lithium acetate	0.1 M Lithium acetate 10 mM Tris/HCl 1 mM EDTA
Detergent Lysis Buffer pH 8.0	100 mM NaCl 10 mM Tris/HCl 1 mM EDTA 2 % (v/v) Triton X-100 1 % (w/v) SDS
TAE-Buffer pH 8.5	40 mM Tris acetate 1 mM EDTA

Table 2.11: Media used in this study. Except for the glycerol and ethanol stock which was sterile filtered, all media were autoclaved and stored at 4°C.

Media	Composition
YPD medium	2.0 % (w/v) Peptone ^[1] _{SEP} 1.0 % (w/v) Yeast extract 2.0 % (w/v) Glucose
SC medium	0.1385 % (w/v) Synthetic complete mix 0.17 % (w/v) Yeast nitrogen base 0.5 % (w/v) Ammonium sulfate
for SCD medium add for SCGE medium add	2.0 % (w/v) Glucose 2.0 % (v/v) Glycerol and 1 % EtOH (v/v) (sterile filtered)
LB medium	2.0 % (w/v) LB-powder
SOC medium	1.0 % (w/v) Peptone 0.5 % (w/v) Yeast extract

Error! Use the Home tab to apply Überschrift 1 to the text that you want to appear here.

Table 2.12: Agar-plates used in this study. All plates were stored at 4°C.

Agar-plates	Composition
LB plates	3.5 % (w/v) LB agar
YPD plates	2.0 % (w/v) Peptone 1.0 % (w/v) Yeast extract 2.0 % (w/v) Agar 1 pellet NaOH per litre → Autoclave and add glucose afterwards 2.0 % (w/v) Glucose
YPG plates	2.0 % (w/v) Peptone 1.0 % (w/v) Yeast extract 2.0 % (w/v) Agar 1 pellet NaOH per litre 3.0 % (w/v) Glycerol → Autoclave
SCD plates	x % (w/v) Synthetic complete mix (see below) 0.17 % (w/v) Yeast nitrogen base 0.5 % (w/v) Ammonium sulfate 2.0 % (w/v) Agar 1 pellet NaOH per litre → Autoclave and add glucose afterwards 2.0 % (w/v) Glucose

Table 2.13: Amount of the respective synthetic complete dropout mix used in this study.

Synthetic complete dropout mix % (w/v)								
SC complete	SC-HTLUA Met	SC-HTLUA	SC-Met	SC-Ade	SC-Ura	SC-His	SC-Leu	SC-Trp
0.1385	0.1085	0.1105	0.1365g	0.1345	0.1365	0.1365	0.1265	0.1305

Error! Use the Home tab to apply Überschrift 1 to the text that you want to appear here.

Table 2.14: Synthetic complete mix composition. All amino acids were mixed and stored at 4°C. For dropout plates, the respective amino acid was left out.

Composition	Amino acids/ supplements
0.01 % (w/v)	Aspartic acid
0.005 % (w/v)	Glutamic acid
0.003 % (w/v)	Phenylalanine
0.0375 % (w/v)	Lysine
0.02 % (w/v)	Serine
0.015 % (w/v)	Threonine
0.003 % (w/v)	Valine
0.0375 % (w/v)	Tyrosine
0.003 % (w/v)	Isoleucine
0.002 % (w/v)	Arginine
0.002 % (w/v)	Methionine
0.004 % (w/v)	Adenine
0.002 % (w/v)	Uracil
0.002 % (w/v)	Histidine
0.012 % (w/v)	Leucine
0.008 % (w/v)	Tryptophan

2.9. Cell cultivation

2.9.1. Cultivation of wild-type and *Whi5*-inducible *S. cerevisiae* strains

For long-term storage the *S. cerevisiae* strains were maintained in a 15% (v/v) glycerol solution diluted with SC-medium. The glycerol stocks were stored at -80°C and cultured on YPD agar plates at 30°C before transfer to liquid culture. All liquid cultures were incubated at 30°C in a shaking incubator at 250 rpm and harvested at 3,220 x g.

For experiments performed on non-fermentable medium (SCGE), strains were first cultured on full medium (YPD) for at least 6 hours. Cells were then washed twice with SCGE and transferred to SCGE. Cell cultures without cell volume manipulation were grown to log-phase for approximately 24 h and used directly for experiments. In preparation of *Whi5*-induction, cells were grown for 12-24 h on SCGE. Afterwards β -estradiol was added, and cells were grown for another 24 h. For manipulation of cell volume, *WHI5* expression was induced with concentrations of 0 nM, 10 nM, and 30 nM β -estradiol for haploid strains and 0 nM, 15 nM, and 60 nM β -estradiol for diploid strains were used. Optimal concentrations have been determined by growth rate and cell size measurements.

For experiments using fermentable medium, cells were inoculated directly into synthetic complete medium containing 2% dextrose (SCD). After approximately 12 h, β -estradiol concentrations of 0 nM, 15 nM, 60 nM, 100 nM (only in Fig. 3.1b) and 150 nM for haploids and 0 nM, 15 nM, 60 nM, and 150 nM for diploids were added. Cultures were grown for 24 h and cell size measurements were performed using a Coulter counter.

To ensure that the cultures were in exponential growth ($OD_{600} < 1$), optical density measurements were performed regularly using a spectrophotometer (NanoDrop OneC).

2.9.2. Cultivation for induction of G1 arrest in *S. cerevisiae*

G1 arrests were performed in collaboration with Alissa Finster. To arrest cells in G1 phase, a *cln1/2/3* deletion strain was used in which *Cln1* is expressed from an β -estradiol-inducible promoter (Ewald et al. 2016). As a consequence, the cells can only undergo complete cell cycle with the addition of β -estradiol. Once estradiol is removed from the medium, the cells remain in G1. First, cells were cultured on YPD containing 30 nM β -estradiol for at least 6 hours and then transferred to SCGE containing 30 nM β -estradiol. When SCD medium was used, cells were directly inoculated into SCD containing 60 nM β -estradiol, allowed to grow for at least 6 h, diluted, and incubated for 24 h. The cells were then transferred to SCD containing 60 nM β -estradiol. Subsequently, cells were pelleted, washed with the respective medium, and

Error! Use the Home tab to apply Überschrift 1 to the text that you want to appear here.

then harvested hourly (SCGE 0-7 h; SCD 0-5 h). To document the progression of the G1 arrest, bud counts were done in parallel (see 2.11.7).

2.9.3. Cultivation of the hormone-inducible Mip1-mCitrine (ASY40-1)

To manipulate concentrations of Mip1 and in parallel measure Mip1 concentrations, a β -estradiol regulated promoter was cloned upstream of the Mip1 sequence (see 2.11.5) and, for detection, Mip1 was endogenously tagged with mCitrine. By adding different β -estradiol concentrations to the cell cultures, Mip1 concentrations could be manipulated and, by epifluorescence microscopy, levels of Mip1 could be determined.

The cells were cultivated as described before, however, β -estradiol was added to the medium and plates, to ensure proper mtDNA synthesis and cell growth. Non-toxic β -estradiol concentrations were determined by performing a serial dilution growth test, with the haploid hormone-inducible (HI) *MIP1-mCitrine/MIP1-mCitrine* strain (parental strain of HI-Mip1-mCitrine, KSY252-1) which still contains MIP1-mCitrine in the endogenous locus. The strain shows a growth defect at 10 nM β -estradiol and higher concentrations on YPG (non-fermentable). Based on the growth test on plates (Fig 2.1) and repetition on liquid medium, for an initial cultivation of the HI-Mip1-mCitrine strain (ASY40) 2.5 nM β -estradiol was added to the plates and the liquid medium. After growing for 20-24 h in SCGE, 0 nM, 2.5 nM, 5 nM, 7.5 nM, 10 nM and 20 nM were added and the cells were grown for another 20-24 h. The cultures were harvested and shock frozen to allow mtDNA analysis the next day. Cells from the same cultures were used for microscopy and cell size measurements in parallel.

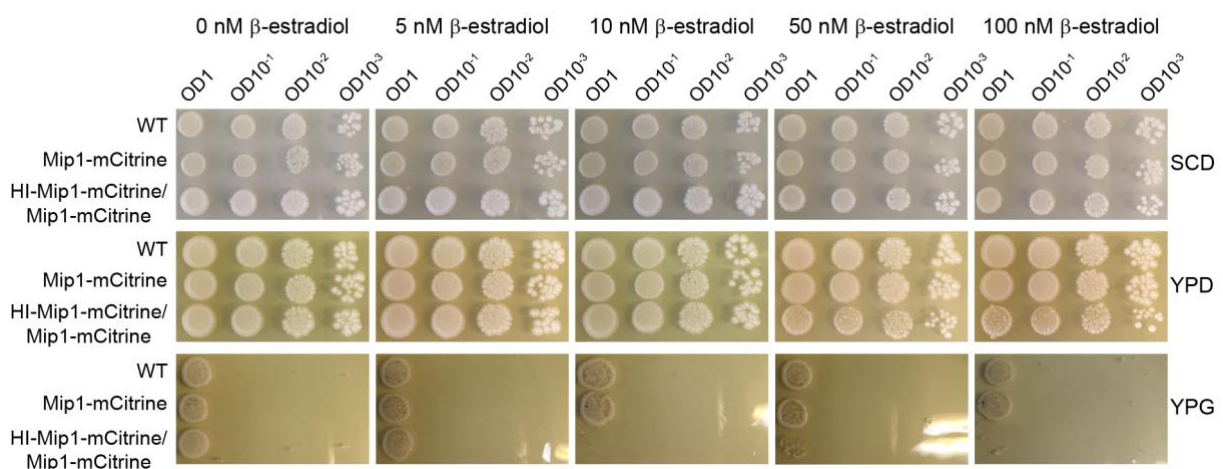


Figure 2.1: Growth test of wild-type, Mip1-mCitrine and Mip1-mCitrine+HI-Mip1-mCitrine. Growth was tested at the indicated β -estradiol concentrations on fermentable medium (SCD, YPD), and non-fermentable medium (YPG). Thus, for each strain a serial dilution was prepared and dropped onto the respective plate which were incubated at 30°C for 2 days.

Error! Use the Home tab to apply Überschrift 1 to the text that you want to appear here.

2.9.4. Cultivation of *E. coli*

E. coli was cultivated in LB medium with 100 µg/mL ampicillin at 37°C in a shaking incubator at 250 rpm.

2.9.5. Transformation of *E. coli* and plasmid isolation

Competent *E. coli* cells were prepared as described earlier (Inoue et al. 1990). For transformation, competent cells were thawed on ice. Afterwards, the plasmid DNA was added in a volume ratio of 1:20 and the mixture was incubated for 30 min on ice. Then, the cells were heat-shocked for 90 sec, transferred on ice for 2 min and 800 µL SOC medium was added. After the cells were incubated in a shaking incubator at 37 C for 45 min, 100 µL of the cell suspension were plated on LB plates containing 100 µg/mL ampicillin and incubated at 37°C. After around 16 h colonies could be picked.

Prior plasmid isolation *E. coli* cells were cultivated as described, with the respective antibiotic. For plasmid isolation the NucleoSpin Plasmid Kit was used and instructions for isolation of high-copy DNA from *E. coli* was followed.

2.9.6. Transformation of *S. cerevisiae*

Cells were inoculated in YPD, grown to log phase, pelletized and washed with ddH₂O. Next, the cells were washed with 800 µL 0.1 M TE/Lithium acetate, solved in 400 µL 0.1 M TE/Lithium acetate and stored on ice. 50 µL of the cell suspension were mixed with 1 µg of DNA (linearized plasmid or PCR product), 25 µL of a 2 mg/mL salmon sperm carrier DNA solution, 240 µL of 50 % PEG and 32 µL of a 1M TE/Lithium acetate solution. The mixture was vortexed, incubated at 30°C for 30 min during continuous rotation and afterwards heat-shocked for 20 min at 42°C. Cells were spun down at 3,500 x g, washed with ddH₂O and plated on selective medium plates. After 2 to 4 days, single colonies became visible and were streaked on selective plates. For this purpose, either SCD dropout plates or antibiotic containing plates (0.1 mg/mL) were used.

Error! Use the Home tab to apply Überschrift 1 to the text that you want to appear here.

2.10. Cloning, DNA purification and DNA analysis

2.10.1. Polymerase chain reaction (PCR) and purification

For amplification of specific DNA fragments, polymerase chain reactions with sequence specific oligonucleotides were performed. Denaturation of the DNA double strands was conducted at 95°C, followed by the annealing of the primers, whereby the annealing temperature depended on the melting temperature of the primers. For high annealing temperatures annealing and elongation were fused to one single step. Elongation was performed at 72°C and either the Phusion-polymerase or, for GC-rich sequences, the Q5 polymerase was used. Elongation time was selected according to the product size. Finally, after ending all cycles, the reaction was stored at 4°C.

Phusion-polymerase reaction		3-step PCR program			
1x	5 x HF Phusion buffer	95 °C	3 min	Initial denaturation	} 30 cycles
0.2 mM	dNTPs	95 °C	30 s	Denaturation	
1 µM	Forward primer	x	30 s	Annealing	
1 µM	Reverse primer	72 °C	1 min/kb	Elongation	
50-100 ng	Template DNA	72 °C	10 min	Final extension	
1.25 U	Phusion-polymerase				

PCR purification was performed with the NucleoSpin Gel and PCR Clean-up Kit.

2.10.2. Agarose gel electrophoresis

Agarose gel electrophoresis was performed to analyze PCR products for their size. For product sizes between 250 bp – 5000 bp, 1% (w/v) agarose in 1 x TAE was used. For smaller fragments 1.5% (w/v) agarose gels, and for larger fragments 0.8% (w/v) agarose gels were used. Gels were heated until completely solved, supplemented with 1 x Sybr Safe DNA Gel stain and cast in trays with combs. The solidified gel was placed into the electrophoresis tank and the PCR samples were mixed with 6 x loading dye and loaded onto the gel. Product size was controlled by loading a DNA marker. The gel was run at 100 V for 30 min. Using UV-light (U:Genius3 Transilluminator), the separated DNA fragments were visualized.

Error! Use the Home tab to apply Überschrift 1 to the text that you want to appear here.

2.10.3. Digestion with restriction enzymes

For modification of plasmid sequences, enzymatic digestion was used to cut the plasmid at a chosen restriction site. If a DNA sequence was inserted into the plasmid DNA, the same restriction sites were added to both ends of the DNA sequence with the help of specific primers by PCR. Both, plasmid DNA and DNA sequence were digested with the same enzymes. For this purpose, the enzyme specific buffer, enzyme and plasmid or DNA sequence were mixed and incubated for 3h at the optimal temperature of enzymatic activity. To impede digested ends from re-ligation, calf intestinal alkaline phosphatase (CIP) was added and incubated for 1 h to dephosphorylate 5' and 3' DNA phosphomonoesters. Then, the fragments were purified with the NucleoSpin PCR purification kit and either immediately used for ligation or stored at -20°C. If an integrative plasmid DNA was used for yeast transformation, plasmid DNA had to be linearized before by enzymatic digestion.

20 µL restriction digest reaction

1 x	enzyme specific buffer
1 U	enzyme
1000 ng	DNA/Plasmid

2.10.4. Ligation of DNA fragments

To create new plasmids, plasmid DNA and insert DNA needed to be ligated. Therefore, plasmid DNA and insert DNA were mixed in relation to their size, usually in a ratio of 1:2. T4 Ligase Buffer and T4 ligase were added and the reaction mix was incubated at 16°C overnight. Subsequently, 2 µL of ligation mixture were used for E. coli transformation.

20 µL ligation reaction

2 µL	T4 ligation buffer
0.3 µL	T4 ligase
100 ng	Plasmid
200 ng	Insert

2.10.5. Sequencing

New plasmids or control PCRs of endogenously modified sequences were sent for sequencing to verify correct position as well as correctness of the new sequences. Therefore, 50-100 ng/µL of plasmid DNA or 1-10 ng/µL purified PCR product (depending on the product length) in a volume of 20 µL were sent with specific primers (20 µL of a 10 nM dilution) to Eurofins Genomics Germany GmbH (Ebersberg).

Error! Use the Home tab to apply Überschrift 1 to the text that you want to appear here.

2.11. Molecular biological methods with yeast

2.11.1. Gene deletion in yeast

To disrupt the gene of interest, a PCR fragment containing a marker cassette and overlaps flanking the coding regions of the gene of interest was constructed by PCR. Primers were used, each consisting of ~60 base pairs before the start codon and ~60 base pairs after the stop codon, and containing about 20 base pairs of the forward or reverse sequence of the marker. As knock-out markers, the *C. glabrata TRP1* gene, *K. lactis URA3*, *C. glabrata LEU2*, and/or clonNAT (Table 2.8) were used. After amplification, the construct was purified and used for yeast transformation. Integration into the corresponding gene loci was achieved via homologous recombination.

To generate hemizygous strains, a diploid wild-type or *Whi5*-inducible strain was transformed with one of the given marker genes. To verify that only one copy of the gene of interest was deleted, the DNA of the clones was extracted and tested with specific primers by PCR for amplification of the knock out sequence and the gene of interest. Before performing experiments, final strains were verified by sequencing (see 2.10.5).

2.11.2. Generation of mtDNA microscopy strains

For detection of mtDNA and the mitochondrial network (haploid, diploid, ρ^0) microscopy strains were generated from parental strains with LacO arrays in the mtDNA (yCO380, yCO381) (Osman et al. 2015). To get a *Whi5*-inducible strain, the endogenous *WHI5* in yCO380 was first deleted, followed by endogenous integration of a plasmid containing the β -estradiol transcription factor (FRP880) (Ottoz et al. 2014), obtaining ASY11-2B. Subsequently, the plasmid ASE001-5 carrying the LacI protein tagged with two copies of mNeon and mKate2 with a Su9 targeting sequence was transformed into the HO-locus, resulting in the haploid microscopy strain ASY13-1. The diploid strain (ASY15-1) was generated by transforming ASY001-5 in yCO381 and crossing the resulting strain with ASY11-2B.

2.11.3. Integration of additional gene copies

For integration of additional gene copies of *MIP1* and *ABF2*, both genes were cloned into a vector backbone consisting of an ampicillin resistance cassette and a yeast marker gene. The genes to be inserted were amplified from the yeast genome with enzymatic cleavage sites, then digested as described in section 2.10.3 and cloned into the vector backbone. Promoter sequences of *ABF2* and *MIP1* were chosen to start 1000 bp upstream of the coding sequence.

Error! Use the Home tab to apply Überschrift 1 to the text that you want to appear here.

The *ABF2* terminator sequence ended 287 bp after coding *ABF2* and the *MIP1* terminator sequence ended 271 after coding *MIP1*. Cloning resulted in ASE002-2 (*MIP1*) and ASE003-1 (*ABF2*).

Prior to yeast transformation, the final plasmids were cut by enzymatic digestion within the yeast marker gene and then integrated in the corresponding marker locus via homologous recombination.

2.11.4. Insertion of chromosomal C-terminal protein tags and modification of terminator sequences

Insertions of chromosomal C-terminal protein tags were also performed via homologous recombination. The respective tag was amplified together with a selection cassette and 60 bp overlaps of the target locus by PCR and then transformed into the target locus.

For terminator experiments, the long *ADH1* terminator sequence consisted of 20 bp (GGCGCGCCACTTCTAAATAA) which were added upstream of the 188 bp after coding *ADH1*. The 188 bp after coding *ADH1* were defined as the short *ADH1* terminator sequence.

2.11.5. Modification of promoter sequences

Sequences for histone promoters were directly integrated by amplifying the promoter sequence with around 60 bp overhangs of the target locus. This was performed as described in section 2.11.1. The *HTB1* promoter consisted of 817 bp and the *HTB2* promoter consisted of 699 bp upstream of the coding histone sequence, respectively.

The β -estradiol promoter and the *MIP1*-mCitrine were first cloned together into a vector backbone and then transformed into the corresponding marker locus. To retain only the β -estradiol-expressed Mip1-mCitrine in the strain, the endogenous *MIP1* was deleted from the genome.

2.11.6. Genomic DNA extraction and RNase A digestion

If DNA was required for DNA analysis by PCR, cells were picked directly from the plate and dissolved in 50 μ L of double-distilled water.

For quantitative PCR, the DNA was extracted from cells which were cultured in 50 mL of the respective medium with the addition of the corresponding β -estradiol concentrations (see 2.9). First, cell volume distributions and optical density were measured, and subsequently cells were

Error! Use the Home tab to apply Überschrift 1 to the text that you want to appear here.

harvested at 3,220 x g and washed with 1 mL of double-distilled water. To isolate complete genomic DNA (gDNA), a phenol-chloroform-isoamyl alcohol (PCI) extraction was used. For this, the pellets were first dissolved in 200 µL DNA extraction buffer (pH 8.0) and 200 µL PCI. Using approximately 250 µg of glass beads, the cells were mechanically disrupted by vortexing at 3000 oscillations using a Mini-BeadBeater 24 and then centrifuged at 17,000 x g for 5 min. The aqueous phase was then transferred to a new reaction vessel and 500 µL of 100% EtOH were added to precipitate the gDNA for 2 min at room temperature. The mixture was then centrifuged again for 5 min at 17,000 x g and the supernatant was discarded. The gDNA pellet was washed with 70% EtOH, centrifuged at 17,000 x g for 2 min, and the supernatant was again discarded. The pellet was dried at 40°C for 5 min and dissolved in 50-100 µL of nuclease-free water, depending on the pellet size.

DNA used for PCR amplification was used directly after this step. DNA for quantitative PCR was subjected to RNase A digestion to remove RNA residues. Therefore, the solubilized pellet was treated with 1 mg/mL RNase A (DNase-free) and incubated at 37°C for 30 min. To inactivate RNase A, DNA extraction buffer and PCI were added and the extraction steps were repeated. However, for this purpose the addition of glass beads and mechanical disruption were omitted. Instead, a vortexer was used.

To determine the DNA concentrations and purity, the extinction at 260 nm and 280 nm was determined using a spectrophotometer (NanoDrop OneC). The ratio of both extinctions should be 1.8 for pure DNA. For qPCR, 1 ng of DNA was used.

2.11.7. Quantitative DNA PCR and analysis

The number of mtDNA was determined by DNA-qPCR. This was achieved by the fluorophore SYBR® Green binding exclusively to double stranded DNA. The fluorescence intensity of DNA-bound fluorophore increases compared to unbound fluorophore. Thus, with every amplification cycle, fluorescence increases in direct proportion to the amount of amplified sequence, allowing quantitative analysis of mtDNA levels.

The master mix was prepared with the SsoAdvanced Universal SYBR® Green Supermix and specific primer pairs with a final concentration of 0.5 µM for each primer. For nDNA genes *ACT1*, *MIP1* and *MRX6* and for mtDNA genes *COX2* and *COX3* were used. These genes were chosen arbitrarily and several genes were used to make the data more robust. 8 µL of the master mix and 2 µL of 0.5 ng/µL DNA were pipetted on a Light Cycler 480 Multiwell Plate 96. Then, qPCR was performed on a Light Cycler® 96.

Error! Use the Home tab to apply Überschrift 1 to the text that you want to appear here.

Settings	Temperature	Time	Cycles
Pol. activation	95°C	600 sec	1
Denaturation	95°C	10 sec	} 40
Annealing	60°C	30 sec	
Melting	95°C	60 sec	1

Each sample was measured in technical triplicates. For technical replicates the same sample was measured three times. In contrast, for biological replicates different samples were generated on at least three different days. Thus, for qPCR at least three biological replicates were measured each with three technical replicates. For analysis, mean Cq-values of the technical replicates were used. If the standard deviation within the technical replicas was higher than 0.5, the technical replica in question was excluded from the analysis.

Differences in primer efficiencies were corrected by a qPCR calibration standard. Therefore, all amplified sequences were fused to one PCR product and a qPCR dilution series was performed to obtain standard curves for all used primer pairs (Fig. 2.2). By using a linear fit through the standard curves, it was possible to calculate the concentration for each gene. Next, the calculated nDNA concentrations (*ACT1*, *MIP1*, *MRX6*) and mtDNA (*COX2*, *COX3*) concentrations were pooled by calculating the mean, respectively and mtDNA concentrations were normalized on nDNA, thereby getting the relative mtDNA copy number per nDNA. This analysis was performed for each biological replicate, respectively and the average of the biological replicates was plotted. For hemizygous, multicopy and mCitrine experiments, *MIP1* was excluded from analysis.

Error! Use the Home tab to apply Überschrift 1 to the text that you want to appear here.

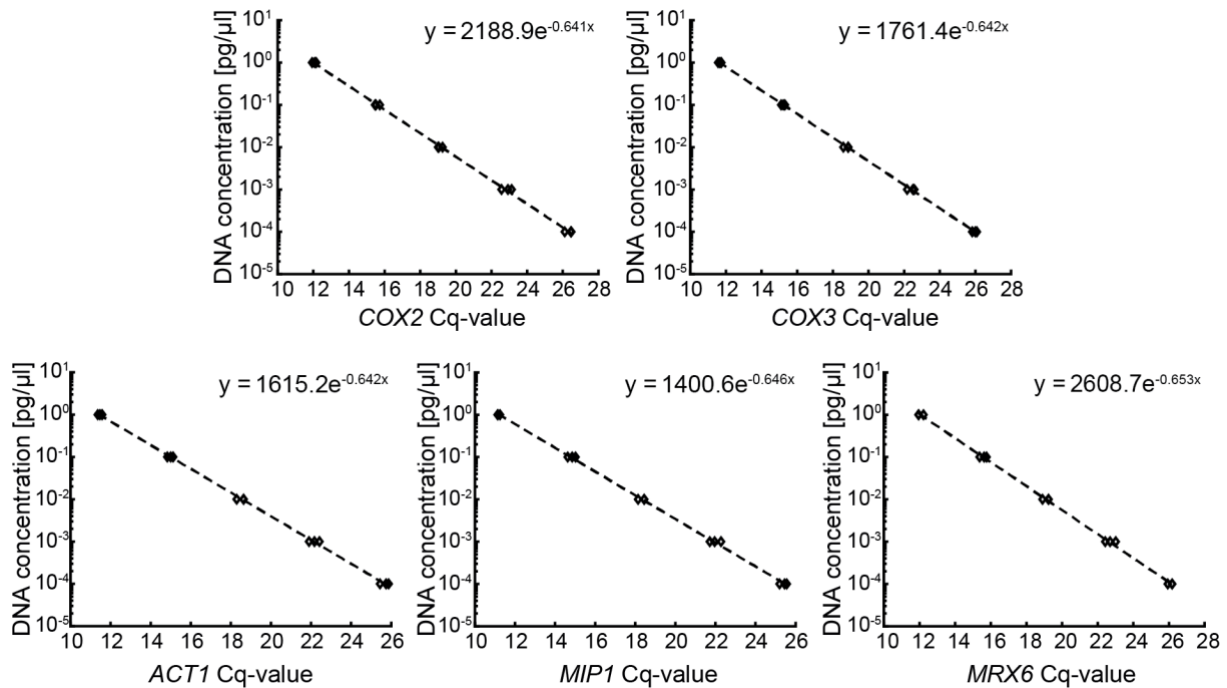


Figure 2.2: qPCR calibration standard curves. Standard curves were measured for COX2, COX3, ACT1, MIP1 and MRX6. The resulting equations of the linear fit were used to calculate mtDNA concentrations from Cq-values.

By performing bud counts, the nDNA per cell was determined for all cell populations, assuming one copy for haploid unbudded cells and two copies of nDNA for budded haploid cells. For diploids twice the nDNA copies were assumed. Per biological replicate 200 cells were counted.

$$\frac{nDNA(haploids)}{cell} = \frac{(\% buds * 2) + (\% no-buds * 1)}{100} \quad \text{or} \quad \frac{nDNA(diploids)}{cell} = \frac{(\% buds * 4) + (\% no-buds * 2)}{100}$$

The average nDNA amount per cell of three biological replicates was then multiplied with mtDNA copies resulted in the relative mtDNA copy number per cell.

2.11.8. Cell volume measurements

Cell volume measurements were performed with a Coulter counter. Therefore, 1 mL of cell culture was sonicated to separate cells. Depending on the OD₆₀₀ and Whi5-induction 50-600 μL of the sonicated culture were added to the Isoton II Diluent containing cuvette. Ideally, 20,000-40,000 cells should be counted. Due to technical limitations of the measurable range, Whi5-induced cells with the highest β-estradiol concentrations (30 nM on SCGE and 150 nM on SCD) had to be measured within two ranges.

Error! Use the Home tab to apply Überschrift 1 to the text that you want to appear here.

Table 2.15: Coulter counter settings for mean cell volume measurements. Range 1 was used for all strains and conditions. Range 2 was measured only for Whi5-inducible strains grown at 30 nM on SCGE and 150 nM on SCD.

	Volume [fL]	Gain	Current [ma]
Range 1	10 – 328	256	0.707
Range 2	328 – 1856	256	0.125

The number of cell counts of each range was used to calculate the combined average cell volume of both ranges:

$$Cell\ volume_{total} = Cell\ volume_{range1} \times \left(\frac{Cell\ number_{range1}}{Cell\ number_{total}} \right) + Cell\ volume_{range2} \times \left(\frac{Cell\ number_{range2}}{Cell\ number_{total}} \right)$$

2.11.9. Extraction of total RNA from yeast

Two different methods were used for total RNA extraction. RNA samples in Figure 3.6b (left) were taken from experiments carried out in the study by Claude et al., Fig. 2b-c (Claude et al., 2021). Here, RNA was extracted using hot, acid phenol chloroform using a modified protocol of Collart and Oliviero (Collart and Oliviero 1993).

The cells were harvested and the pellet was resuspended in RNase-free water. The lysis buffer and acid phenol were prewarmed to 65°C and 10-times the volume of resuspension was added, respectively. The batch was incubated at 65°C for 1 h and vortexed every 10-20 min. It was then placed on ice for 10 min and then centrifuged at 10,000 x g. The supernatant was removed, transferred to a new tube, and the same volume of acid phenol was added. The mixture was vortexed and centrifuged again at 10,000 x g. The supernatant was transferred to a fresh tube and this time the same volume of chloroform was added. After vortexing, centrifugation was performed at 10,000 x g and the supernatant was transferred to a new tube. Then, 3 M NaOAc was added at a ratio of 1:10 and 100 % ethanol at a ratio of 2:1. For precipitation, the extraction was incubated at -20°C. After about 24 h, the RNA was pelleted at 10,000 x g for 20 min, the supernatant discarded, and resuspended again in 400 µL RNase-free H₂O. Again, 1/10th of the reaction volume 3 M NaOAc and 2-fold reaction volume 100 % ethanol were added. RNA was precipitated for 2-4 h at -80°C, then pelleted, dissolved in 50 - 100 µL H₂O and stored at -80°C.

RNA extractions in Figures 3.6b (right), 3.6c and 3.7f-g were carried out with the YeaStar RNA kit according to the manufacturer's instructions. Afterwards, to remove DNA contamination, a DNA digestion step using DNase I was performed and the samples were stored at -80°C. To confirm that RNA was not degraded, samples from both extraction methods were always

Error! Use the Home tab to apply Überschrift 1 to the text that you want to appear here.

loaded onto a 1% agarose gel, checking ribosomal RNA bands for 25 S, 18 S, and 5.8 S subunits. Purity and RNA concentration were determined using a NanoDrop.

2.11.10. cDNA synthesis and quantitative reverse transcription PCR (RT-qPCR)

RT-qPCR was used to quantify mRNA expression levels. Prior RT-qPCR, complementary DNA (cDNA) had to be synthesized using same amounts of total RNA (1000 ng, before DNase I digestion), random primers, and following the protocol of the high-capacity cDNA reverse transcription kit (Thermo Fisher Scientific). As negative controls, samples without reverse transcriptase and samples without template RNA were treated equally. Samples were either stored at -20°C or immediately used for RT-qPCR. Therefore, the SYBR® Green master mix was prepared as depicted in the manufacturer's protocol with a specific primer pair for the RNA of interest. For *MIP1*, *ABF2*, *PIM1*, *MTF1*, *RPO41* and *MRX6*, 2 µL of a 1:10 dilution of the cDNA was used. For the highly expressed ribosomal RNA *RDN18*, 2 µL of a 1:200 dilution was used. Each sample was measured in technical triplicates of which the mean was taken for normalization to *RDN18*.

Settings	Temperature	Time	Cycles
Pol. activation	95°C	60 sec	1
Denaturation	95°C	10 sec	} 40
Annealing	60°C	30 sec	
Melting	95°C	60 sec	1

2.12. Microscopy and image analysis

2.12.1. Live-cell imaging by confocal microscopy

To get insights into the quantity of nucleoids and mitochondrial network volume during cell growth live-cell imaging was performed. Cells were cultivated as already described in 5 mL SCD or SCGE with corresponding hormone concentrations (see 2.9.1). To ensure cells stay in place during imaging, slides (µ-Slide 8 Well, ibi-Treat) were treated with 200 µL Concanavalin A (ConA, 1 mg/mL in H₂O). After incubation for 5-10 min, the slides were washed twice with H₂O and left to dry on air. The ConA treated well was covered with 200 µL of a sonicated cell suspension and the cells were allowed to settle down for about 5 min. Next, the supernatant was removed and the well was washed twice and covered with 200 µL of fresh medium.

Error! Use the Home tab to apply Überschrift 1 to the text that you want to appear here.

Living cells were imaged with a Zeiss LSM 800 microscope (software: Zen 2.3, blue edition) containing an airyscan detector and a Zeiss AxioCam 506 camera. Using the confocal mode and a 63x /1.4 Oil DIC objective, z-stacks were acquired in 0.35 μm steps over a depth of 15.05 μm . The mitochondrial network was imaged using mKate2 as fluorophore which was excited at 561 nm and detected between 610-700 nm. Visualization of nucleoids was achieved by exciting mNeon at 488 nm detecting between 410-546 nm. After imaging the fluorescence channels, the transmitted light detector (T-PMT) was used to acquire bright-field images.

2.12.2. Cell segmentation

To determine the cell volume, the imaged cells first had to be segmented. For this purpose, brightfield images were analyzed using Cellpose v0.6 (Stringer et al. 2021). The parameter 'cell diameter' was set to 50 pixels, 'flow threshold' set to 0.4, and 'cell probability threshold' set to 0. With the help of Cell-ACDC (Padovani et al. 2021), cell segmentation was manually corrected and buds were assigned to the corresponding mother cells and finally the cell volume the cell volume was computed by Cell-ACDC.

2.12.3. Nucleoid counting and network volume calculation

Quantification of nucleoids and mitochondrial network volume was performed with a Python routine written by Dr. Francesco Padovani (Kurt Schmoller Lab, Helmholtz Zentrum München). The analysis was done in 3D using images acquired as described above (see 2.12.1).

The analysis process can be divided into 7 different steps. 1) First, to reduce noise, a 3D gaussian filter with a small sigma (0.75 voxel) was applied for both the nucleoids and mitochondria signals. 2) Subsequently, instance segmentation, a combination of object and semantic segmentation, was applied to classify each pixel into mitochondria signals using automatic Li thresholding (Li and Tam 1998) (*threshold_li* function from the library *scikit-image* (van der Walt et al. 2014)). 3) The mitochondria signal was then normalized on the median of the voxel intensities. 4) By using the *peak_local_max* function from the library *scikit-image* local maxima (peaks) were detected in 3D. 5) If the intensity of these peaks was below the threshold defined by the automatic Li thresholding algorithm, peaks were excluded from the analysis. 6) In addition to that, if several peaks are found within the same resolution limited volume, only the one with the highest intensity was kept. 7) All peaks that remain after step 5 and 6 were filtered again. Mitochondria voxels from step 2 were further classified to be inside (within the resolution limited volume) or outside of the nucleoids. Then the mean of all mitochondria voxels outside of a nucleoid was used for normalization of the nucleoid signal.

Error! Use the Home tab to apply Überschrift 1 to the text that you want to appear here.

This normalized nucleoid signal was compared to the same voxels from the mitochondria signal and tested for significance by using a Welch's t-test. A p-value above 0.025 or a negative t-statistic (i.e., nucleoid signal is lower than mitochondria signal) leads to exclusion of the peaks. Step 7 was repeated until the number of peaks stayed constant. Those peaks were counted as nucleoids (true positives).

To calculate the mitochondrial network volume, all voxels classified as mitochondria signal were added up. Here it is important to note that the mitochondrial network width was not measured accurately, due to limitations in the optical resolution. For this reason, the determined mitochondrial network volume is not an absolute measure.

To validate the Python routine the mitochondrial network data were compared to MitoGraph, an already established, automated image processing method (Viana et al. 2015, 2020). MitoGraph calculates the network volume from three-dimensional images either from network length by assuming a constant diameter or from the voxel volume. The MitoGraph network volume calculated from voxels correlates in linear proportion with the network volume calculated by the Python routine (Fig. 2.3a). In comparison, the MitoGraph network volume calculated from length differs more from the volume calculated by the Python routine (Fig 2.3b). One suggestion might be that MitoGraph underestimates changes in mitochondrial diameter, in this case specifically for SCD medium (Fig. 3.5). Thus, this supports the approach to calculate mitochondrial network volume from voxels and confirms that the Python routine is well suited for the analysis of the mitochondrial network volume.

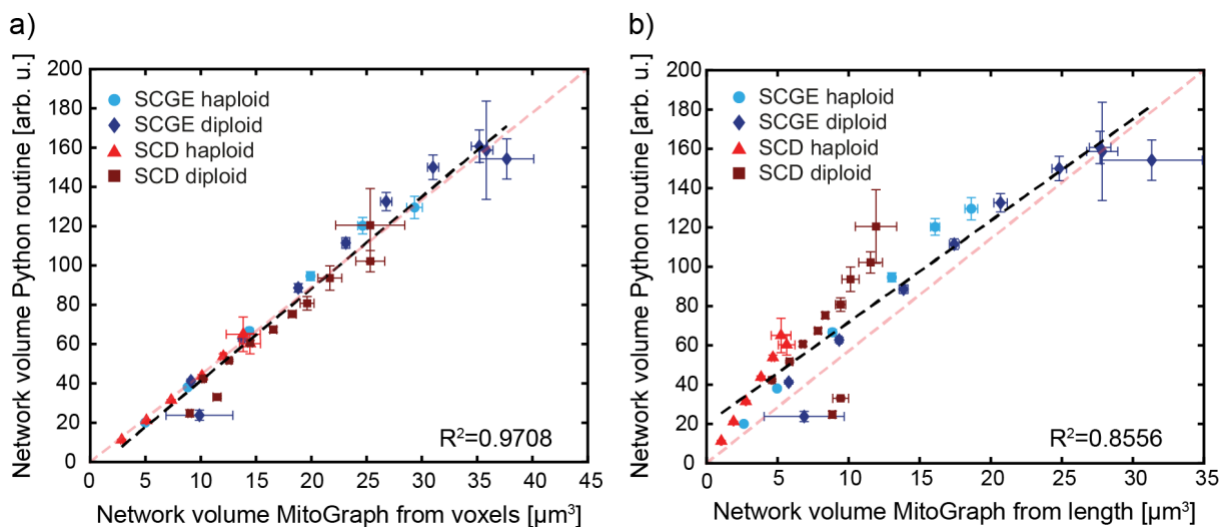


Figure 2.3: Comparison of mitochondrial network volume calculated by Python routine and MitoGraph. Data correspond to Fig. 3.3 d-e. Network volume from three biological replicates was binned in 50 fL intervals and the means of the bins were plotted against each other. Error bars indicate standard errors. Bins containing only one cell were excluded from the analysis. Dashed black line is a trendline through all data points. **a)** Network volume calculated from Python routine as a function of mitochondrial

Error! Use the Home tab to apply Überschrift 1 to the text that you want to appear here.

network volume MitoGraph from voxels. **b)** Network volume calculated from Python routine as a function of mitochondrial network volume MitoGraph from length assuming a constant diameter.

2.12.4. Mip1-mCitrine fluorescence intensity measurements

Microscopy was performed with the Zeiss LSM 800 microscope (software: Zen 2.3, blue edition) using a plan-apochromat 40×/1.3 oil immersion objective. Therefore, cell suspension was transferred to a slide and immediately imaged taking 30 z-stacks over a depth of 9.3 μm. mCitrine was excited at 508 nm with 20% intensity and emission was detected at 524 nm. In addition, phase-contrast images were acquired to allow analysis of the cell volume.

For analysis of the Mip1-mCitrine concentration a Python analysis routine written by Dr. Francesco Padovani (Schmoller lab) was used. Prior to concentration calculation, cells were segmented as described above (see 2.12.2). To calculate the mCitrine concentration per cell, first the amount per cell was determined. For this purpose, the pixel intensities of the segmented area were summed, then the mean intensity was calculated and finally, the background intensity was subtracted. Multiplication with the segmented area resulted in the amount, which was divided by the volume to obtain the concentration. The mCitrine concentration was then manually corrected for autofluorescence of the parent strain without mCitrine. This experiment was done in three biological replicates, each consisting of at least 30 cells per strain and condition.

2.12.5. Electron Microscopy

Electron microscopy was performed in collaboration with Moritz Mayer (Till Klecker Lab, University of Bayreuth). For electron microscopy wild-type and Whi5-inducible strains were cultivated as described above and both were treated with equal hormone concentrations. For cell volume quantification, samples from same cell cultures were used to take DIC images with a Zeiss Axiophot microscope equipped with a Plan-Neofluar 100×/1.30 Oil objective (Carl Zeiss Lichtmikroskopie, Göttingen, Germany) and a Leica DFC360 FX camera operated with the Leica LAS AF software version 2.2.1 (Leica Microsystems, Wetzlar, Germany). Cell segmentation was performed in collaboration with Dr. Francesco Padovani (Kurt Schmoller Lab) with Cell-ACDC (Padovani et al. 2021).

For fixation of yeast cells with glutaraldehyde and potassium permanganate the protocol of Perkins and McCaffery was followed (Perkins and McCaffery 2007). The following modifications were made: Cells were fixed with 3% glutaraldehyde, 0.1 M cacodylic acid, 1 mM

Error! Use the Home tab to apply Überschrift 1 to the text that you want to appear here.

CaCl₂, pH 7.2, washed with 0.1 M cacodylic acid, 1 mM CaCl₂, pH 7.2, and then treated with potassium permanganate. Subsequently, the fixed cells were embedded in agarose and fibrillated with 2% uranyl acetate overnight at room temperature.

The next steps were performed with minor variations according to Unger et al (Unger et al. 2017). The chemically fixed cells were dehydrated with ethanol and propylene oxide at 4°C. Epon infiltration was then performed at room temperature. Contrast enhancement of ultrathin sections was conducted with 2% uranyl acetate for 15 minutes and lead citrate for 3 minutes.

After completion of the steps above, electron micrographs were taken with a JEOL JEM-1400 Plus transmission electron microscope at 80 kV equipped with a JEOL Ruby CCD camera with 3296x2472 pixels using TEM Center software, either ver.1.7.12.1984 or ver.1.7.19.2439 (JEOL, Tokyo, Japan). To quantify mitochondrial diameter, widest point of the shorter edge was measured using Fiji (Schindelin et al. 2012). The average diameter was obtained by measuring 100 mitochondria in three biological replicates, respectively.

2.13. Flow Cytometry

Flow cytometry was performed by Daniela Bureik (Kurt Schmoller Lab, Helmholtz Zentrum München) and analysis was done by Dr. Kurt Schmoller. Strains used for flow cytometry contained either Mip1 or Abf2 endogenously tagged with the fluorophore mCitrine. Cells were grown for 16-20 h on SCGE, then diluted and divided into 3 technical replicates. The cells were sonicated for 10 sec and kept on ice. Flow cytometry measurements were performed with a CytoFlex S Flow Cytometer (Beckman Coulter).

To evaluate whether SSC (side scatter) or FSC (forward scatter) is the better measure for cell volume, both measurements were compared with each other and with Coulter counter measurements (Fig. 2.4 a-c). For this purpose, SCGE grown cell cultures were Whi5-induced and SSC (Fig. 2.4a), FSC (Fig. 2.4b) and Coulter counter cell volume (Fig. 2.4a-b) were measured in technical duplicates. It was found, that both SSC measurements correlate well with the Coulter counter measurements. In addition, to test if SSC-A is proportional to cell volume, independent of the cell cycle stage the percentiles of the scatter signal were compared with the percentiles of Coulter counter measurements for a wild-type strain. The data nicely show that SSC-A is proportional to cell volume and thus for the experiments in this study SSC-A data were used.

Cells were analyzed at a slow flow rate (10 µL/min) and total fluorescence intensity using the FITC channel (excitation at 488 nm and detection with a 525/40 nm filter) and SSC-A (side-scatter area) were collected from 50.000 events per sample. Cell debris, particles and doublets

Error! Use the Home tab to apply Überschrift 1 to the text that you want to appear here.

were excluded from the analysis, by using a standard gating strategy (Fig. 2.4d). Measurements were corrected for autofluorescence by measuring the parent strain without mCitrine tag. The technical replicates from one day were pooled and binned using SSC-A. Afterwards, autofluorescence was corrected by subtracting the mean signal of the control strain from the mCitrine strain at same SSC-A bins. The complete experiment including analysis was repeated a second time and the data of both biological replicates were averaged. To estimate the experimental error, for each bin the maximum (minimum) of the two signals plus (minus) the standard error associated with the measurement of the fluorescent strain was used.

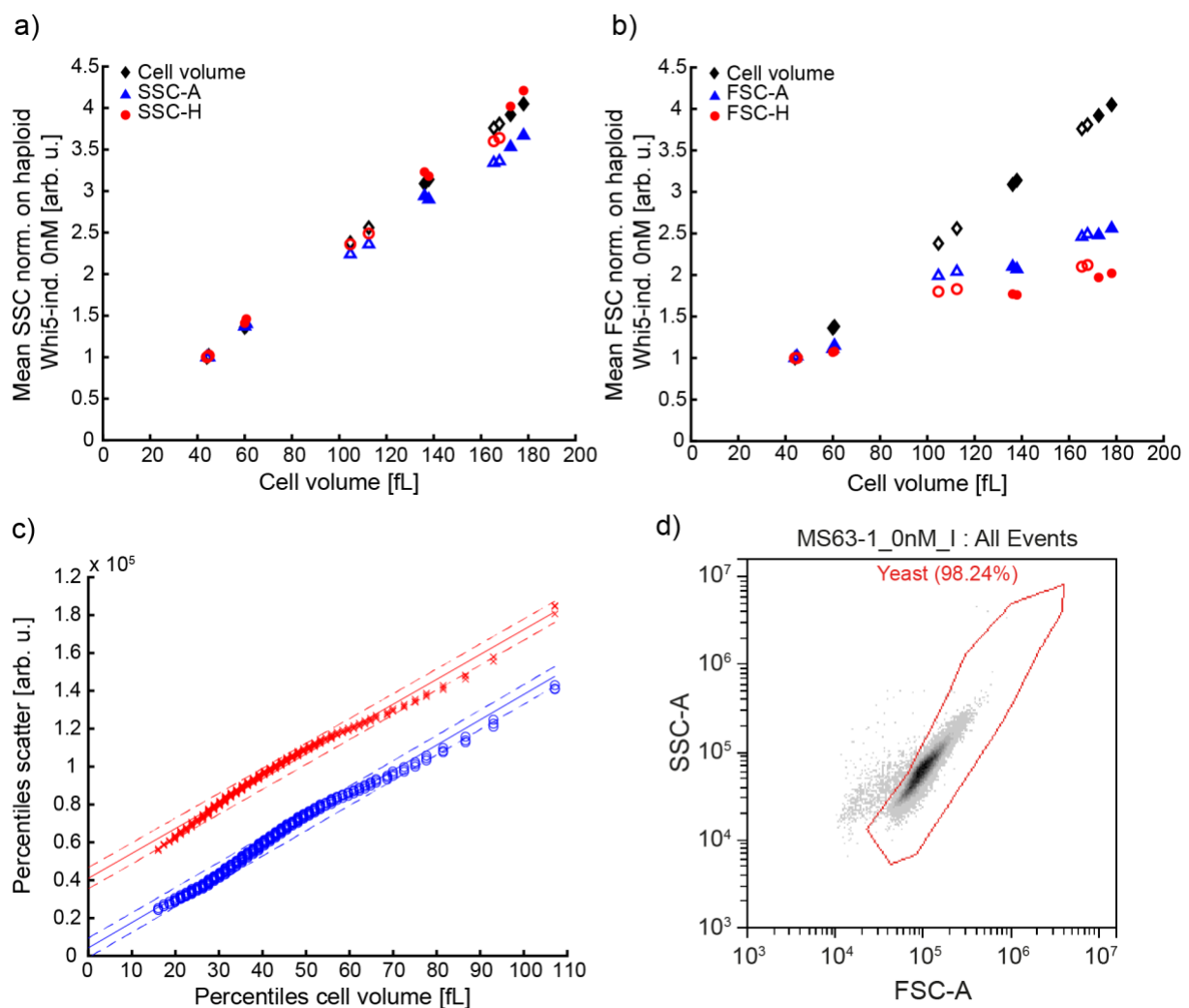


Figure 2.4: Comparison of flow cytometry side scatter and forward scatter measurements with Coulter counter measurements. a-b) Cell populations of haploid (open symbols) and diploid cells (filled symbols) were grown on SCGE with β -estradiol (haploids 0 nM, 10 nM, 30 nM; diploids 0 nM, 25 nM, 50 nM). Samples were measured using a CytoFlex S flow cytometer in technical duplicates, with SSC (a) and FSC (b) recorded. SSC (a) and FSC (b) are compared with mean cell volumes determined by Coulter counter measurements. Flow cytometry data and coulter counter measurements were each normalized to the Whi5-inducible strain grown with 0 nM β -estradiol. Blue triangles show area (SSC-A, FSC-A) measurements, red circles show height (SSC-H, FSC-H) measurements and black diamonds

Error! Use the Home tab to apply Überschrift 1 to the text that you want to appear here.

represent Coulter counter measurements. Both side scatter measurements correlate well with the Coulter counter cell volume measurements. **c)** SSC-A should be proportional to cell volume, regardless of cell cycle stage. To test this, the percentiles of the scatter signal (SSC-A: blue circles, FSC-A: red crosses) were compared with the percentiles of Coulter counter measurements for a wild-type strain. Data from three biological replicates are shown. Solid lines show linear fits to the pooled data. Dashed lines represent 95% confidence prediction intervals. **d)** Example of gating strategy.

2.14. Statistical analysis

Before calculating significances, data were tested for gaussian distribution by performing a Shapiro-Wilk test. As all data were normally distributed, a two-sided two-tailed t-test was performed to calculate significances (* $p < 0.05$, ** $p < 0.01$, *** $p < 0.001$).

3. Results

3.1. mtDNA copy number increases with cell volume modulated by nutrients

While it is quite well investigated how nDNA copy number is regulated with cell growth, little is known about mtDNA copy number regulation. nDNA replication is strictly coupled to the cell cycle and occurring only during S phase, ensuring only one doubling of nDNA content per cell cycle. In contrast, mtDNA replication takes place rather independently of the cell cycle, leading to the question: What is the mechanism which promotes constant mtDNA copy numbers? Recent studies found that mitochondrial network increases in linear proportion with cell size (Rafelski et al. 2012) and that the number of nucleoids, which contains several mtDNA genomes and mtDNA binding proteins, increases with mitochondrial network volume (Osman et al. 2015). These results indicate that cell size is a driving parameter regulating mitochondrial biogenesis. To shed light on this hypothesis, the first aim of this study is to get an insight into the influence of cell size on mtDNA copy number.

To get cell cultures of different cell sizes, the expression of the cell cycle inhibitor Whi5 was manipulated (Kukhtevich et al. 2020, Claude et al. 2021). As previously reported, Whi5 represses SBF-transcription, however, with increasing cell volume during G1, Whi5 concentration in the cell is diluted allowing SBF-transcription and transition from G1 to S phase (Schmoller et al. 2015). By expressing Whi5 under the β -estradiol inducible promoter system Whi5 can be overexpressed depending on the hormone concentration added to the cell culture (Ottoz et al. 2014). In steady state this results in increased volume and a slightly prolonged G1 phase, most likely because cells have to increase their cell volume to dilute Whi5 and continue cell cycle progression (Fig 3.1a). Moreover, to achieve a natural variation in cell size both, haploid and diploid strains were tested in combination with the Whi5-inducible system. As a result, cell sizes can be reproducibly regulated between 50 fL and 200 fL.

To examine how mtDNA copy number depends on cell size, cells were grown in the absence or presence of β -estradiol. For each culture, cell volume measurements were performed using a Coulter counter. Additionally, as a proxy for cell cycle phases bud fractions were determined to estimate the number of cells in G1 and S phase. Then cellular DNA of asynchronous, size-induced cell populations was extracted and qPCRs on mtDNA genes normalized on nDNA were performed. The nDNA per cell was calculated from bud counts, which was multiplied with mtDNA per nDNA to get the mtDNA copy number per cell (see 2.11.7). First, cells were grown on non-fermentable medium (SCGE), which is a condition where subunits of the electron

Error! Use the Home tab to apply Überschrift 1 to the text that you want to appear here.

transport chain (ETC) encoded by the mtDNA are essential for metabolic activity and thus for cell growth.

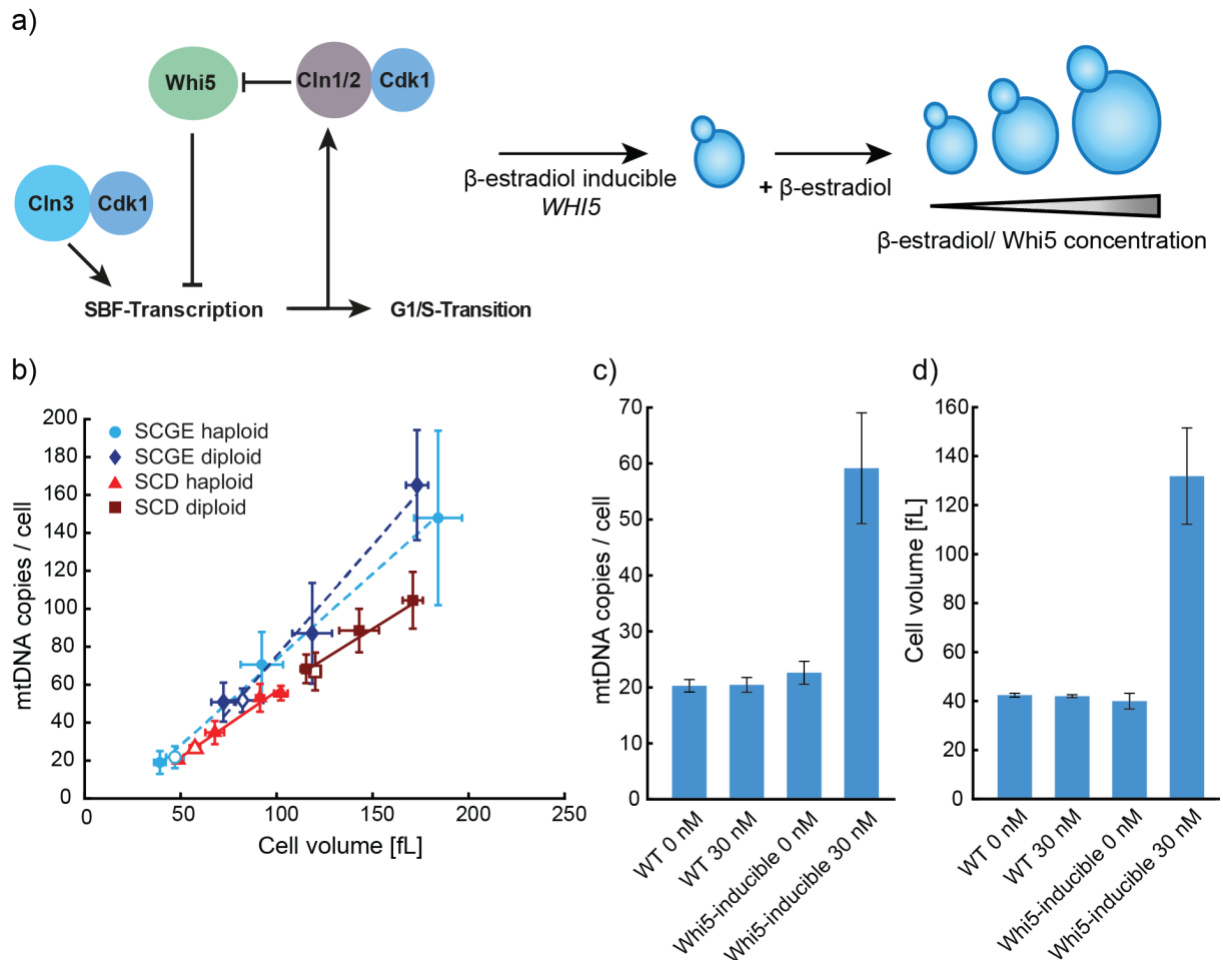


Figure 3.1: mtDNA copy number increases with cell volume. **a)** The cell volume was increased by manipulating the concentration of the SBF transcription inhibitor *Whi5*. Therefore, *Whi5* was expressed under the β -estradiol inducible promoter. By addition of increasing hormone concentrations, the *Whi5* concentration was increased leading to a prolonged G1 phase and bigger cell volumes. **b)** mtDNA copy number per cell as a function of cell volume. Haploid and diploid wild-type (open symbols) and *Whi5*-inducible (filled symbols) asynchronous cell populations were grown with different β -estradiol concentrations on fermentable (SCD, solid line) and non-fermentable medium (SCGE, dashed line). Total DNA was extracted and qPCR was performed on mtDNA genes (*COX2*, *COX3*) and nDNA genes (*ACT1*, *MIP1*, *MRX6*). Concentrations were calculated for mtDNA and nDNA allowing the normalization of mtDNA on nDNA. Using the budding index, the nDNA copies per cell were estimated **c)** β -estradiol alone does not affect mtDNA copy number. To verify that the increase of mtDNA copy number does not depend on β -estradiol concentrations, haploid wild-type and *Whi5*-inducible strains were grown with 0 nM and 30 nM β -estradiol. **d)** Mean cell volumes were determined from same cultures as in c). All cell volume measurements were performed using a Coulter counter. Error bars display standard deviation of at least three biological replicates.

For both, haploid and diploid cells, mtDNA copies increase linearly with cell volume (Fig. 3.1b). To test conditions where the ETC and thus mtDNA is not essential for cell growth, fermentable medium (SCD) was used. As shown for the non-fermentable medium, mtDNA increases in

Error! Use the Home tab to apply Überschrift 1 to the text that you want to appear here.

proportion to cell volume, however, at same cell volumes cells grown in SCD have ~10-30% less mtDNA copies compared to cells grown on SCGE (Fig. 3.1b).

To verify, that the effect is not caused by β -estradiol itself, non-inducible wild-type cells were grown on β -estradiol as well (Fig. 3.1c-d). In contrast to the Whi5-inducible strain, neither for the mtDNA copy number (Fig. 3.1c) nor for the cell volume (Fig. 3.1d) any significant effect of β -estradiol on wild-type cells was observed, confirming that the mtDNA increase is specific to the Whi5-induced cell volume increase and not directly dependent on β -estradiol.

3.2. mtDNA copy number increases with cell volume during G1 arrest

To ensure that the mtDNA increase is not directly caused by higher Whi5 concentrations a G1 arrest was used as an alternative approach to manipulate cell size. For this purpose, a haploid *CLN1/2/3* deletion strain with a β -estradiol inducible *CLN1* was used (Ewald et al. 2016). These cyclin proteins are cell-cycle regulators, interacting with Cdk1 and thereby promoting the G1/S transition (*Start*). As only one of the three cyclins is necessary for complex formation with Cdk1 and inducing G1/S transition (*Start*) (Richardson et al. 1989), expression of *Cln1* from a β -estradiol promoter and addition of the hormone enables cell cycle progression. Thus, removal of the hormone resulted in G1-arrested cells, increasing their cell volume over time (Fig. 3.2a). Experiments were performed in collaboration with Alissa Finster (Kurt Schmoller Lab, Helmholtz Zentrum München). Samples were harvested hourly and for each culture cell size was measured. Additionally, bud counts were performed to ensure G1 arrest and to determine cell cycle fractions. Subsequently, DNA extractions followed by DNA-qPCR were conducted. Again, experiments were performed for cells grown on SCD and SCGE.

Cells grown on SCD reach the maximum of G1-arrested cells around 1 h earlier than cells grown on SCGE (Fig. 3.2c). However, SCD cells increase their cell volume faster and stronger compared to cells grown on SCGE (Fig. 3.2d). This is most likely caused by the fermentation process and the faster conversion of energy leading to increased growth rates on SCD. As observed for the Whi5-inducible approach, mtDNA copy number increases linearly with cell size for G1-arrested cells. Again, for cells grown on fermentable medium mtDNA copies per cell are shifted down by ~10-30% compared to cells grown on non-fermentable medium. Taken together, the data suggest that mtDNA copy number is closely linked to cell volume, even in conditions where mtDNA is not essential. Moreover, mtDNA copy number increases during G1 phase suggesting that cell cycle progression is no requirement for mtDNA replication and copy number maintenance. This observation is consistent with literature, where mtDNA replication was shown to continue during G1 arrest. However, there, the G1 arrest was induced by using α -factor (Petes and Fangman 1973). The alpha factor arrest is a very special state in the cell

Error! Use the Home tab to apply Überschrift 1 to the text that you want to appear here.

cycle, where haploid yeast cells prepare for mating, which might impact metabolic processes. The *CLN1/2/3* mutant is therefore a cleaner method to demonstrate the influence of a G1 arrest on mtDNA.

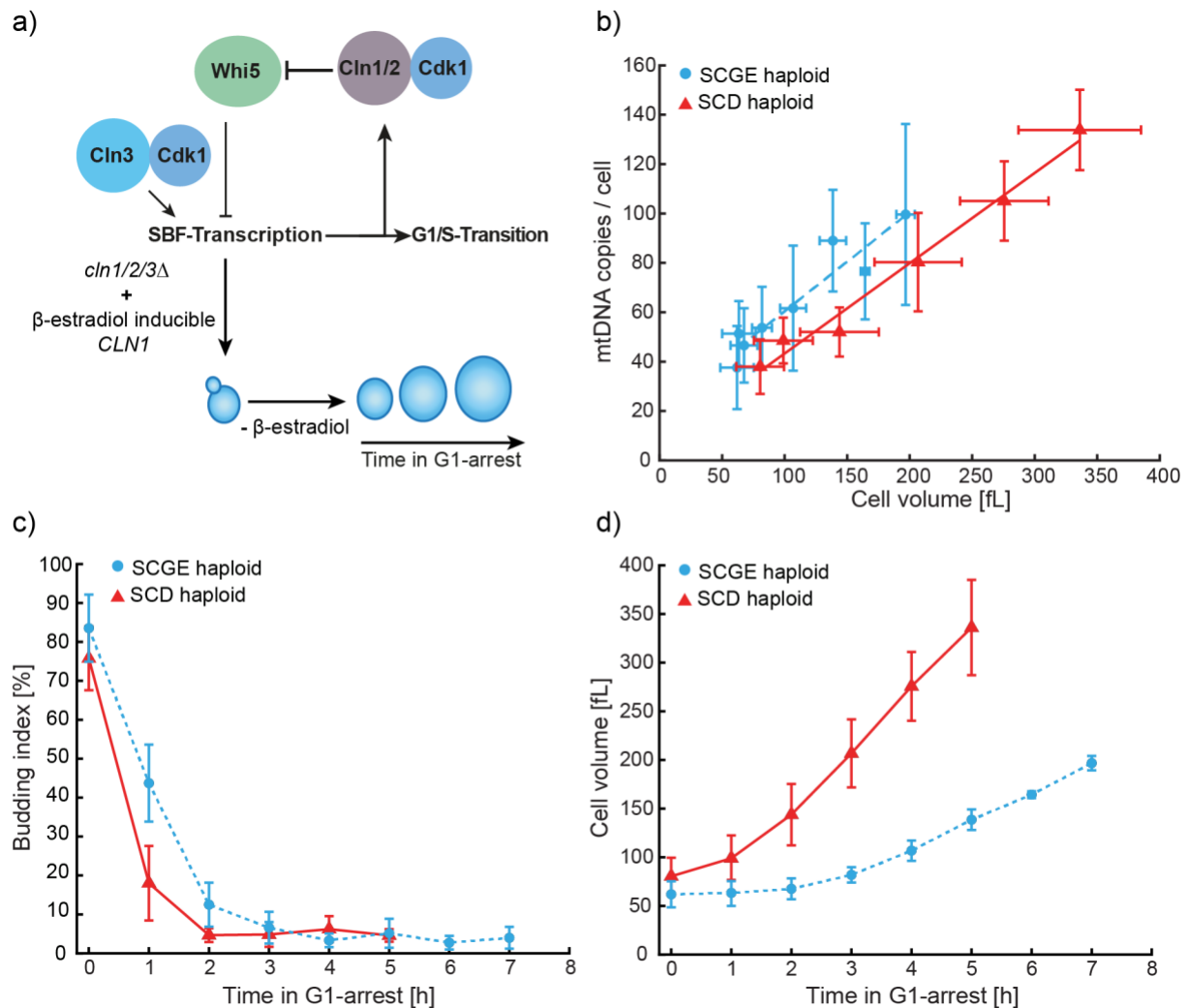


Figure 3.2: mtDNA copy number increases with cell volume during G1 arrest. **a)** To arrest cells in G1, a *cln1/2/3* deletion mutant with *CLN1* expressed under a β -estradiol promoter was used (Ewald et al. 2016). Cells can undergo cell cycle progression only in the presence of β -estradiol and removal of the hormone leads to G1-arrested cells. **b)** mtDNA copy number per cell as a function of cell volume. The haploid *Cln1*-inducible strain was grown on SCD and SCGE medium to log-phase and then arrested in G1. Samples were harvested every hour for 5 h on SCD or 7 h on SCGE starting directly after β -estradiol removal. qPCR was performed and the relative concentration of mtDNA to nDNA was calculated. Using the budding index nDNA copy number per cell was estimated and mtDNA per cell was calculated. Trendlines are fitted through the data. **c)** Cell volume as a function of time in G1 arrest. All mean cell volumes were obtained using a Coulter counter. **d)** Budding index during G1 arrest. Error bars display standard deviation of at least three biological replicates.

Error! Use the Home tab to apply Überschrift 1 to the text that you want to appear here.

3.3. Number of nucleoids increases with cell volume and is modulated by nutrients

mtDNA copies are organized in nucleoprotein complexes, also called nucleoids, which are distributed throughout the mitochondrial network and consist of multiple mtDNA copies and mtDNA binding proteins. The observed increase of mtDNA copies per cell could either apply on the nucleoid level or the mtDNA copy number per nucleoid increases in bigger cell volumes. To determine whether one of the hypothesis holds true, the number of nucleoids was investigated with increasing cell size by confocal live-cell imaging.

For this purpose, a strain in which LacO repeats were integrated into the mtDNA was used (Osman et al. 2015). These LacO repeats can be bound by a LacI repressor tagged with a fluorophore, which allows visualization of nucleoids by live-cell confocal imaging. The system used in this study was improved by replacing the fluorophore GFP with two copies of mNeon. In addition, cells were imaged in medium instead of PBS, since PBS induces fission of the mitochondrial network in yeast after only 30 minutes (Hori et al. 2011). The mitochondrial network volume was investigated by targeting mKate2 to the mitochondrial matrix (Fig. 3.3a-b). In combination with the Whi5-inducible system the number of nucleoids and the mitochondrial network volume could be quantified in a broader range of cell sizes. Image analysis was performed in collaboration with Dr. Francesco Padovani (Kurt Schmoller Lab, Helmholtz Zentrum München). The cell volume was determined by segmenting cells on bright-field images with Cell-ACDC (Padovani et al. 2021). Quantification of the number of nucleoids was performed by identifying local intensity maxima in three dimensions. After filtering the identified peaks, the remaining intensity peaks were classified as nucleoids. For determining the mitochondrial network volume, the mitochondrial network was segmented and the volume was calculated from voxels (see 2.12.3). It needs to be mentioned, that in SCGE the mitochondrial network is due to the denser network and a higher background fluorescence harder to quantify, which could lead to a slight underestimation of the volume.

As for copy number investigations (Fig. 3.1), haploid and diploid strains were grown under respiratory and fermenting conditions. For both conditions the number of nucleoids increase in proportion to cell volume and, similar to mtDNA copy number, the number of nucleoids was shifted down under fermenting conditions (Fig. 3.3c). Moreover, the mitochondrial network volume increases in linear proportion to cell volume, comparable to the number of nucleoids, which is in agreement with the results shown by Rafelski et al., 2012. Similar to the number of nucleoids, cells grown on SCD have less mitochondrial network volume (Fig. 3.3d).

Error! Use the Home tab to apply Überschrift 1 to the text that you want to appear here.

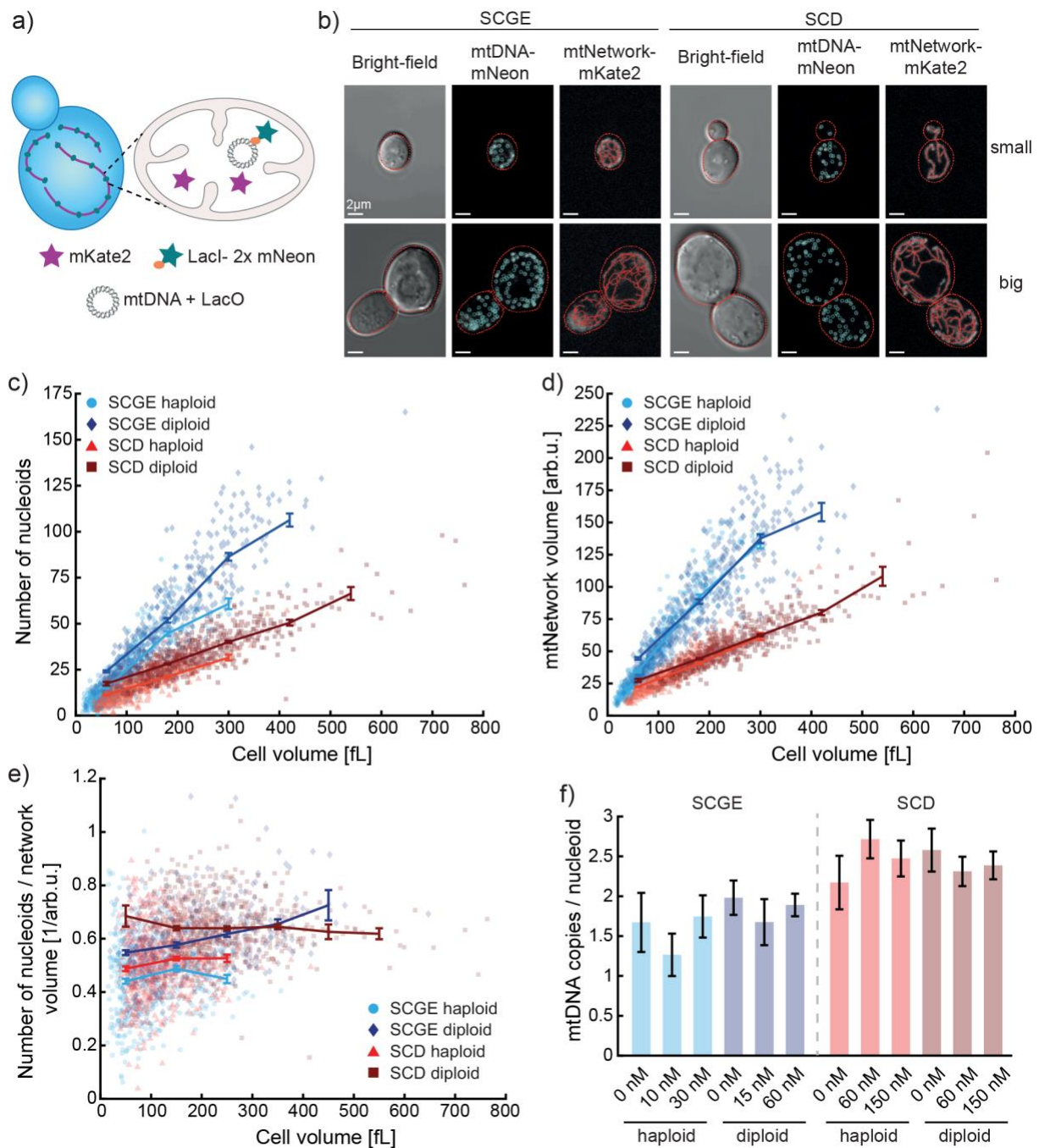


Figure 3.3: Number of nucleoids and the mitochondrial network volume increase with cell volume. **a)** For visualization of mtDNA a strain with integrated LacO arrays was used (Osman et al. 2015). LacO arrays are specifically bound by the nuclear encoded fluorescently tagged LacI protein. Detection of the mitochondrial network was achieved by targeting mKate2 to the mitochondrial matrix. **b)** Representative bright-field and confocal live-cell images (maximum intensity projections). Diploid *Whi5*-inducible microscopy strains were grown on SCGE or SCD at 0 nM (small) or 60 nM (big) β -estradiol concentrations. **c)** Number of nucleoids as a function of cell volume. **d)** Mitochondrial network volume as a function of cell volume for same cells as in c). **e)** Nucleoid concentration as a function of cell volume. In the range between 95-105 fL the data were tested for significances with a two-tailed, two-sided t-test. Haploids and diploid cells grown on SCD are significantly different from each other ($p < 0.01$), as well as haploids and diploid cells grown on SCGE ($p < 0.001$). Haploids grown on SCGE or SCD are significantly different from each other ($p < 0.01$), however for the diploids no significant difference was found ($p > 0.05$). **f)** Average mtDNA copies per nucleoid for *Whi5*-inducible haploid and diploid strains. Average mtDNA copy number per cell from Fig. 3.1b. was normalized on cell volume and

Error! Use the Home tab to apply Überschrift 1 to the text that you want to appear here.

divided by the average number of nucleoids per cell volume from Fig. 3.3c. Error bars indicate propagated standard errors of at least three biological replicates.

In addition, the concentration of nucleoids per mitochondrial network volume was calculated in dependence of cell volume (Fig. 3.3e). Here it was shown that the nucleoid concentration within the network seems to be slightly upshifted on SCD compared to SCGE. Moreover, for both conditions the diploid strain has an overall higher concentration of nucleoids within the network compared to the haploid strain. For both strains and conditions, the number of nucleoids per network volume is almost constant over cell volume.

To further investigate the nucleoid composition regarding to mtDNA copies, the mtDNA copy number from Fig. 3.1b was used to calculate the mtDNA copy number per nucleoid (Fig. 3.3f). For this purpose, the number of nucleoids per cell for each condition was pooled and divided by the cell volume measured with the Coulter counter to obtain the nucleoid concentration. By dividing the mtDNA concentration by the nucleoid concentration the mtDNA copy number per nucleoid was estimated. Nucleoids for cells grown in SCGE contain 1-2 copies mtDNA, whereas nucleoids for cells grown on SCD contain rather 2-3 copies. Again, the mtDNA copy number per nucleoid is almost constant over cell volume. When referring to literature, the composition of nucleoids was found to be quite variable depending on the study. This might be due to an improvement of the methodology, but also due to different culturing strategies. A previous report identified 1-2 mtDNA copies per nucleoid under aerobic growth conditions (Miyakawa et al. 2004). There, the medium contained glucose and the cells were grown to stationary phase, limiting the comparability of the results. For different media and growth conditions up to 20 mtDNA copies per nucleoid were identified (Miyakawa et al. 2004). This, in combination with the data shown in Fig. 3.3f, clearly highlights that the growth condition is crucial for the composition of the nucleoids.

The data suggest that the nucleoid concentration per network and the nucleoid composition in regard to mtDNA copy number are independent of cell volume. However, both seem to be slightly modulated by the nutrient availability and nucleoid concentration significantly depends on ploidy. Moreover, as observed for mtDNA copies, the number of nucleoids is closely linked to cell volume, which holds true for mitochondrial network volume also under fermenting conditions where mtDNA is not needed for cell viability.

3.4. Mitochondrial network increases independent of mtDNA

To test if the increase of the mitochondrial network volume was caused by increasing mtDNA amount, the capability of yeast to grow without mtDNA while fermenting was used. Therefore, a ρ^0 strain was constructed by knocking out the mtDNA polymerase Mip1 in the haploid

Error! Use the Home tab to apply Überschrift 1 to the text that you want to appear here.

microscopy strain, containing the LacO arrays, LacI-2xmNeon and mKate2. The loss of mtDNA was confirmed by DNA-qPCR shown in table 3.1, where Cq-values for the mitochondrial genes COX2 and COX3 were either not measurable or higher than 34.

Table 3.1: Test of ρ^0 strain for mtDNA by DNA-qPCR. Cq-values are displayed for mtDNA genes (COX2, COX3) and nDNA (ACT1) including standard deviation of three biological replicates.

Gene	WT Cq-value	ρ^+ Cq-value	ρ^0 Cq-value
COX2	18.96 +/-0.19	19.30 +/- 0.15	Cq-values not measurable or higher than 36
COX3	18.53 +/- 0.30	18.73 +/- 0.15	Cq-values not measurable or higher than 34
ACT1	22.83 +/- 0.33	22.70 +/- 0.33	21.84 +/- 0.26

Strains were grown on SCD medium in the absence or presence of β -estradiol and the mitochondrial network was visualized by confocal microscopy. It is noticeable that ρ^0 cells are overall larger than ρ^+ cells. However, in the given cell volume range of ρ^+ cells (up to 400 fL) the mitochondrial network volume of ρ^0 cells increases similar to that of ρ^+ cells (Fig. 3.4a). Also, beyond that, the mitochondrial network volume of ρ^0 cells increases in linear proportion to cell volume. Additionally, the mitochondrial network in ρ^0 cells shows morphological changes in form of increased fragmentation (Fig. 3.4b-c). Taken together, the results suggest that the increase of mitochondrial network with cell volume is independent of mtDNA.

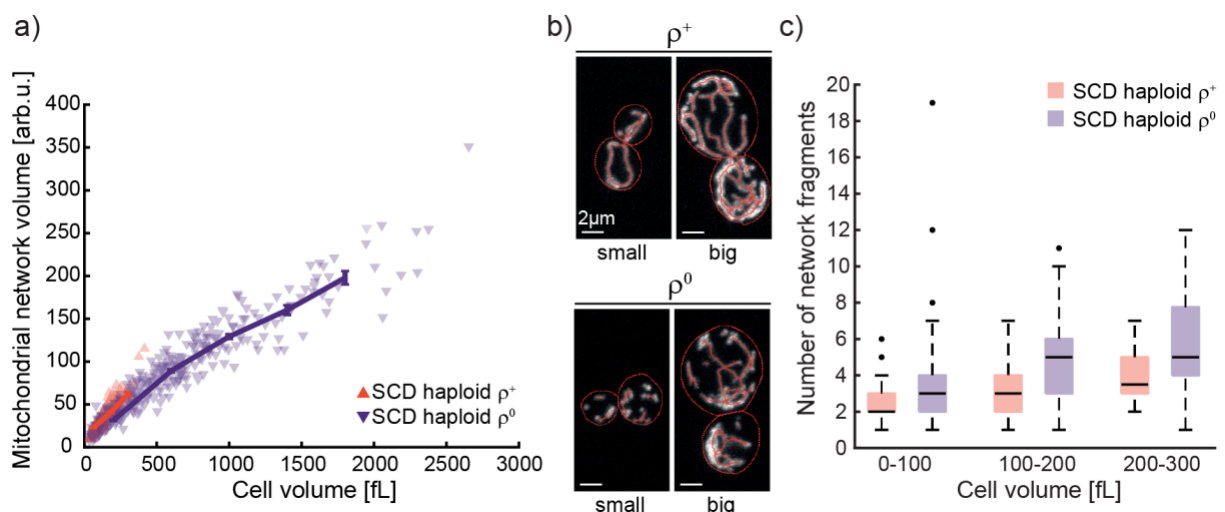


Figure 3.4: Mitochondrial network volume increases with cell volume independent of mtDNA. **a)** mtNetwork as a function of cell volume. mtNetwork volume and cell volume were quantified in a haploid ρ^0 (*mip1 Δ*) and ρ^+ strain (wild-type, same data as in Fig. 3.3b) grown on SCD. The data consist of three biological replicates with each $n = 50$ cells. **b)** Representative confocal images of the mtNetwork in ρ^0 and ρ^+ cells for 0 nM β -estradiol (small) and 150 nM β -estradiol (big). **c)** Quantification of network fragments. The data were binned according to the indicated cell volume. Box plots depict median (black

Error! Use the Home tab to apply Überschrift 1 to the text that you want to appear here.

line), 25th, 75th percentile (box). Whiskers indicate extreme values still within 1.5 interquartile ranges and outliers are depicted as single black points.

3.5. Mitochondrial diameter stays constant with increasing cell volume

The volume of the mitochondrial network increases proportionally to cell volume. Whether this is caused by changes in the local mitochondrial structure, i.e., mitochondrial diameter, is not clear due to limitations in the resolution of confocal microscopy. Therefore, the mitochondrial diameter was investigated with increasing cell volume by transmission electron microscopy. For this purpose, non-inducible and *Whi5*-inducible haploid strains were grown on SCD and SCGE to log-phase and fixed for electron microscopy. Mitochondrial diameter was measured from electron micrographs, acquired and analyzed in collaboration with Moritz Mayer (Till Klecker Lab, University of Bayreuth). Cell volume analysis was performed in collaboration with Dr. Francesco Padovani (Kurt Schmoller Lab, Helmholtz Zentrum München) by segmenting bright-field images with Cell-ACDC (Padovani et al. 2021), which were acquired from the same cultures as investigated by electron microscopy.

Data for both SCD and SCGE show a constant mitochondrial diameter for increasing cell volume, suggesting that the mitochondrial diameter is independent of cell volume (Fig. 3.5a). Interestingly, even though the total mitochondrial volume is reduced in SCD compared to SCGE cells (Fig. 3.3b), the average mitochondrial diameter in SCD (418 nm) is significantly higher than in SCGE (338 nm), indicating that the diameter is modulated by nutrient availability. However, as the experiments for SCD and SCGE were performed separately, the data need to be evaluated by a simultaneous experiment. Nevertheless, it could be ruled out that β -estradiol itself has an influence on the mitochondrial diameter in wild-type cells. The average mitochondrial diameter for SCGE is in agreement with a previous study (Egner et al. 2002), where cells were grown on YPG. Interestingly, they did not observe an increase in the mitochondrial diameter for cells grown on YPD. This opposes the hypothesis that the increase is due to structural changes during respiration and fermentation. Furthermore, compared to cells grown on SCGE, the mitochondrial diameter for cells grown on SCD also shows a higher mean variation (Fig. 3.5.b), which cannot be explained by variations in the cell volume, as the cell volume distributions are comparable for SCD and SCGE (Fig 3.5d). In conclusion, the data suggest that the mitochondrial diameter is constant over cell volume, but is modulated by nutrient availability.

Error! Use the Home tab to apply Überschrift 1 to the text that you want to appear here.

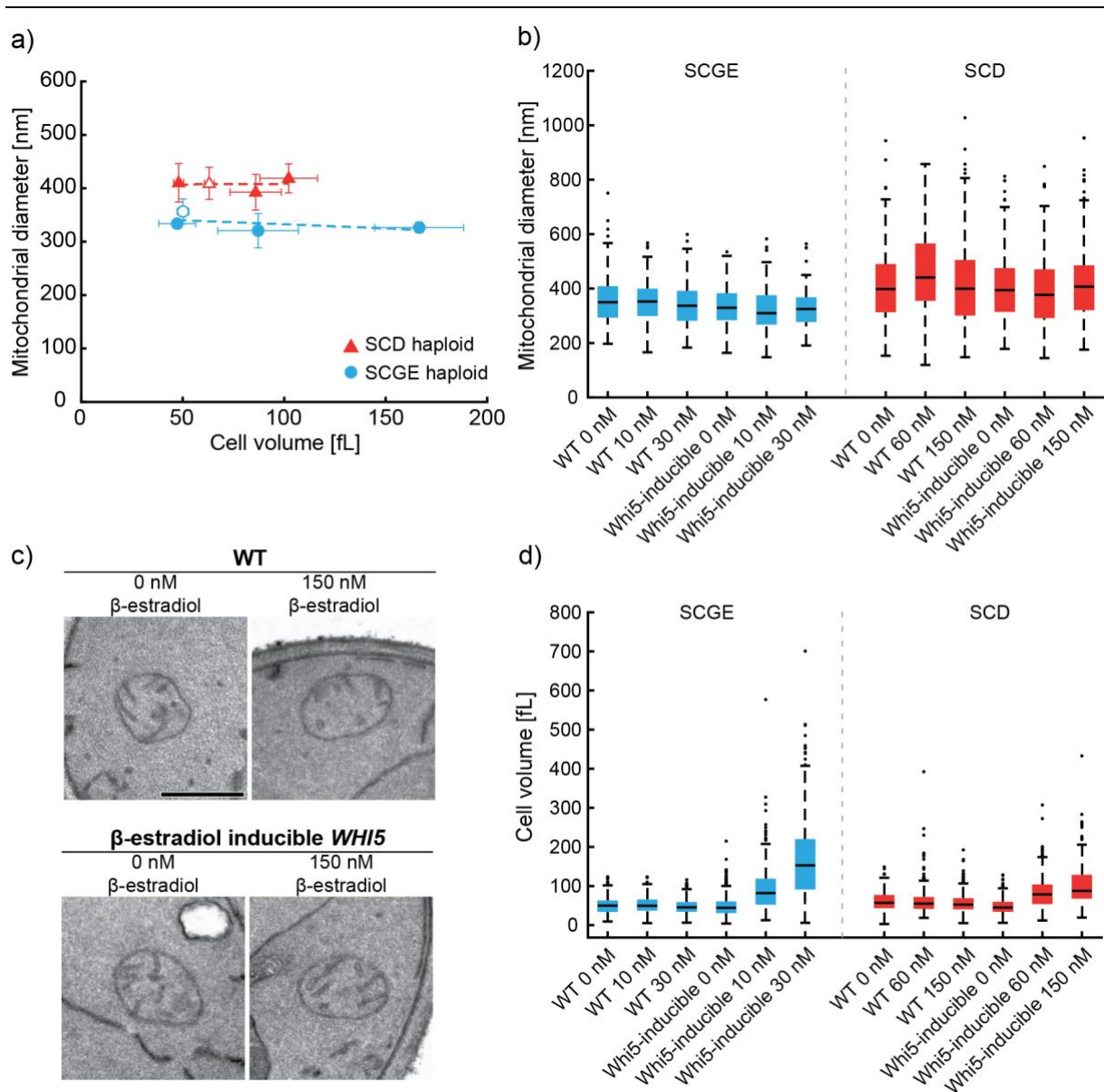


Figure 3.5: Mitochondrial diameter stays constant with increasing cell volume but is modulated by nutrients. **a)** Mitochondrial diameter as a function of cell volume. Wild-type (open symbols) and Whi5-inducible (filled symbols) strains were grown on SCGE and SCD medium and analyzed by transmission electron microscopy. The mean of three biological replicates is plotted, each consisting of 100 mitochondrial diameter measurements. For cell volume measurements DIC images from same cultures were segmented ($n \geq 50$). Error bars are indicating the standard deviation of the means **b)** Mitochondrial diameter measurements from a). Data from three biological replicates, each containing $n=100$ diameter measurements, were pooled. Box plots indicate median (black line), 25th, 75th percentile (red or blue box). Whiskers indicate extreme values still within 1.5 interquartile ranges and outliers are depicted as single black points. **c)** Representative electron micrographs of wild-type (WT) and Whi5-inducible cells grown on SCGE or SCD medium. Scale bars represent 500 nm. **d)** Cell volume measurements from a) depicted as boxplots.

Error! Use the Home tab to apply Überschrift 1 to the text that you want to appear here.

3.6. Amount of mtDNA maintenance factors increases with cell size

The data suggest that mtDNA copy number and mitochondrial network are coupled to cell volume. However, the mechanism leading to the scaling of mitochondrial content with cell volume is unknown. In recent studies it was shown that during cell growth the total RNA and protein abundance increases for most proteins (Marguerat and Bähler 2012). Thus, a possible explanation is that a higher expression of mitochondrial maintenance factors passively leads to an increased production of mitochondrial building blocks in larger cells.

To further investigate this possibility, the expression levels of mitochondrial maintenance factors were analyzed on mRNA level for cells grown on SCGE. As representative mitochondrial maintenance factors the genes *MIP1*, *ABF2*, *RPO41*, *MTF1*, *MRX6* and *PIM1* were investigated for their mRNA concentrations in small and big cells. The corresponding proteins are all involved in either mtDNA replication (Mip1), stabilization (Abf2), transcription and replication initiation (Rpo41, Mtf1) or degradation (Mrx6, Pim1). In addition, all proteins have been shown to be important for maintaining a stable mtDNA copy number (Contamine and Picard 2000). For comparison, the mRNAs *ACT1* and *HTA1* were as well measured. As a structural protein in the cytoskeleton, *ACT1* is often considered as a housekeeping gene and its concentration on mRNA is kept nearly constant with cell volume (Claude et al. 2021). In contrast, the amount of several histone mRNAs and proteins was shown to be constant. Thus, the concentration of histones is decreasing with increasing cell volume (Claude et al. 2021) (Fig. 3.6a). This also applies for the *HTA1* mRNA (Claude et al. 2021).

RNA samples from Claude et al., 2021 were re-analyzed and *ACT1* and *HTA1* values were directly taken from Claude et al., 2021, Fig.2b. There, total RNA was extracted from Whi5-induced and non-induced cells, grown on non-fermentable medium and RT-qPCR was performed. The Cq-Values were normalized on the rRNA *RDN18* before calculating concentrations. By plotting ratios of mRNA concentrations from big cells over small cells, it was estimated if the concentrations of factors are kept constant with increasing cell size. When comparing the mRNA ratios of the mitochondrial biogenesis factors with the benchmark mRNAs *ACT1* and *HTA1*, it is shown that their concentration slightly decreases, however, the amount significantly increases with cell volume (Fig. 3.6b, left). Independent repetition for *ACT1*, *MIP1* and *ABF2* using a different extraction method and DNA digestion shows that concentrations of *MIP1* and *ABF2* are almost constant with increasing cell volume (Fig. 3.6b, right). The differences between the two experiments are non-significant for any of the three factors. This further emphasizes that the amount of mitochondrial biogenesis factors is increasing with cell size. To exclude that hormone treatment impacts mRNA expression, wild-type cells were treated with 0 nM and 30 nM β -estradiol (Fig. 3.6c). An effect of the hormone on mRNA level could be excluded, as no significant changes were observed.

Error! Use the Home tab to apply Überschrift 1 to the text that you want to appear here.

Overall, the transcript amounts of the tested proteins increase with cell volume, creating the fundament for the hypothesis that higher amounts of mitochondrial maintenance factors lead to an increase of the mitochondrial content.

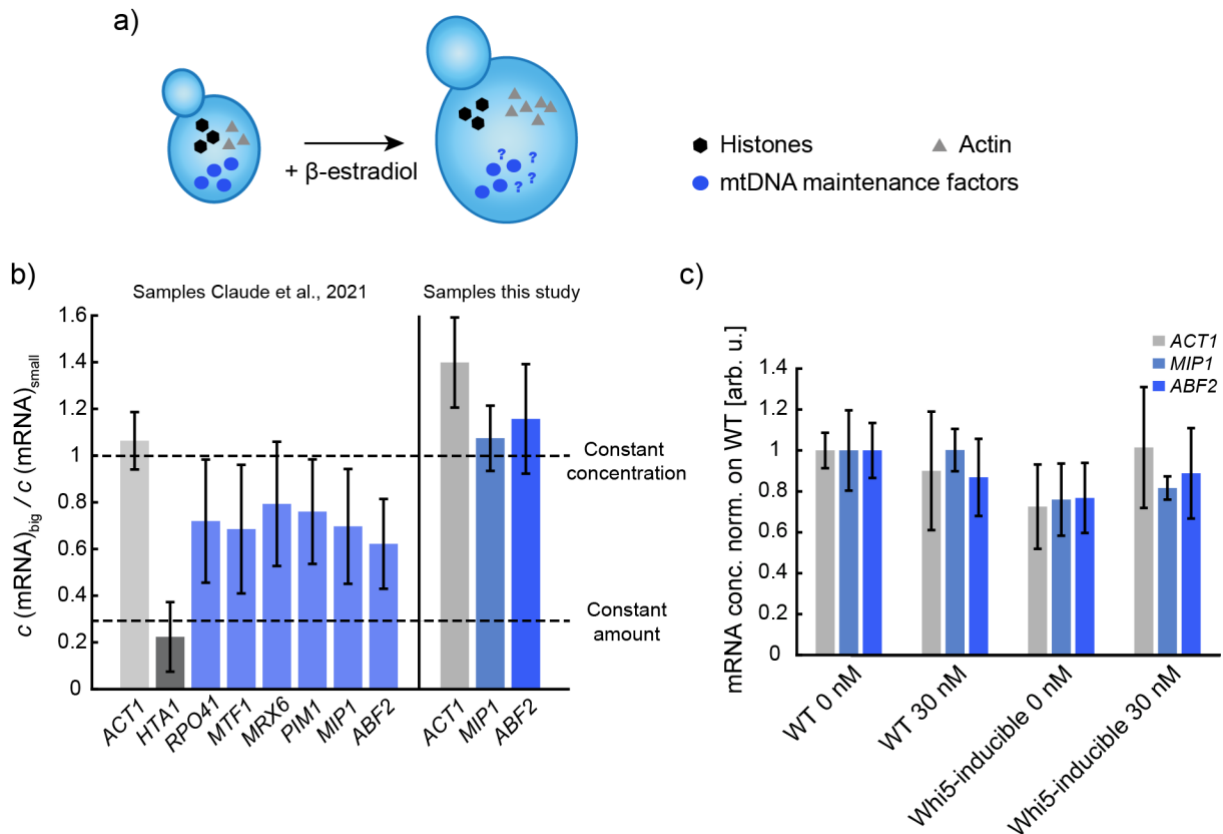


Figure 3.6: Abundance of mtDNA maintenance factors increases with cell volume. **a)** Actin concentration is kept constant over cell volume whereas histone concentration is decreasing with cell volume and kept at a constant amount. **b)** mRNA concentration in haploid, big Whi5-induced asynchronous cell populations relative to small non-induced cell populations. *ACT1* and *HTA1* are shown as reference for constant concentration or constant amount, respectively. Concentrations for *ACT1* and *HTA1* on the left were directly taken from Claude et al., 2021. Data for *RPO41*, *MTF1*, *MRX6*, *PIM1*, *MIP1* and *ABF2*, were generated from RNA samples from Claude et al., 2021. Data on the right were independently generated in this study. Error bars indicate the propagated standard error of at least three biological replicates. **c)** mRNA concentrations measurements for wild-type and Whi5-inducible cells at 0 nM and 30 nM β -estradiol. Whi5-inducible data are the same as for **b)** right. Concentrations of *ACT1*, *MIP1* and *ABF2* were normalized on wild-type at 0nM. Bars represent the mean of at least three biological replicates. Error bars show normalized standard deviations.

To validate that the observed increase of mitochondrial maintenance factors also applies on the protein level, flow cytometry was performed. For this purpose, the mtDNA polymerase Mip1 and the histone-like protein Abf2, both important for mtDNA maintenance, were endogenously tagged with the fluorophore mCitrine, allowing intensity measurements as a proxy for protein expression level, i.e., the protein amount.

Error! Use the Home tab to apply Überschrift 1 to the text that you want to appear here.

To ensure protein functionality, the effects of the tags on mtDNA copy number and mRNA levels were examined by qPCR. For Abf2-mCitrine, no significant influence of the tag on mtDNA and mRNA level was detected (Fig. 3.7d,f). For Mip1-mCitrine, on the other hand, the mtDNA copy number increased significantly by ~70% compared to the wild-type, while *MIP1* mRNA concentration remains constant. This suggests that the C-terminus of Mip1 is important for a balance of mtDNA copy number. However, both strains grow with similar doubling times as wild-type, supporting the assumption that both proteins remain functional with a C-terminal tag. To test if the volume-dependency of the mtDNA copy number is still present, even if mtDNA copy number is increased by ~70%, Mip1 was endogenously tagged with mCitrine in a *Whi5*-inducible strain and DNA-qPCR was performed. The data reveal that mtDNA copy number in the Mip1-mCitrine strain remains volume-dependent, however, again mtDNA copy number is upshifted by ~70% as observed for the non-inducible strain. The results suggest that regulation of Mip1 is not impaired by the mCitrine tag and thus flow cytometry was performed.

The flow cytometry experiment was performed in collaboration with Daniela Bureik (Kurt Schmoller Lab, Helmholtz Zentrum München) and analysis was performed by Dr. Kurt Schmoller (Helmholtz Zentrum München). The cells were grown on SCGE medium and to exclude the measurement of doublets, samples were sonicated prior the experiment. Additionally, cell debris, particles and doublets were excluded from the analysis, by using a standard gating strategy (see 2.13, Fig. 2.4d). To correct for autofluorescence, the non-fluorescent wild-type strain was measured. The cell volume was quantified using side scatter A (SSC-A) data (see 2.13, Fig. 2.4a-c).

For both, Mip1-mCitrine and Abf2-mCitrine, the fluorescence intensity, i.e., the amount, strongly increases with cell volume confirming the results observed on the mRNA level. This is consistent with an analysis performed by Swaffer et al., showing an increase for the mitochondrial biogenesis factors Abf2, Mhr1, Pim1 and Rpo41 with cell size (Swaffer et al. 2021). This supports the hypothesis that the expression of the mitochondrial maintenance machinery is linked to global protein expression and thus to cell volume.

Error! Use the Home tab to apply Überschrift 1 to the text that you want to appear here.

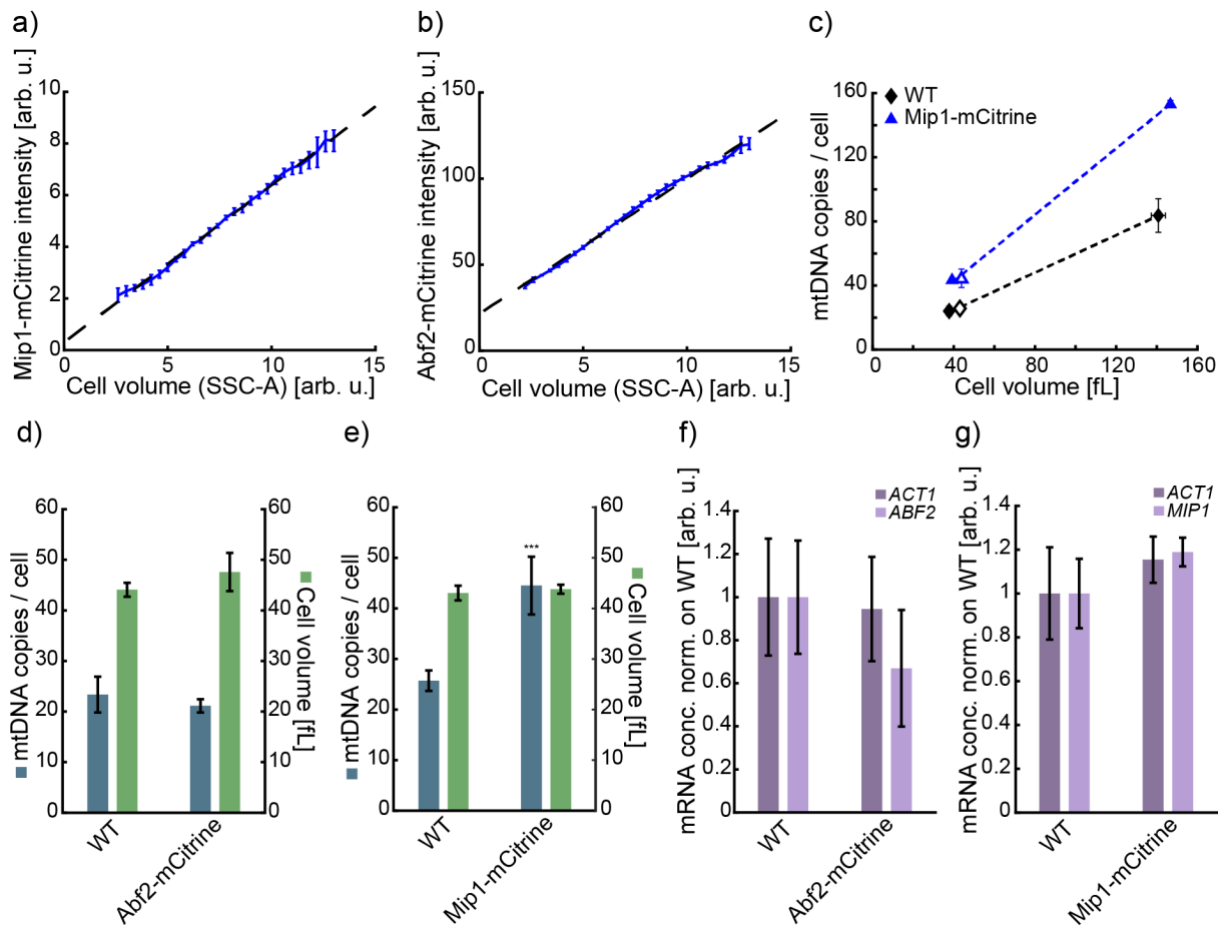


Figure 3.7: Protein concentrations of Mip1-mCitrine and Abf2-mCitrine increase with cell volume. **a-b)** Mip1-mCitrine or Abf2-mCitrine intensity as a function of cell volume. In a haploid non-inducible strain *MIP1* or *ABF2* were endogenously tagged with mCitrine. Fluorescence intensity was measured by flow cytometry and SSC-A data were used as a measure for cell volume. Dashed lines show linear fits to the binned means. Error bars show the estimated error of binned means. **c-g)** Functionality tests for Mip1-mCitrine and Abf2-mCitrine. **c)** mtDNA copies increase with cell volume in a Whi5-inducible Mip1-mCitrine strain. A non-inducible (open symbol) and a Whi5-inducible strain with 0 nM and 30 nM β -estradiol were grown asynchronously on SCGE and harvested to perform DNA-qPCR. Error bars show the standard error of three biological replicates. **d-e)** mtDNA copies per cell and cell volume measurements. **f-g)** mRNA concentration for *MIP1* (**f**) in Mip1-mCitrine strain and *ABF2* (**g**) in Abf2-mCitrine strain normalized on wild-type. Error bars depict the normalized standard error of three biological replicates. Significances were determined by a two-tailed t-test (* $p < 0.05$, ** $p < 0.01$, *** $p < 0.001$).

Error! Use the Home tab to apply Überschrift 1 to the text that you want to appear here.

3.7. mtDNA copy number in Mip1-mCitrine strain is slightly affected by *ADH1* terminator variants

The C-terminal mCitrine-tag of Mip1 influences mtDNA copy number unexpectedly strong. To ensure that it was solely an effect of the mCitrine, the terminator sequences were examined. Since the open reading frame of mCitrine is terminated in the original construct with an *ADH1* terminator, this sequence was swapped for the endogenous *MIP1* terminator sequence. DNA-qPCR on two transformant clones revealed a slight, non-significant, decrease of mtDNA by < 20% (Fig. 3.8a). Next, either the short endogenous or a longer *ADH1* terminator sequence was integrated after the non-tagged wild-type *MIP1* gene. The long sequence consisted of additional 20 bp upstream of the shorter *ADH1* terminator sequence, without any known function. For both, the short and the long *ADH1* terminator sequences a comparable increase of mtDNA by < 20% for each of the clones was found, indicating that the additional base pairs upstream of the *ADH1* terminator sequences do not further mtDNA copy number. The slight increase in mtDNA copy number when terminating *MIP1* expression with the *ADH1* terminator was also observed when terminating *MIP1*-mCitrine expression with the *ADH1* terminator sequence, compared to *MIP1*-mCitrine-*MIP1*term. However, only a small fraction of the total increase in mtDNA copy number observed for the *MIP1*-mCitrine-*ADH1*term is caused by the *ADH1* terminator sequence itself. As no significant changes on the mRNA levels were observed for *MIP1*-mCitrine compared to the wild-type *MIP1*, the main increase of mtDNA copy number is most likely caused by the C-terminal mCitrine tag that alters Mip1 properties. Here, two possible explanations are conceivable. Firstly, it is possible that Mip1-mCitrine is less accessible to degradation on the protein level leading to increased concentrations of Mip1. Secondly, it has been shown that the C-terminal domain of Mip1 is crucial for mtDNA copy number regulation (Viikov et al. 2012). The data suggest that C-terminal extension of Mip1 is important for the balance between mtDNA synthesis and degradation. It was found that mutations in the C-terminal extension of Mip1 influences the binding affinity and thereby alters Mip1 processivity. Thus, higher binding affinity resulted in increased Mip1 processivity. The C-terminal mCitrine tag might impact the binding affinity of Mip1, thereby influencing the polymerase activity leading to an increased mtDNA copy number.

Error! Use the Home tab to apply Überschrift 1 to the text that you want to appear here.

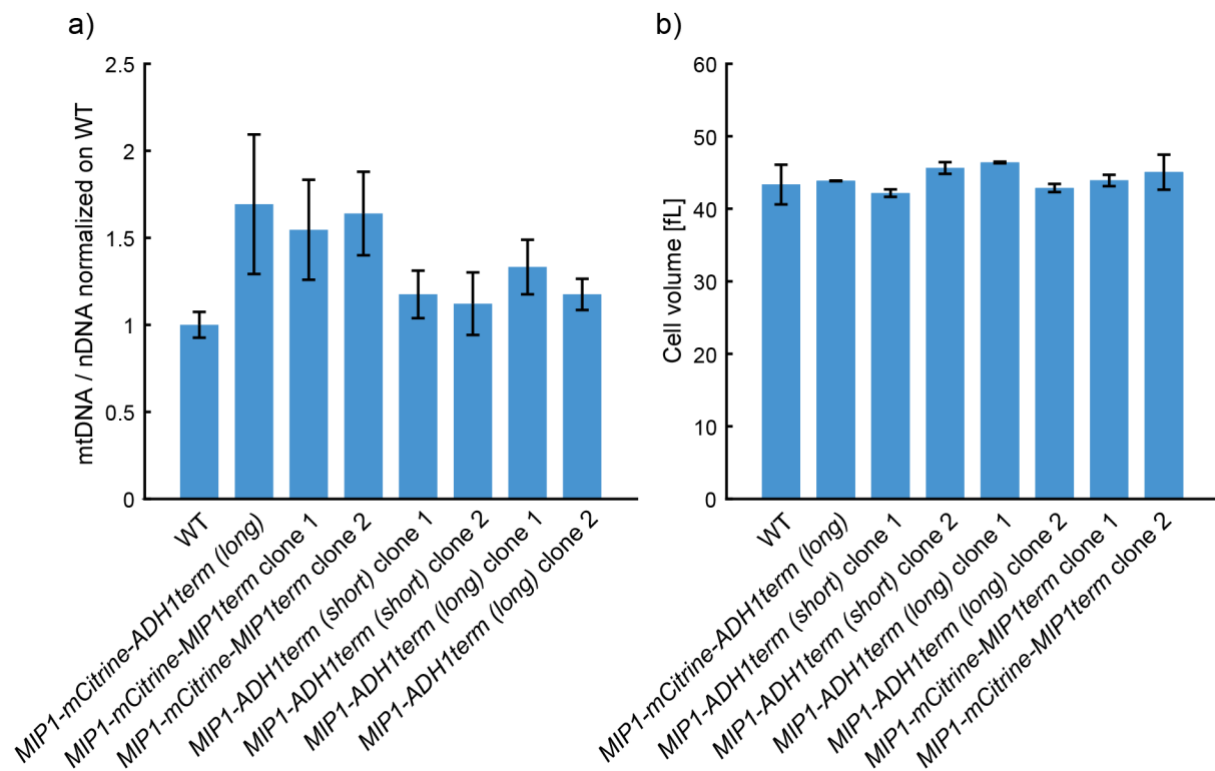


Figure 3.8. Increase of mtDNA copy number by mCitrine tagged Mip1 is not influenced by the terminator sequence. a) mtDNA copy number in Mip1 clones with varying terminator sequences normalized on wild-type. Tested was the endogenous Mip1 with a short and a long version of the *ADH1* terminator sequence and Mip1-mCitrine with the *MIP1* terminator sequence. **b)** Cell volume measurements for strains from a) performed with a Coulter Counter. Each clone consists of two biological replicates. Error bars depict the standard deviation.

3.8. Reducing the expression of mtDNA maintenance factors leads to altered mtDNA copy numbers

3.8.1. Mip1 and Abf2 are limiting for mtDNA maintenance

So far, the results suggest that larger cells have more mitochondrial biogenesis factors, which could lead to an increase in mtDNA copy number. If this is indeed the case, a reduction in protein concentration should also lead to a reduction in mtDNA copy number. For this purpose, several factors involved in mtDNA maintenance were chosen to manipulate their concentration (Contamine and Picard 2000). This includes proteins important for mtDNA replication such as the mtDNA polymerase Mip1 (Stumpf et al. 2010), recombination factors (Mhr1, Mgm101) (Ling and Yoshida 2020), helicases (Hmi1, Pif1, Rrm3) (Sedman et al. 2005, Crider et al. 2012, Muellner and Schmidt 2020), mtDNA priming (Rpo41, Mtf1) (Sanchez-Sandoval et al. 2015) and ssDNA stabilization (Rim1) (Van Dyck et al. 1992). In addition, the packaging factor Abf2 (Zelenaya-Troitskaya et al. 1998) and the protein kinase Rad53 were investigated (Crider et al. 2012).

Error! Use the Home tab to apply Überschrift 1 to the text that you want to appear here.

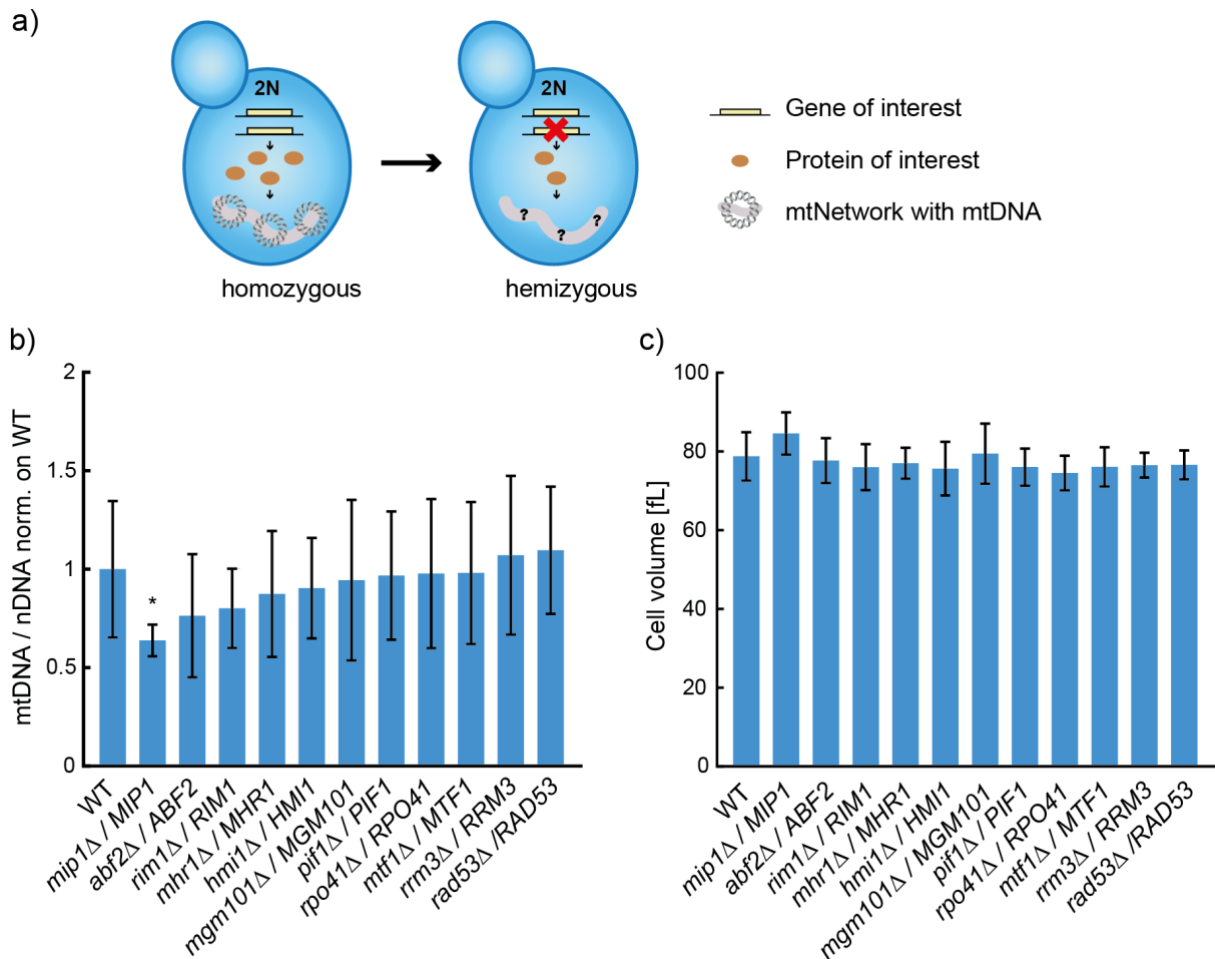


Figure 3.9: Identification of mtDNA limiting factors using hemizygous deletion mutants. a) Depiction of the experimental set-up. In a diploid wild-type strain, one copy of the gene of interest was deleted, aiming the reduction of the protein concentration by 50%. Variations in mtDNA copy number were detected by DNA-qPCR. b) mtDNA copies per nDNA normalized on wild-type for asynchronous non-induced cell cultures of hemizygous deletion strains grown on SCGE. c) Cell volume measurements performed with a Coulter counter for same cultures as in b). Error bars indicate the normalized standard deviation (b) or standard deviation (c) of at least three biological replicates. Significances were determined by a two-tailed t-test (* $p < 0.05$, ** $p < 0.01$, *** $p < 0.001$).

To reduce concentrations of the above-mentioned mtDNA maintenance factors, diploid strains were used to delete one copy of the gene of interest, aiming for a reduction in protein concentration by 50% (Fig. 3.9a). Previous studies suggest that budding yeast does not exhibit dosage compensation neither on mRNA level (Torres et al. 2016) nor on protein level (Springer et al. 2010). Thus, a knock-out of one gene copy should result in a reduction of protein concentration to 50%. If one of the tested factors should be perfectly limiting, a decrease of the DNA copy number to 50% is expected. For this purpose, a series of hemizygous deletion strains was constructed and all strains were investigated for their mtDNA levels by DNA-qPCR. The strongest impact on the mtDNA copy number was observed for the hemizygotes Mip1, Abf2 and Rim1 which show a reduction to ~65%, ~70% and to ~80% of wild-type levels,

Error! Use the Home tab to apply Überschrift 1 to the text that you want to appear here.

respectively (Fig. 3.9b). For none of the hemizygotes any significant changes in cell volume were observed (Fig. 3.9c). However, no reduction to 50% of wild-type level was observed for any of the hemizygotes, suggesting that concentrations of mitochondrial maintenance factors are not perfectly limiting.

3.8.2. Reduction of Mrx6 expression increases mtDNA copy number

A recent study identified a protein-complex involved in mtDNA quality control (Göke et al. 2020). Part of this complex are Mrx6, Pet20 and the protease Pim1. This complex is likely involved in the degradation of proteins important for mtDNA maintenance. Both, Mrx6 and Pim1 were found to be important maintaining stable mtDNA copy numbers (Göke et al. 2020). Independently of Mrx6 and Pim1, also Sue1 and Pim1 form a complex, which is rather involved in the degradation of proteins encoded by the mtDNA (Göke et al. 2020). To get an impression of how these complexes impact mtDNA copy number, the concentrations of Sue1, Pet20 and Mrx6 were manipulated by constructing hemizygous strains.

For all three hemizygotes an increase of the mtDNA copy number was observed. The strongest increase of mtDNA was shown for the hemizygote *mrx6Δ/MRX6*. Thus, to determine whether a size-dependent effect was present, *MRX6* was deleted in the haploid *Whi5*-inducible strain, the cell size was induced and subsequently DNA-qPCRs were performed. Here, mtDNA levels are doubling for all sizes compared to wild-type. However, no additional effect of cell size was observed for the *mrx6Δ* strain. Consistent with Göke et al., 2020, Mrx6 and Pet20 are, via interaction with the protease Pim1, involved in the degradation of the mtDNA synthesis machinery factors. Thus, depletion of these factors increases mtDNA copy number independently of cell size. However, a dose-dependent effect for all three proteins on mtDNA copy number is present, especially for Mrx6. While the mtDNA copy number in the hemizygote *mrx6Δ/MRX6* increases to ~1.6-fold of wild-type levels the complete deletion of *MRX6* leads to an increase to roughly 2-fold.

Error! Use the Home tab to apply Überschrift 1 to the text that you want to appear here.

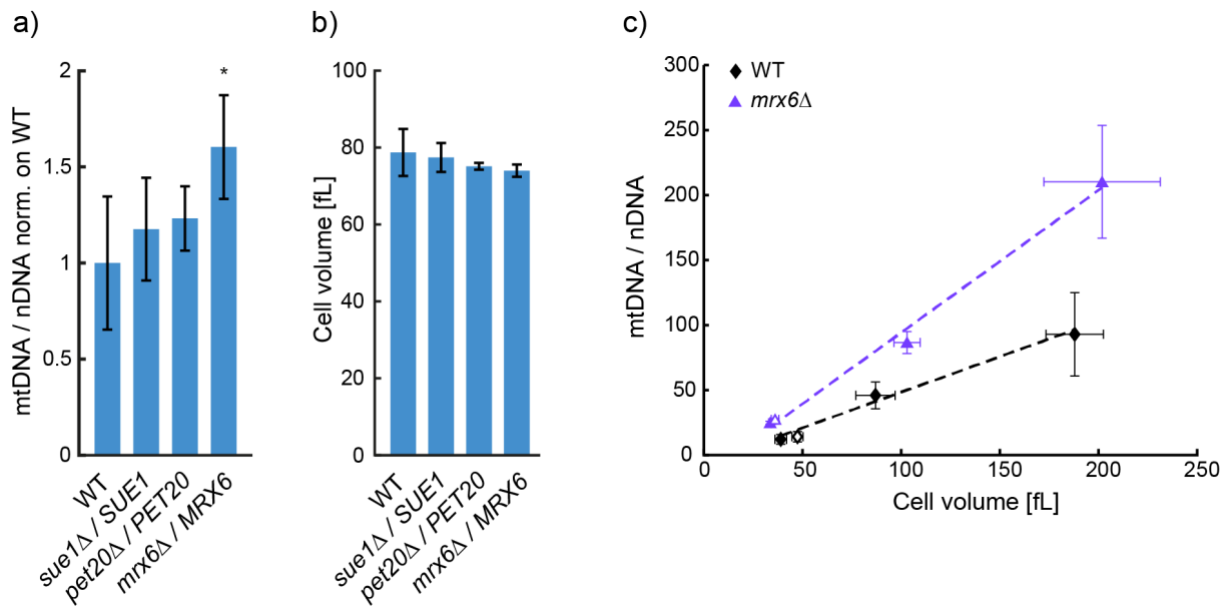


Figure 3.10: *mrx6* deletion increases mtDNA copy number. a) Hemizygous mtDNA copies per nDNA Same wild-type as in Fig. 3.9. b) Cell volume measurements for the hemizygotes from a). c) mtDNA per nDNA in *mrx6*Δ (triangle) and wild-type (diamond) as a function of cell volume. Whi5-inducible (filled symbols) and non-inducible (open symbols) cells were grown on SCGE in the absence or presence of β -estradiol. Error bars indicate the normalized standard deviation (a) or standard deviation (b-c) of at least three biological replicates. Significances were determined by a two-tailed t-test (* $p < 0.05$, ** $p < 0.01$, *** $p < 0.001$).

3.8.3. Double hemizyote *MIP1/ABF2* shows a stronger decrease of mtDNA copy number

To validate the data for the hemizygotes *Mip1* and *Abf2*, experiments were repeated independently, which are showing now a significant decrease of mtDNA concentration to ~76% for *Mip1* and ~65% for *Abf2* (Fig. 3.11a). Additionally, to test the size-dependency of the effect, hemizygous deletions were integrated into a diploid *Whi5*-inducible strain which was subsequently tested for mtDNA levels. The strains maintained the proportional scaling of mtDNA and neither the *Mip1* hemizyote nor the *Abf2* hemizyote showed an additional size-dependent effect on the mtDNA copy number (Fig. 3.11b).

Of all factors examined, *Mip1* and *Abf2* hemizygotes showed the strongest reduction of mtDNA, however, the expected reduction to 50% was not observed. To rule out dosage compensation, mRNA concentrations were determined in parallel. In both strains mRNA concentrations for *MIP1* and *ABF2* were decreased to around ~50%, respectively (Fig. 3.11c-e). Thus, *Mip1* and *Abf2* alone are not perfectly limiting mtDNA copy number. A possible explanation for this observation could be a stabilization of mtDNA levels by multiple proteins, resulting in a decreased impact of single factors. To test this hypothesis, a strain hemizygous for both *MIP1* and *ABF2* was constructed. Strikingly, the mtDNA level decreases to ~58%,

Error! Use the Home tab to apply Überschrift 1 to the text that you want to appear here.

while the mRNA concentrations again decrease to around 50% (Fig. 3.11c-e). This supports the hypothesis that more than one factor is limiting for mtDNA maintenance (Fig. 3.11a). Again, mtDNA copy number increases linearly with cell volume, however, no further effect of cell size has been observed (Fig. 3.11b). The results suggest that Mip1 and Abf2 stabilize mtDNA copy number alone and even stronger in combination, independently of cell size.

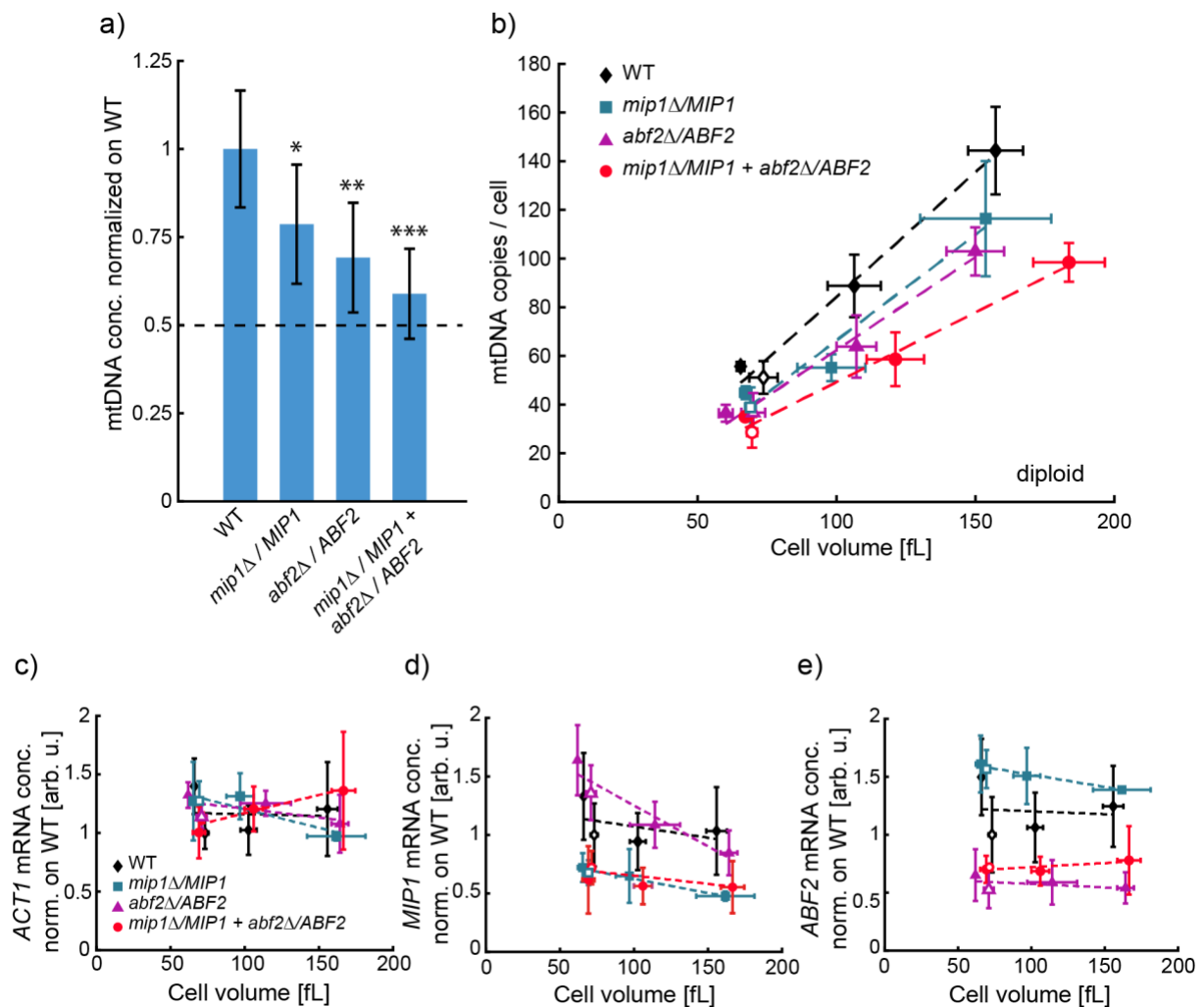


Figure 3.11: mtDNA copy number depends on concentrations of Mip1 and Abf2. **a)** mtDNA concentration for non-inducible wild-type, single and double hemizygous *MIP1* and *ABF2* strains determined by DNA-qPCR. Bars indicate means from 6 biological replicates and significances were determined by a two-tailed t-test (* $p < 0.05$, ** $p < 0.01$, *** $p < 0.001$). **b)** mtDNA copies per cell as a function of cell volume for non-inducible (data from b, open symbols) and *Whi5*-inducible strains (filled symbols), consist of at least three biological replicates. **c-e)** mRNA concentrations for **c)** *ACT1* **d)** *MIP1* and **e)** *ABF2*, determined for the same cultures as in **b)**. Non-inducible and *Whi5*-inducible strains were measured by RT-qPCR and normalized on the non-inducible wild-type strain (open diamond). Error bars indicate standard deviation (**b-e**).

Error! Use the Home tab to apply Überschrift 1 to the text that you want to appear here.

3.9. Overexpression of Mip1-mCitrine shows limited mtDNA increase

The previous results demonstrate that mtDNA copy number is dependent on the concentrations of the mtDNA maintenance factors Mip1 and Abf2. To see how the mtDNA copy number depends on Mip1 concentrations over a larger concentration range, the endogenous Mip1 promoter was replaced with the β -estradiol promoter (Ottoz et al. 2014). Addition of increasing β -estradiol concentrations led to a continuous increase of Mip1 concentration (Fig. 3.12a). By tagging Mip1 with mCitrine and using epifluorescence microscopy the fluorescence intensity was determined for every condition. This allowed the calculation of Mip1-mCitrine concentration by determining the total amount of Mip1 per cell and dividing it by the cell volume (see 2.12.14). In parallel, mtDNA concentrations and cell volume distributions were determined for every replicate. As slight differences in hormone concentrations can lead to higher differences in Mip1-mCitrine concentrations, all three replicates were plotted without taking the average (Fig. 3.12b-c). Surprisingly, without addition of β -estradiol, the Mip1-inducible strain was able to grow on non-fermentable medium, indicating leakiness of the β -estradiol promoter (Fig 3.12b-d). Addition of increasing β -estradiol concentrations to the cell cultures also increases the expression of Mip1-mCitrine, resulting in a higher mtDNA concentration (Fig. 3.12b). However, at about 5-fold Mip1-mCitrine concentration compared to the non-inducible Mip1-mCitrine, a plateau of mtDNA concentration is reached. Importantly, the mtDNA only slightly exceeds the concentration reached of the non-inducible Mip1-mCitrine strain. (Fig. 3.12b,d). Even 50-fold overexpression of Mip1 does not lead to a further increase. mtDNA concentration rather slightly decreases which in combination with a decreased growth rate and an abnormal cell volume indicates that Mip1-mCitrine concentration becomes toxic to the cells. The results suggest that Mip1 concentration and mtDNA copy number are tightly linked, however, only until a plateau is reached. This indicates that either mtDNA is actively degraded, or more likely, other mtDNA synthesis factors or building blocks, such as dNTPs become limiting. In agreement with the previous results, the plateau supports the assumption that Mip1 alone is not perfectly limiting for mtDNA copy number.

Error! Use the Home tab to apply Überschrift 1 to the text that you want to appear here.

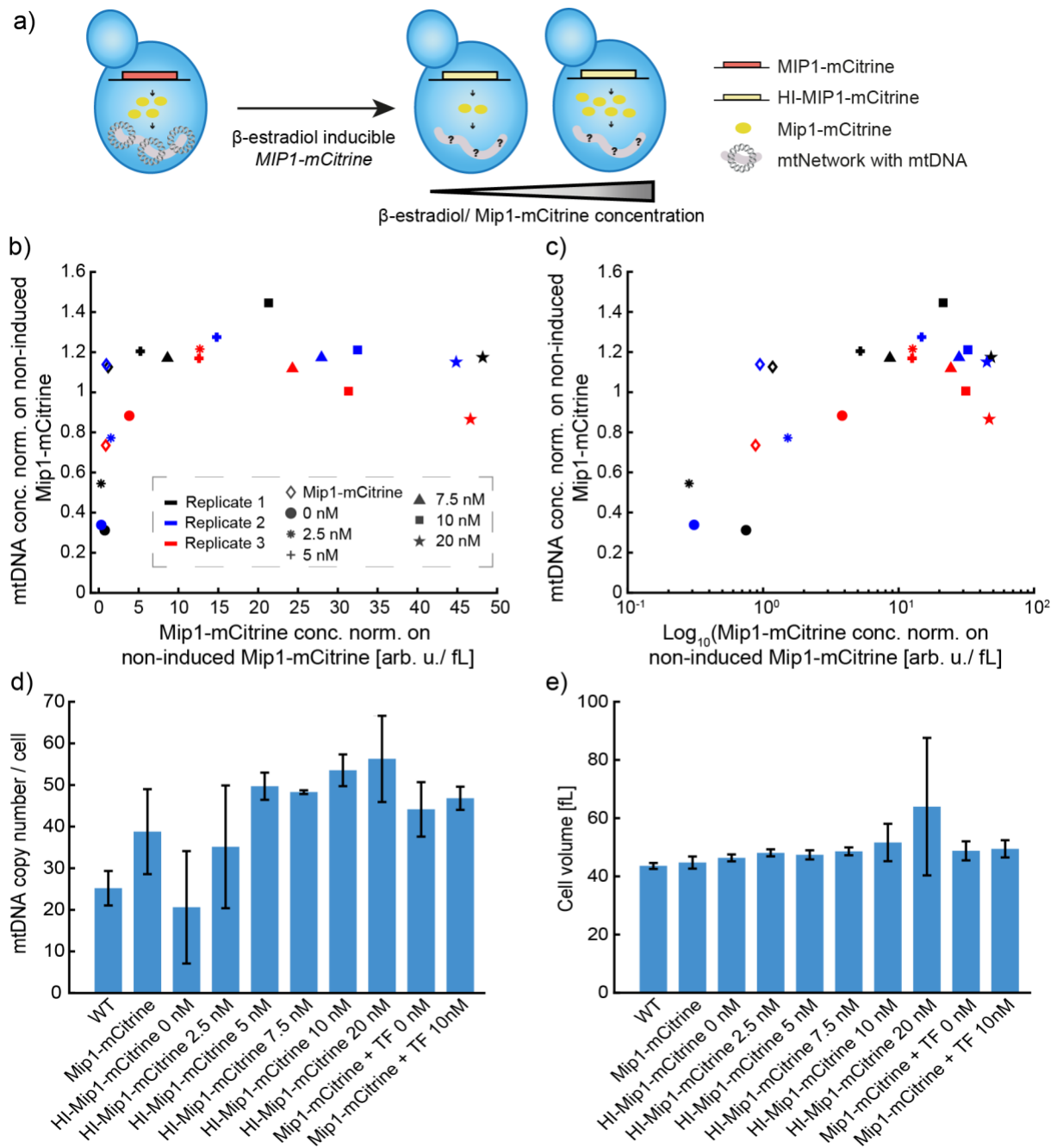


Figure 3.12: Impact of Mip1 concentration on mtDNA copy number is limited. **a)** Experimental set-up. To manipulate the Mip1 concentration, a *MIP1* allele C-terminally tagged with mCitrine, expressed from a β -estradiol inducible promoter was integrated into the nuclear genome and the endogenous *MIP1* copy was deleted. Adding different concentrations of β -estradiol allowed the modulation of Mip1 expression. **b)** mtDNA concentration in dependence of Mip1-mCitrine concentration. Mip1-mCitrine fluorescence intensity was detected in 3D by live-cell epifluorescence microscopy. The amount of Mip1-mCitrine fluorescence intensity was calculated and divided by the cell volume to get the concentration per cell. Mip1-mCitrine concentration was then normalized to the average of the non-inducible Mip1-mCitrine (open diamonds). In parallel, cells were harvested from same cultures to perform DNA-qPCR. mtDNA concentrations were calculated from mean cell volume measurements conducted with a Coulter counter, and normalized on the average mtDNA concentration of the non-inducible Mip1-mCitrine. **c)** Same data as in b) as semi-log plot. **d)** mtDNA copy number per cell for increasing concentrations of HI-Mip1-mCitrine (same data as in b), including the non-inducible Mip1-mCitrine with β -estradiol transcription factor (TF) at 0 nM and 10 nM β -estradiol. **e)** Cell volume

Error! Use the Home tab to apply Überschrift 1 to the text that you want to appear here.

measured with a Coulter counter. Bars display the mean of three biological replicates and error bars indicate standard deviations (d-e).

3.10. Expression of *ABF2* and *MIP1* from histone promoters increases mtDNA copy number

As observed on mRNA and protein level, the amount of mitochondrial maintenance factors increases with cell size and so does mtDNA. As a next question, it was asked whether the amount of mtDNA can be kept constant with increasing cell volume. Thus, by keeping the amount of mitochondrial maintenance factors constant over size, it was aimed to test whether a cell-size dependent expression of the factors is responsible for mtDNA increase.

For this purpose, the mtDNA polymerase Mip1 and the histone like protein Abf2 were expressed under histone promoters in *Whi5*-inducible strains. Expression of *HTB1* and *HTB2* promoters was described to be solely sufficient to keep the histone amount constant over different cell sizes (Claude et al. 2021). This was shown by expressing the fluorophore mCitrine from the *HTB1* and *HTB2* promoters. Its amount on mRNA and protein level was kept constant. Thus, the *HTB1* promoter (*HTB1pr*) was used to modify the expression of Abf2 and Mip1, at first both alone and then together in one strain. In parallel to DNA measurements, mRNA levels for *MIP1* and *ABF2* were examined by performing total RNA extractions for every replicate (Fig. 3.13c-d). For better comparison between the different strains, the mtDNA copy number was estimated at 100 fL cell volume, by using the equation of the linear fit through the data points (Fig. 3.13b).

The mtDNA copy number for Abf2 expressed under the *HTB1* promoter is shifted up for small cells (~1.5-fold), however, even stronger (~2.7-fold) for big cell volumes (Fig. 3.13a). The increased amount of mtDNA is most likely caused by the overexpression of Abf2 via the histone promoter (Fig. 3.13e). This is leading to an overexpression of Abf2 by ~9-fold for small cells and ~6-fold for big cells on the mRNA level. The mRNA concentration is slightly decreasing with increasing cell volume, which is in agreement with the data from Fig. 3.6b. Surprisingly, the mRNA amount is not kept constant as expected based on the findings from Claude et al., 2021.

Error! Use the Home tab to apply Überschrift 1 to the text that you want to appear here.

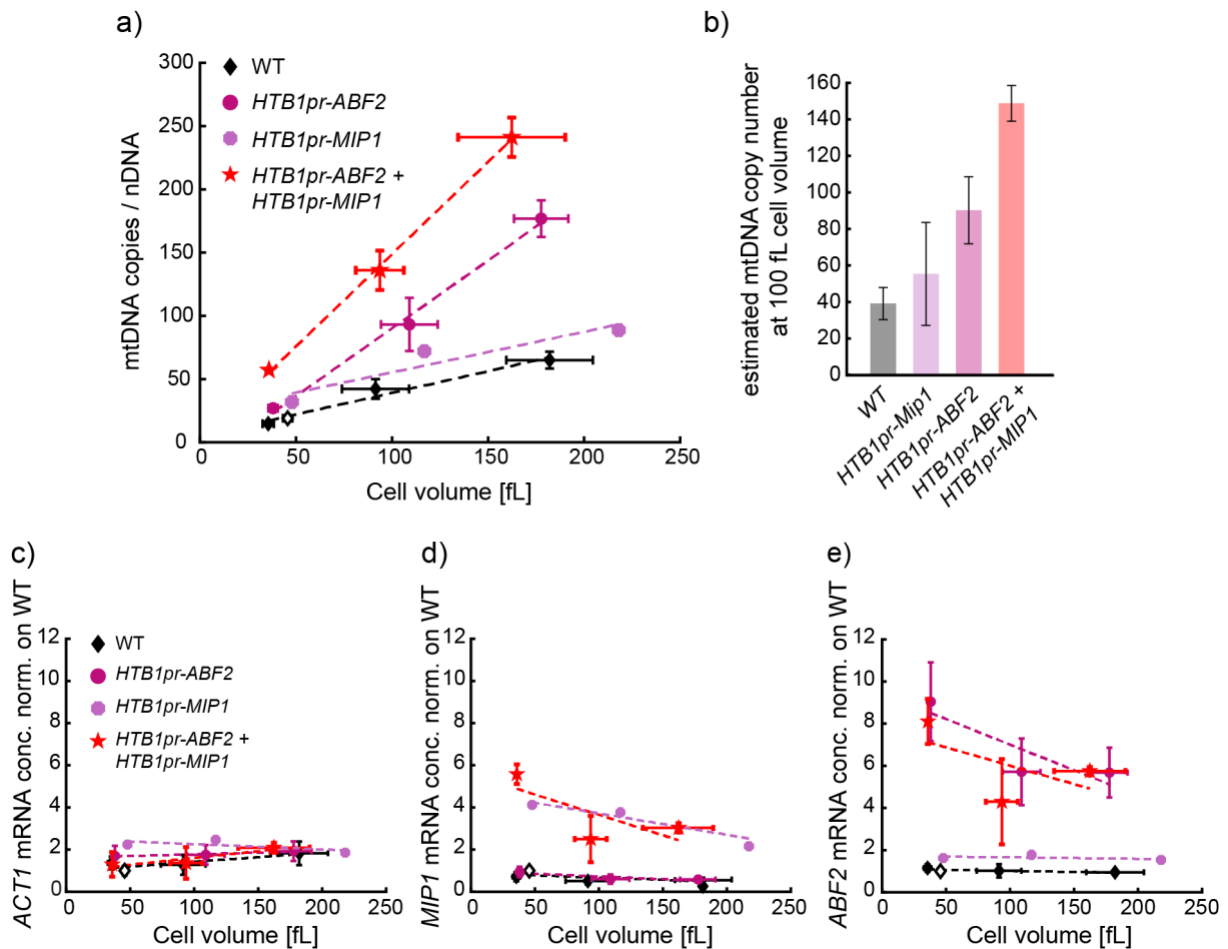


Figure 3.13: Histone promoter leads to overexpression of Mip1 and Abf2 causing increased mtDNA copy numbers. a) mtDNA with increasing cell sizes for Mip1 and Abf2 expressed from the *HTB1* or *HTB2* promoter, with endogenous terminator. All promoter variants were only Whi5-inducible and grown in the absence or presence of β -estradiol, except of wild-type (open diamond). mtDNA copy number was determined by DNA-qPCR. b) Estimated mtDNA copy number at 100 fL cell volume. mtDNA copy number was estimated from the linear fit. Error bars indicate estimated standard errors from the linear fit at 100 fL. c-e) mRNA concentrations for *ACT1*, *MIP1* and *ABF2* in same cultures as in a). Note that data points for *HTB1pr-MIP1* contains only one biological replicate, data points for *HTB1pr-ABF2 + HTB1pr-MIP1* contains two, *HTB1pr-ABF2* and wild-type contain three biological replicates. Fits show trendlines through the data points and error bars indicate wild-type standard deviation.

For this reason, a second histone promoter, *HTB2pr*, was tested for its influence on *ABF2* mRNA and mtDNA levels. Overall, *ABF2* is lower expressed leading to less mtDNA copies compared to the expression under *HTB1pr* (Fig. 3.14a-b). However, as observed for *HTB1pr-ABF2*, the *ABF2* mRNA amount was not kept constant, again contradicting the prediction that histone promoters alone lead to a constant mRNA amount (Fig. 3.14c-e). To further evaluate this result, an effect of the terminator sequence should be excluded. In the study of Claude et al., 2021, expression of *HTB1* was terminated with the *ADH1* terminator. For that reason, the endogenous *ABF2* terminator sequence was replaced with the *ADH1* terminator for *ABF2* expressed from the *HTB1* promoter (1 replicate). The *ABF2* concentration is lower than with

Error! Use the Home tab to apply Überschrift 1 to the text that you want to appear here.

the endogenous terminator, but the amount of *ABF2* mRNA is still not kept constant, indicating that the terminator is not responsible for the rather constant mRNA concentration (Fig. 3.14c-e). On the other hand, *MIP1* expressed from the *HTB1* promoter also shows an increase in mtDNA, but this remains constant over cell volume. However, when evaluating this data set, it should be noted that the data for *HTB1pr-Mip1* contains only one replicate. Again, for the mRNA expression level the expected decrease in concentration as observed for *HTB1* mRNA was not observed. When both, *MIP1* and *ABF2* are expressed in the same strain from the *HTB1* promoter, this leads to a synergistic effect on the mtDNA level and mtDNA copy number further increased. mRNA concentrations are comparable to strains with only *MIP1* or *ABF2* under the *HTB1* promoter (Fig. 3.13a-b).

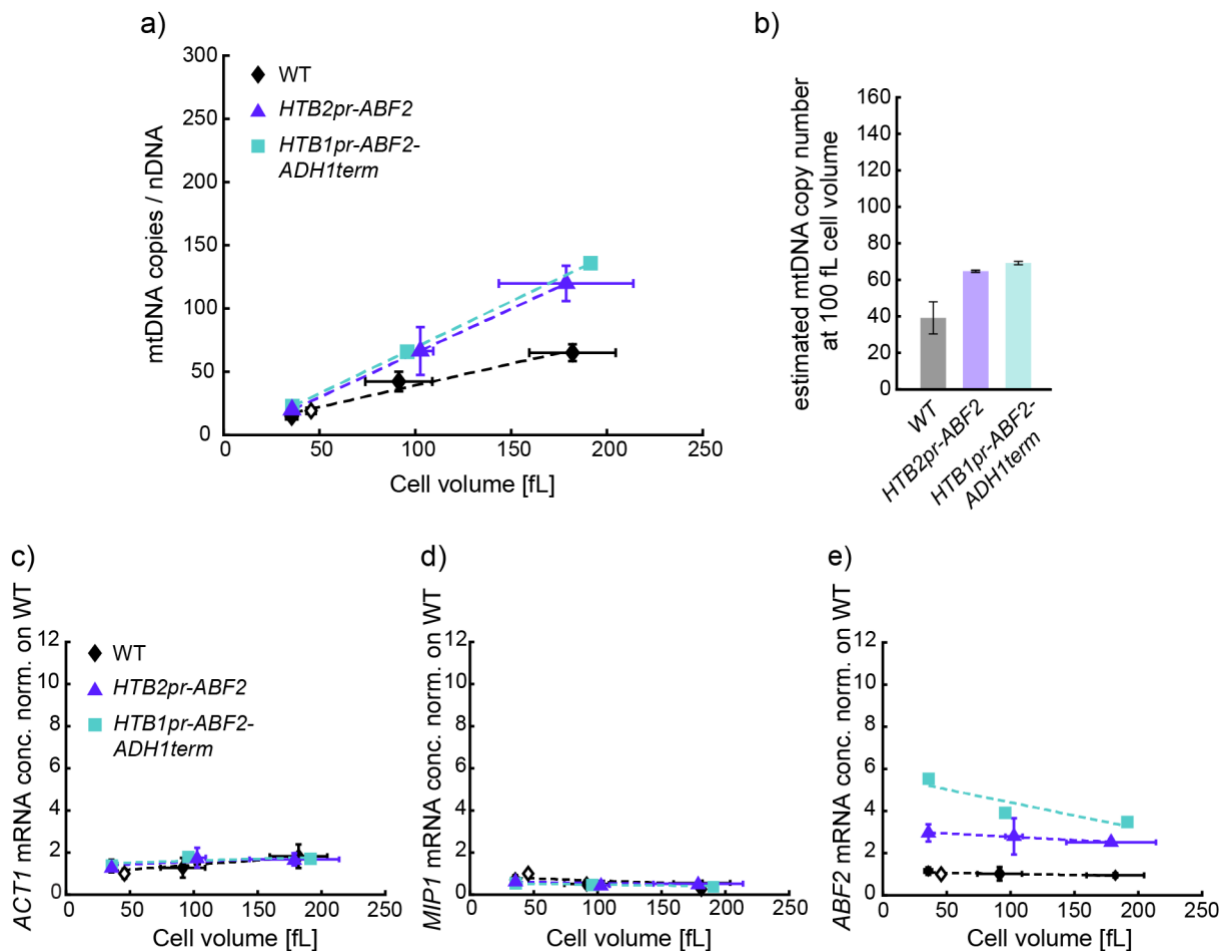


Figure 3.14: Histone promoter leads to overexpression of Abf2 causing increased mtDNA copy numbers. **a)** mtDNA with increasing cell sizes for Abf2 expressed from the *HTB1* or *HTB2* promoter, with either endogenous terminator, or *ADH1* terminator. All promoter variants were only Whi5-inducible and grown in the absence or presence of β -estradiol, except of wild-type (open diamond). mtDNA copy number was determined by DNA-qPCR. Wild-type data are the same as in Fig. 3.13. Error bars indicate the standard deviation. **b)** Estimated mtDNA copy number at 100 fL cell volume. mtDNA copy number was estimated from the linear fit. Error bars indicate estimated standard errors from the linear fit at 100 fL. **c-e)** mRNA concentrations for *ACT1*, *MIP1* and *ABF2* in same cultures as in a). Note that data points for *HTB1pr-ABF2-ADH1term* contains only 1 biological replicate, data points for *HTB1pr-ABF2* +

Error! Use the Home tab to apply Überschrift 1 to the text that you want to appear here.

HTB1pr-MIP1 and *HTB2pr-ABF2* contain two, and wild-type contains three biological replicates. Fits show trendlines through the data points and error bars indicate standard deviation.

Besides the fact that histone promoters alone seem not to be sufficient to express Mip1 and Abf2 at a constant amount, these data suggest that mtDNA copy number can be increased by overexpressing Mip1 and Abf2, respectively. In fact, even higher effects on the copy number were observed when overexpressing both together. This further supports the theory that Mip1 and Abf2 together set mtDNA copy number, and that mtDNA synthesis is limited by the mtDNA replication machinery.

3.11. Mip1 and Abf2 together can upregulate mtDNA copy number

Expression from histone promoters leads to overexpression of Mip1 and Abf2, resulting in increased mtDNA copy numbers, especially when both proteins are overexpressed together. To validate the observations, Mip1 and Abf2 were overexpressed in a more predictable way, independent of the histone promoter. More precisely, additional gene copies of both proteins were inserted into a haploid wild-type strain, to double the respective protein concentration (Fig. 3.15a). By performing DNA-qPCR, mtDNA copy number was determined.

mtDNA concentration of the non-inducible strains shows an increase to ~15% for Mip1 and to ~27% for Abf2 compared to wild-type (Fig. 3.15b). To prove that additional gene copies increase expression of *MIP1* and *ABF2* by 2-fold, total RNA extractions and RT-qPCR were performed. *ACT1* as a control gene was kept at the same concentration for all strains, while the strains with additional copies of *MIP1* and *ABF2* each had double the amount of mRNA (Fig. 3.15d-f).

The histone promoter experiments have shown that *MIP1* and *ABF2* together have a significantly stronger effect on mtDNA copies than alone. This led to the assumption that most likely more than one protein alone limits the mtDNA copy number. In order to show that this effect also occurs independently of the histone promoters, both proteins were transformed together into one strain. Again, increased expression of both proteins by 2-fold was confirmed on mRNA level by RT-qPCR (Fig. 3.15d-f). DNA-qPCR revealed that mtDNA concentration increases to ~55% (Fig. 3.15b). The experiments were repeated in a *Whi5*-inducible strain and are showing a linear increase of mtDNA copies with cell size as observed for non-induced cells (Fig. 3.15c). However, no additional size effect was observed.

In conclusion, Mip1 and Abf2 together limit mtDNA copy number. However, the fact that an increase by 2-fold is not reached indicates that besides Abf2 and Mip1, more factors are limiting mtDNA copy number.

Error! Use the Home tab to apply Überschrift 1 to the text that you want to appear here.

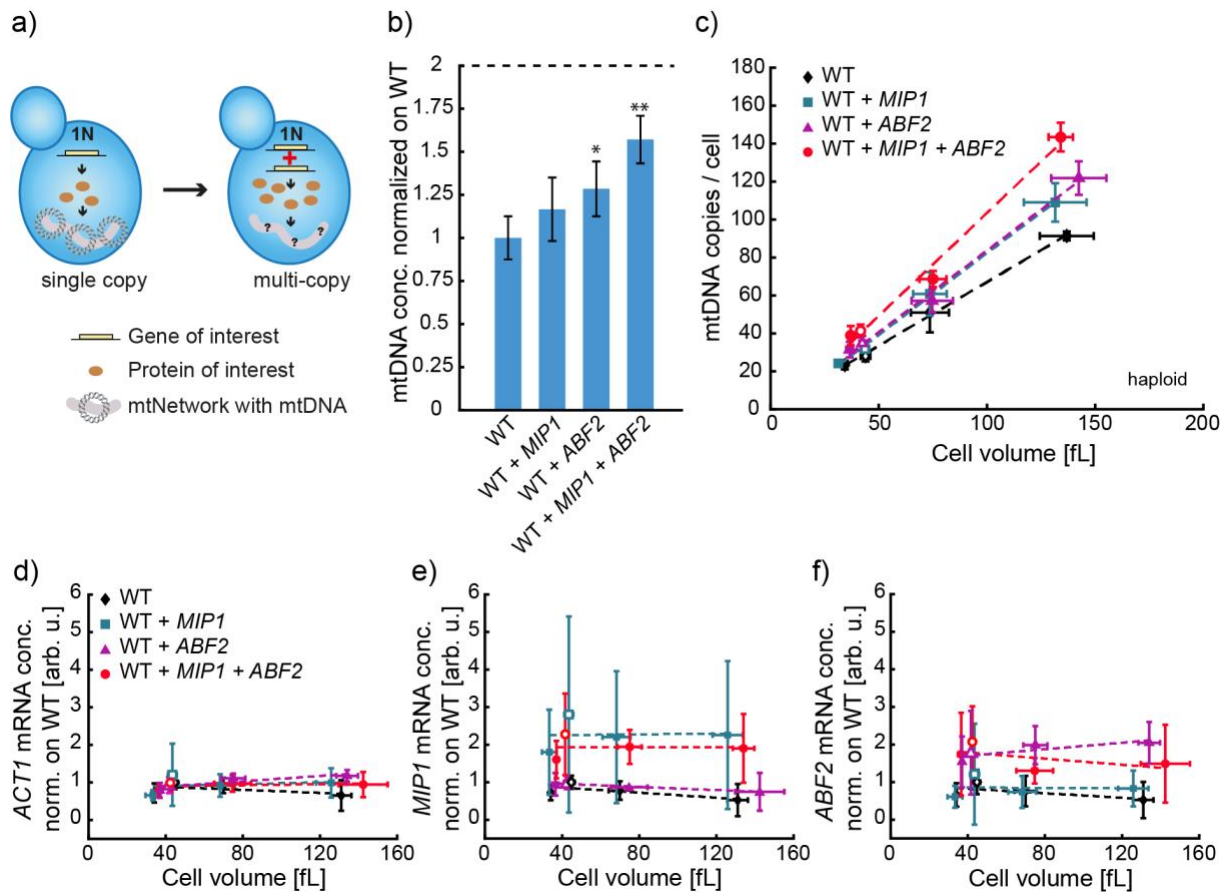


Figure 3.15: Higher concentrations of MIP1 and ABF2 increase mtDNA alone and together. **a)** In haploid non-inducible and Whi5-inducible strains additional copies of *MIP1* and *ABF2* were inserted, aiming the increase of protein concentration by 2-fold. **b)** mtDNA concentration for non-inducible multi-copy strains normalized on wild-type. Significances were determined by a two-tailed t-test (* $p < 0.05$, ** $p < 0.01$, *** $p < 0.001$) **c)** mtDNA copies in multi-copy strains as a function of cell volume. Non-inducible (open symbols) and Whi5-inducible strains (filled symbols). **d-f)** mRNA concentrations for *ACT1*, *MIP1* and *ABF2* for same cultures as in c). Error bars indicate standard deviation of at least three biological replicates.

4. Discussion

The question of how the mtDNA is regulated during cell cycle has been asked frequently in the past years, but a mechanism has not been identified (Petes and Fangman 1973, Newlon and Fangman 1975, Conrad and Newlon 1982). Neither for the mitochondrial network nor for the mtDNA a clear coupling to the cell cycle was identified so far. Instead, increasing evidence suggests that cell size could be an important regulator for mitochondrial content. For both, the mitochondrial network volume and the number of nucleoids an increase with cell volume was observed in recent studies (Rafelski et al. 2012, Jajoo et al. 2016). How exactly cell volume affects mitochondrial content, especially mtDNA copy number, and the mechanism potentially responsible for this, was investigated in this study. In fact, this work identified the cell volume as the main regulator of mtDNA, independently of cell cycle progression. By providing increased amounts of mtDNA maintenance factors during cell growth, cells ensure stable steady state mtDNA concentrations. Thus, coupling mtDNA homeostasis to cell volume is an elegant mechanism to keep mtDNA copy number constant during cell growth, without the necessity of cell cycle-dependent regulation.

4.1. Cell volume regulates mitochondrial biogenesis

To assess the direct influence of cell size on mtDNA, cell size was manipulated and mtDNA was examined within differently sized cell populations. The results clearly show that mtDNA copy number increases roughly in linear proportion with cell volume (Fig. 3.1b). Moreover, cell volume regulates mtDNA copy number maintenance during G1 arrest (Fig. 3.2b), which is consistent with early work in budding yeast (Newlon and Fangman 1975, Conrad and Newlon 1982). Many studies aimed to show a coupling of mtDNA copy number with cell cycle. However most of these studies neglected cell size as an important regulator for mtDNA copy number (Sasaki et al. 2017). Thereby, increases in mtDNA copy number were assigned to specific cell cycle phases rather than to increasing cell size. The findings in this study suggest that mtDNA synthesis rather occurs independent of cell cycle progression in budding yeast. This observation does not exclude cell cycle modulated mtDNA synthesis, as observed in human cells (Sasaki et al. 2017). However, it supports the hypothesis that mtDNA replication occurs throughout the cell cycle and that cell size is a key regulator of mtDNA copy number.

To overcome the limitations of qPCR which only allows the analysis of bulk cell populations, a recently established method based on live-cell imaging was used (Osman et al. 2015). This allowed the analysis of the number of nucleoids and mitochondrial network volume on the single cell level. Nucleoids are nucleoprotein complexes which consist of ~1-2 mtDNA copies

Error! Use the Home tab to apply Überschrift 1 to the text that you want to appear here.

(Miyakawa et al. 2004) and several mtDNA binding proteins. Similar to the increase of mtDNA copies the number of nucleoids is increasing in linear proportion with cell volume (Fig 3.3c). Remarkably, even under fermenting conditions where mtDNA is not essential, mtDNA and the number of nucleoids increase with cell volume. However, at given cell volumes the mtDNA copy number is lower compared to non-fermenting conditions.

Similar to the mtDNA, the mitochondrial network volume increases in linear proportion with cell volume (Fig. 3.3d) which is in agreement with recent data (Rafelski et al. 2012). Additionally, the mitochondrial network volume is increasing independently of mtDNA. Even though the mitochondrial network volume increases with cell volume, the mitochondrial diameter is independent of cell volume, for both fermenting and non-fermenting conditions (Fig 3.5a). When investigating the number of nucleoids per network volume it has been observed that the concentration of nucleoids per network volume was shown to be roughly independent of cell volume. Thus, cell size was identified as the key regulator for mtDNA copy number and mitochondrial network volume with cell growth, even under nutrient conditions when mtDNA is not essential.

4.2. mtDNA copy number maintenance during cell growth relies on increased expression of mtDNA maintenance factors

So far this study has shown that mtDNA and the mitochondrial network volume increase with cell volume. Previous studies have shown that the global transcription and translation is dependent on cell volume (Wu et al. 2010, Padovan-Merhar et al. 2015). Thus, the overall amount of mRNA and proteins increases during cell growth. Additionally, mitochondrial mass and global transcription rate seem to be coupled (das Neves et al. 2010). As most of the mitochondrial biogenesis factors are encoded by the nuclear genome, it is very likely that the global increase of expression during cell growth also applies for mitochondrial biogenesis factors. Thus, simply the increase of mitochondrial biogenesis factors can lead to more mitochondrial content in bigger cells. As a next step, this hypothesis was tested by examining mRNA and protein levels of mitochondrial biogenesis factors in dependence of cell volume. Indeed, selected factors increase in amount on mRNA level with increasing cell volume (Fig. 3.6b). Strikingly, the data provided in this study are supported by RNA-sequencing data acquired by Swaffer et al. (Swaffer et al. 2021). There it is shown that the concentration of mitochondrial maintenance factors increases comparable to that of the housekeeping genes Actin or RNA-Polymerase II, whereas the concentration of histones decreases in big cells. Overall, the data support the hypothesis that global expression leads to more mitochondrial content in larger cells. In order to test whether that this is indeed the case on the protein level,

Error! Use the Home tab to apply Überschrift 1 to the text that you want to appear here.

flow cytometry was performed for the mtDNA polymerase Mip1 and the histone-like protein Abf2. Both proteins are essential for mtDNA maintenance and were tagged with the fluorophore mCitrine. For both proteins an increase with cell volume was observed (Fig. 3.7a-b). Additionally, data generated by Parts et al. (Parts et al. 2014) and published in Swaffer et al. 2021, show that GFP-tagged mitochondrial biogenesis factors are as well coupled to cell volume in budding yeast. Similar observations were made in human epithelial cells where several mitochondrial proteins also increase with cell volume (Lanz et al. 2021). Thus, mitochondrial maintenance factors are likely regulated with global protein expression. This suggests that the mtDNA maintenance machinery is coupled to cell volume and that the increase of mtDNA and nucleoids directly depends on the amount of mtDNA maintenance factors.

4.3. The synergy of Mip1 and Abf2 protein homeostasis regulates mtDNA copy number

If increasing levels of mtDNA maintenance factors indeed lead to more mtDNA, then decreasing protein concentrations should reduce mtDNA copy number. Indeed, by reducing the concentrations of several mitochondrial maintenance factors, three proteins were identified that exhibited a reduction in mtDNA copy number (Fig. 3.9b). Since there is no evidence for dosage compensation in budding yeast (Torres et al. 2016), it was assumed that knocking out a gene copy in a diploid strain would lead to a 50% reduction in protein concentration. Thus, a perfectly limiting factor should show a decrease in mtDNA copy number to 50% when the protein concentration is reduced to 50%. In this study, the strongest effect was observed for the mtDNA polymerase Mip1, the packaging factor Abf2, and the single-strand binding protein Rim1. However, none of the proteins studied showed the expected decrease in mtDNA to 50%, although dosage compensation for Abf2 and Mip1 at the mRNA level was excluded (Fig. 3.11c-e). The fact that none of the proteins showed the expected decrease of mtDNA to 50% raised the idea that potentially more than one protein is limiting.

To get a better understanding of how different factors potentially act together and limit mtDNA replication and maintenance, a minimal model based on Michaelis-Menten kinetics is introduced.

Error! Use the Home tab to apply Überschrift 1 to the text that you want to appear here.

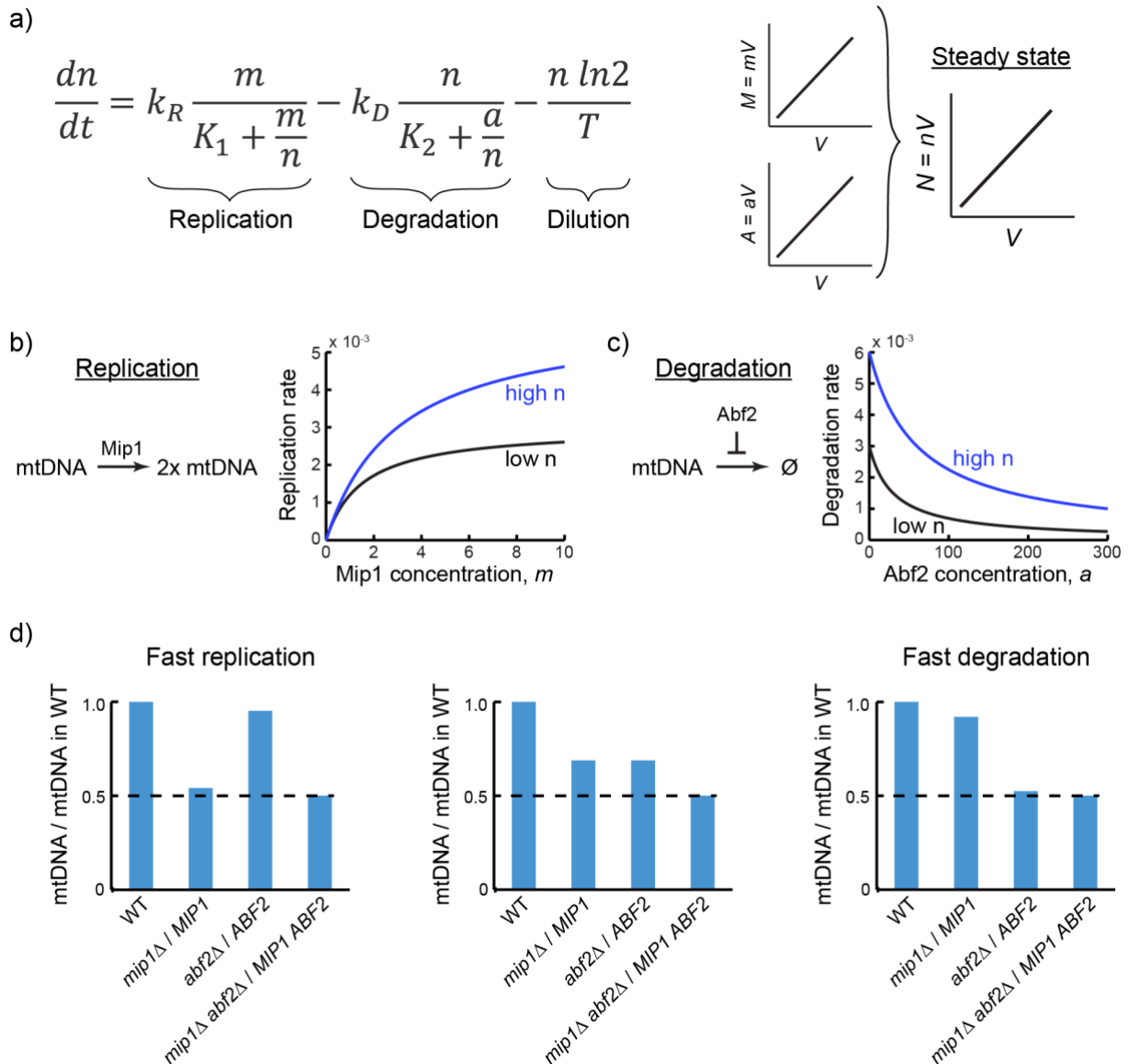


Figure 4.1: Mathematical model to represent the impact of replication and degradation on mtDNA. a) Change of mtDNA is depends on replication, degradation and dilution during cell growth. b) In this model replication is limited by either the Mip1 concentration, m , or by the mtDNA copy number, n , when all molecules are saturated by m . c) Degradation is negatively correlated with the concentration of Abf2. Increasing Abf2 concentrations lead to an exponential decay of the degradation rate. d) mtDNA modeled for hemizygous strains. For both, Mip1 (m) and Abf2 (a) a decrease in protein concentration by 50% was modeled. Depending on the constant values, the impact of a single hemizygote can vary between 50-100% of wild-type mtDNA. In contrast the outcome of the double hemizygote is independent of the chosen constants and is always reduced to 50%.

The model is confined to the two in this study identified limiting proteins Mip1 and Abf2. Mip1 and Abf2 function in the promotion of mtDNA replication or prevention of degradation, respectively. Thus, the rate of replication depends on the concentration of Mip1, m , and the concentration of mtDNA, n such that $\frac{dn}{dt} = k_R \frac{m}{K_1 + \frac{m}{n}}$. K_1 is the dissociation constant describing

Error! Use the Home tab to apply Überschrift 1 to the text that you want to appear here.

the propensity of Mip1 to dissociate from the mtDNA. Thus, the higher K_1 the more Mip1 reversibly dissociates from mtDNA. k_R describes the maximal rate of replication.

As Abf2 is the stabilizing factor for mtDNA, the rate of degradation is negatively correlated with the concentration of Abf2, a , resulting in $\frac{dn}{dt} = -k_D \frac{n}{K_2 + \frac{a}{n}}$. Again, K_2 and k_D are constants describing the dissociation of Abf2 from mtDNA and the rate of degradation, respectively. Cell growth was included by assuming dilution of mtDNA according to exponential growth. Combining replication, degradation and dilution results in $\frac{dn}{dt} = k_R \frac{m}{K_1 + \frac{m}{n}} - k_D \frac{n}{K_2 + \frac{a}{n}} - \frac{n \ln 2}{T}$. If steady state equilibrium is assumed, $\frac{dn}{dt} = 0$. Thereby the copy number of mtDNA is directly coupled to the concentrations of Mip1 and Abf2.

The model is implementing that the rate of replication depends on the Mip1 concentration, m . However, a low mtDNA copy number, n , would limit the impact of high Mip1 concentrations, as replication sites would be fully saturated at a certain Mip1 concentration (Fig. 4.1b). This assumption is also supported by the experimental overexpression of Mip1, which showed first an almost linear increase of mtDNA with increasing Mip1 concentrations, however, then ending in a plateau with a constant mtDNA copy number, independent of the Mip1 concentration (Fig. 3.12b-c). The degradation rate depends on the concentration of Abf2, a , and the higher a is the lower is the degradation rate. With the model the influence of the different protein concentrations for Mip1 and Abf2 on the mtDNA was hypothetically tested. Depending on the chosen constants for replication and degradation, the impact of a decrease in concentration to 50% of Mip1 or Abf2 can be modulated. At fast replication, Mip1 concentration is the limiting parameter for mtDNA copy number (Fig. 4.1d), whereas slow mtDNA replication would increase the impact of Abf2 concentration. Basically, in this model the outcome for the mtDNA in single hemizygotes strongly depends on the exact parameters. Regarding this, it was shown that the C-terminal mCitrine tag on Mip1 shifts the balance in favor of the mtDNA. A possible explanation for this observation could be an increased binding affinity to the mtDNA which leads to an increase in the polymerization rate and lowers the dissociation constant K_1 . Thus, the equilibrium is shifted towards mtDNA replication which underlines the dependence of this model on correct constants. However, as the exact values for the rates of degradation, replication and dissociation are not given, single hemizygotes are not suited to test the model. In contrast, for a double hemizygous strain in which one copy of both, Mip1 and Abf2 are deleted, the model predicts a decrease of the mtDNA copy number to 50% of wild-type levels, independent of the chosen parameters. Strikingly, in the double hemizygote *mip1Δ/MIP1 abf2Δ/ABF2* the mtDNA concentration further decreases to about 55% of the wild-type level (Fig. 3.11a), roughly matching the model prediction. This finding further supports the hypothesis that the concentration of several factors limits mtDNA homeostasis. In addition, the

Error! Use the Home tab to apply Überschrift 1 to the text that you want to appear here.

effect of the hemizygous deletions was predicted to be independent of cell volume. Again, the prediction was confirmed by experimental results showing for the single hemizygotes as well as the double hemizygote a similar reduction for all cell volumes.

To understand the effects of an overexpression of Mip1 and Abf2 on mtDNA, the effect on mtDNA copy number was modeled by assuming a 2-fold overexpression for both strains alone and in combination. The model predicts an increase of mtDNA by 2-fold, when both proteins are 2-fold overexpressed. In this case, the experimental data differ stronger from the prediction. An increase of mtDNA was observed, however not to the expected 2-fold (Fig. 3.14b). The histone promoter experiment also shows that the balance of the mtDNA copy number strongly depends on the expression of the respective factors Mip1 and Abf2. Here, as observed by the 2-fold overexpression, it becomes clear that an overexpression of the individual factors can already lead to an overproduction of the mtDNA, however, if both factors are present in excess at the same time mtDNA copy number is even higher. As described in the model, the replication by Mip1 is dependent on the number of mtDNA molecules. As soon as all free DNA molecules are occupied, no further synthesis can occur. However, if extra Abf2 stabilizes additional mtDNA molecules, Mip1 can continue to replicate. This in turn leads to further molecules that are stabilized by Abf2. The equilibrium is reached at the number of mtDNA molecules, where the concentration of at least one of the factors limits mtDNA homeostasis. This also implies that strong overexpression of single factors at a certain concentration does only weakly impact mtDNA copy number. Indeed, this was shown that upon 5-fold Mip1 overexpression the mtDNA concentration stops increasing (Fig. 3.12).

The restricted influence of Mip1 and Abf2 suggests that besides these proteins also other factors act limiting on mtDNA copy number. In this regard, all factors of the replication machinery are conceivable, such as Rim1, which has already shown an effect in the hemizygous screen. Thus, to gain further insight into the regulation of mtDNA and to test the hypothesis put forward here, Rim1 and other factors need to be tested. Besides the replication machinery, also the building blocks of mtDNA might can become limiting, such as dNTPs. It was shown that increased amounts of dNTPs seem to increase mtDNA copy number (Blázquez-Bermejo et al. 2019). Thus, a balanced availability of all factors and building blocks involved in the maintenance of mtDNA is necessary for mtDNA homeostasis.

4.4. mtDNA copy number is modulated by additional mechanisms

4.4.1. mtDNA copy number can be regulated by quality control mechanisms

Error! Use the Home tab to apply Überschrift 1 to the text that you want to appear here.

Maintaining a balanced mtDNA maintenance machinery during cell growth is proposed to be achieved by a constant increase of global expression induced by cell size. A major advantage of the mechanism proposed here, is that it allows for the regulation of mtDNA by additional mechanisms. For example, mechanisms important for mitochondrial quality control may also modulate mtDNA copy number, for example in response to heteroplasmy. In this context, it has been shown that reduction or deletion of Mrx6, a protein that may degrade factors of the mtDNA replication machinery (Göke et al., 2020), leads to a large increase in mtDNA copy number. In Fig. 3.10c, it was additionally shown that this effect is almost independent of cell size, meaning that mtDNA copy number in the *mrx6* Δ strain increases with cell size. This also shows that the regulation of mtDNA with cell volume persists.

Moreover, it was shown in this work that this effect is dose-dependent, i.e., the mtDNA depends on the Mrx6 concentration. In combination with the observations of the hemizygote screen and the multi-copy experiments, this means that the balance of all factors requires well balanced expression during cell growth. This is also shown by a recent study in which the incorrect distribution of mtDNA maintenance factors resulted in altered mtDNA replication and mtDNA nucleoid distribution (Ramos et al., 2019). Therefore, coupling mitochondrial maintenance factors to global expression represents the ideal mechanisms that makes cell size the basic regulator but also allows for other regulatory mechanisms.

4.4.2. mtDNA copy number is modulated by nutrients

In addition to quality control mechanisms, environmental changes, such as available carbon sources can affect mtDNA levels. Here, it was observed that fermenting cells had overall less mtDNA and nucleoids than non-fermenting cells (Fig. 3.1 - Fig. 3.3). The differences of mtDNA copy numbers in fermenting and non-fermenting conditions are in agreement with earlier findings (Ulery et al. 1994). This observation can be explained by the phenomenon of glucose-repression. Glucose-repression mainly affects the transcriptional level (Gancedo, 1998), potentially leading to reduced concentrations of mtDNA synthesis factors. For Abf2 and other factors (Rim1, Rpo41, Mtf1, Mhr1, Mgm101, Rad53) it has indeed been shown that the total protein copy number per cell is reduced during growth on glucose (Morgenstern et al. 2017). However, Mip1 and additional important factors (e.g. Pif1, Rrm3, Hmi1) have not been investigated. Thus, future studies should address the question of how the amount of these factors is influenced by the carbon source.

Also, the packaging of mtDNA copies appears to depend on the carbon source. Cells on fermentable medium contain ~0.5-1 copy of mtDNA per nucleoid more than cells on non-fermentable medium (Fig. 3.3f). This indicates an altered organization of nucleoids under

Error! Use the Home tab to apply Überschrift 1 to the text that you want to appear here.

fermenting and non-fermenting conditions. Potentially, the accessibility of mtDNA is not essential under fermenting conditions which allows an altered and denser packaging of mtDNA.

Similar to the mtDNA, the network volume is decreased in fermenting conditions. Data on mitochondrial network volume in different nutrient conditions are rare to find. However, in fission yeast it was found that the number of mitochondrial network fragments is reduced on high glucose levels, supporting the findings of this study (Zheng et al. 2019). Also Jurkat cells obtain a lower membrane potential in fermenting compared non-fermenting conditions, which might result from a reduced network volume (Miettinen and Björklund 2016). Interestingly, the mitochondrial diameter is larger for cells grown under fermenting conditions compared to non-fermenting conditions. Indeed, the data for non-fermenting conditions (~338 nm) are in agreement with a recent study where the diameter was determined to be ~360 nm. However, while the EM data in Fig. 3.5 show a significantly higher diameter on fermentable medium (~418 nm), Egner et al. did not find differences for fermentable medium compared to non-fermentable medium (~339 nm) (Egner et al. 2002). Based on these data, it cannot be clearly concluded whether the differences observed here are exclusively due to fermentation and respiration. However, the data clearly show that growth conditions can be an important factor for modulation of the mitochondrial diameter. A hypothetical explanation for the increased mitochondrial diameter in fermentable medium could be the altered function of the mitochondria during fermentation, where the mitochondrial membrane surface is less needed. As glycolysis is the main pathway of energy generation during fermentation, oxidative phosphorylation and therefore simply the membrane surface is less crucial for cellular metabolism. However, mitochondrial volume is essential as other processes continue to take place within the mitochondrial matrix. Thus, by increasing the mitochondrial diameter, potentially less membrane surface is needed.

The data highlight that the carbon source is an important modulator of the mitochondrial network and the mtDNA. Overall, the carbon source appears to adjust the initial level of mtDNA and network volume and also modulates the mitochondrial network morphology and the organization of nucleoids. It is also conceivable that other environmental influences, or for example ploidy (Fig. 3.3e), may lead to altered mtDNA organization and changes in mtDNA copy number. However, the underlying mechanism that provides stable steady state mtDNA copy number during cell growth remains the coupling to cell volume and the associated control of global expression.

Error! Use the Home tab to apply Überschrift 1 to the text that you want to appear here.

4.5. Further experimental validation of the proposed model is required

Overall, this work has shown that the cell volume, by controlling the expression levels of mitochondrial biogenesis factors, is the key regulator of mtDNA homeostasis. However, there are several questions that need further investigations. For example, this study hypothesizes that the coupling of the mtDNA replication machinery with cell growth is related to global expression. To further validate this assumption, a next step could be to uncouple the factors from global expression to observe the effects on mtDNA during cell growth. As shown in this study, histone promoters are not suitable for this purpose (Fig. 3.13; Fig. 3.14). However, expression could be controlled using an artificial promoter during cell growth.

Furthermore, it is hypothesized that besides Mip1 and Abf2, additional factors limit mtDNA copy number. Thus, components of the replication machinery, such as Rim1, need to be examined in combination with Mip1 and Abf2 in hemizygous and multicopy experiments. This will provide valuable information on the correctness of the model but also provides insights into the interplay of the different mtDNA maintenance factors and its influence on mtDNA copy number.

In addition, it would be highly interesting to gain insight into the actual impact of variations in mtDNA copy number on the metabolic activity. While evidence has been found for higher eukaryotes showing that abnormal mtDNA levels are associated with various disease patterns, little is known for budding yeast. However, even in higher eukaryotes, the impact of altered mtDNA copy numbers is not clear. Altered mtDNA copy numbers could arise upstream of a disease pattern and thus trigger a disease pattern, but could also arise downstream, due to altered metabolic processes. Therefore, the hemizygotes *mip1Δ/MIP1*, *abf2Δ/ABF2*, and the double hemizygote *mip1Δ/MIP1 abf2Δ/ABF2* described here could be used to observe the influence of altered mtDNA levels on metabolic activity, using a Seahorse assay (Divakaruni et al. 2014).

Regarding nutrient-dependence, it would be important to further investigate whether mtDNA levels depend on glucose concentrations, as has been observed for the transcription factor Mig1, which is involved in catabolite repression (Treitel and Carlson 1995). Therefore, studying the expression levels of mitochondrial biogenesis factors under fermenting and non-fermenting conditions with defined concentrations of the respective carbon source, could provide further information on the control of mtDNA synthesis by global protein expression. In this context, investigations of the nutrient-dependency of mtDNA copy number in yeast could provide further insights about the differences in mtDNA copies in tissues. Different tissues have very specific concentrations of mtDNA. This is probably due to different metabolic needs (Dickinson et al. 2013) and thus to the cell- and tissue-specific biogenesis of the OXPHOS system. This in turn is dependent on mtDNA expression (Kühl et al. 2017), which is why the mtDNA content in cells

Error! Use the Home tab to apply Überschrift 1 to the text that you want to appear here.

and tissues must be adjusted. Therefore, mtDNA copy number is finely regulated in a cell- and tissue-specific manner by a balance between replication and turnover. Budding yeast can help to understand this specific regulation, as cultivation under many different metabolic conditions is possible.

4.6. Regulation of mtDNA copy number with cell size is likely conserved across eukaryotes

The mechanism identified in this work proposes that the regulation of mtDNA copy number during cell growth is tightly linked to cell size. This is achieved by coupling global protein expression to cell size. By limiting the abundance of the mitochondrial replication machinery via the global transcription rate, a reproducible range of mtDNA copies is ensured during cell growth (Fig. 4.2). This allows for a cell cycle-independent regulation of mtDNA homeostasis. In addition, steady-state mtDNA copy number does not require an active feedback mechanism but is rather passively regulated due to the cell volume-dependent adjustment of the limiting machinery. This is in agreement with observations in fission yeast where the production of nucleoids appeared to be rather passively regulated (Jajoo et al. 2016).

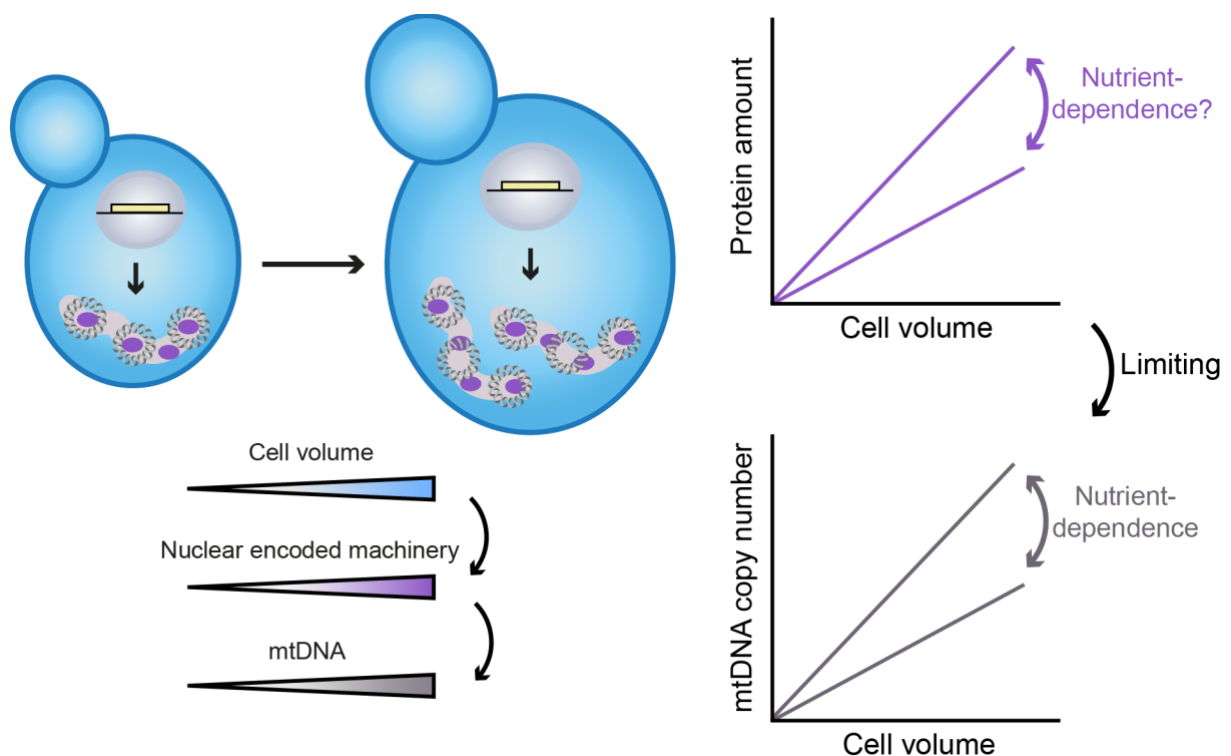


Figure 4.2: Illustration of mtDNA copy number homeostasis during cell growth by the limiting-machinery mechanism. Cell volume determines the amount of mitochondrial replication machinery, which can be modulated by the carbon source. The larger the cell volume, the more

Error! Use the Home tab to apply Überschrift 1 to the text that you want to appear here.

machinery is expressed. This leads to an increase in mtDNA copy number. Thus, mtDNA copy number is limited by the coupling of the mtDNA maintenance factors, such as Mip1 and Abf2, to global protein expression, which ensures mtDNA homeostasis during cell growth.

In this thesis, the advantages of budding yeast, such as its good fermenting capacity and easy genetic manipulability, were used to study strains lacking genes critical for the maintenance of mtDNA in differently sized cell populations. Moreover, the visualization of mtDNA in living yeast cells provided a major advantage since physiological conditions are maintained. In addition, the basic machinery of mtDNA replication between budding yeasts and higher eukaryotes is partly conserved (Shadel, 1999). Therefore, yeast is an excellent model organism to study the fundamental question of mtDNA homeostasis, and to improve the regulatory understanding in higher eukaryotes. It is very likely that the coupling of mtDNA copy number to cell volume is conserved across eukaryotes, but with variations in the core components of the limiting machinery. For example, the human replication machinery contains the mitochondrial helicase TWINKLE (Tynismaa et al. 2004), which has no homolog in yeast. However, TWINKLE as well as the Abf2 homolog TFAM (Larsson et al. 1998, Matsushima et al. 2003, Ekstrand et al. 2004) have a dose-dependent effect on mtDNA copy number in human cells. Moreover, in human epithelial cells, the amount of many mitochondrial proteins increases with increasing cell volume (Lanz et al. 2021), suggesting that the increase in global protein amounts is conserved widely across eukaryotes. Thus, the coupling of global protein expression to cell volume provides a robust mechanism to ensure mtDNA homeostasis during cell growth.

Bibliography

Allen JF. 1992. Protein phosphorylation in regulation of photosynthesis. *Biochimica et Biophysica Acta (BBA) - Bioenergetics* 1098: 275–335.

Allen JF. 2015. Why chloroplasts and mitochondria retain their own genomes and genetic systems: Colocation for redox regulation of gene expression. *Proceedings of the National Academy of Sciences* 112: 10231–10238.

Altmann K, Dürr M, Westermann B. 2007. *Saccharomyces cerevisiae* as a Model Organism to Study Mitochondrial Biology. Pages 81–90 in Leister D and Herrmann JM, eds. *Mitochondria*, vol. 372. Humana Press.

Anderson S, Bankier AT, Barrell BG, de Bruijn MHL, Coulson AR, Drouin J, Eperon IC, Nierlich DP, Roe BA, Sanger F, Schreier PH, Smith AJH, Staden R, Young IG. 1981. Sequence and organization of the human mitochondrial genome. *Nature* 290: 457–465.

Backert S, Dörfel P, Lurz R, Börner T. 1996. Rolling-circle replication of mitochondrial DNA in the higher plant *Chenopodium album* (L.). *Molecular and Cellular Biology* 16: 6285–6294.

Bahhir D, Yalgin C, Ots L, Järvinen S, George J, Naudí A, Krama T, Krams I, Tamm M, Andjelković A, Dufour E, González de Cózar JM, Gerardis M, Parhiala M, Pamplona R, Jacobs HT, Jöers P. 2019. Manipulating mtDNA in vivo reprograms metabolism via novel response mechanisms. *PLOS Genetics* 15: e1008410.

Bendich AJ. 1996. Structural Analysis of Mitochondrial DNA Molecules from Fungi and Plants Using Moving Pictures and Pulsed-field Gel Electrophoresis. *Journal of Molecular Biology* 255: 564–588.

Berk AJ, Clayton DA. 1974. Mechanism of mitochondrial DNA replication in mouse L-cells: Asynchronous replication of strands, segregation of circular daughter molecules, aspects of topology and turnover of an initiation sequence. *Journal of Molecular Biology* 86: 801–824.

Bertalanffy L. 1934. Untersuchungen über die Gesetzmäßigkeit des Wachstums: I. Teil: Allgemeine Grundlagen der Theorie; Mathematische und physiologische Gesetzmäßigkeiten des Wachstums bei Wassertieren. *Wilhelm Roux' Archiv für Entwicklungsmechanik der Organismen* 131: 613–652.

Björkholm P, Ernst AM, Hagström E, Andersson SGE. 2017. Why mitochondria need a genome revisited. *FEBS Letters* 591: 65–75.

Blázquez-Bermejo C, Carreño-Gago L, Molina-Granada D, Aguirre J, Ramón J, Torres-Torronteras J, Cabrera-Pérez R, Martín MÁ, Domínguez-González C, Cruz X, Lombès A, García-Arumí E, Martí R, Cámara Y. 2019. Increased dNTP pools rescue mtDNA depletion in

human POLG-deficient fibroblasts. *The FASEB Journal* 33: 7168–7179.

Bleeg HS, Bak AL, Christiansen C, Smith KE, Stenderup A. 1972. Mitochondrial DNA and glucose repression in yeast. *Biochemical and Biophysical Research Communications* 47: 524–530.

Brandt T, Mourier A, Tain LS, Partridge L, Larsson N-G, Kühlbrandt W. 2017. Changes of mitochondrial ultrastructure and function during ageing in mice and *Drosophila*. *eLife* 6: e24662.

Brewer LR, Friddle R, Noy A, Baldwin E, Martin SS, Corzett M, Balhorn R, Baskin RJ. 2003. Packaging of Single DNA Molecules by the Yeast Mitochondrial Protein Abf2p. *Biophysical Journal* 85: 2519–2524.

Burger G, Gray MW, Forget L, Lang BF. 2013. Strikingly Bacteria-Like and Gene-Rich Mitochondrial Genomes throughout Jakobid Protists. *Genome Biology and Evolution* 5: 418–438.

Busch KB, Kowald A, Spelbrink JN. 2014. Quality matters: how does mitochondrial network dynamics and quality control impact on mtDNA integrity? *Philosophical Transactions of the Royal Society B: Biological Sciences* 369: 20130442.

Carlson M. 1999. Glucose repression in yeast. *Current Opinion in Microbiology* 2: 202–207.

Chan Y-HM, Marshall WF. 2010. Scaling properties of cell and organelle size. *Organogenesis* 6: 88–96.

Chan Y-HM, Reyes L, Sohail SM, Tran NK, Marshall WF. 2016. Organelle Size Scaling of the Budding Yeast Vacuole by Relative Growth and Inheritance. *Current Biology* 26: 1221–1228.

Chen H, Vermulst M, Wang YE, Chomyn A, Prolla TA, McCaffery JM, Chan DC. 2010. Mitochondrial Fusion Is Required for mtDNA Stability in Skeletal Muscle and Tolerance of mtDNA Mutations. *Cell* 141: 280–289.

Chen X, Prosser R, Simonetti S, Sadlock J, Jagiello G, Schon EA. 1995. Rearranged mitochondrial genomes are present in human oocytes. *American Journal of Human Genetics* 57: 239–247.

Chen XJ, Butow RA. 2005. The organization and inheritance of the mitochondrial genome. *Nature Reviews Genetics* 6: 815–825.

Chen XJ, Clark-Walker GD. 2018. Unveiling the mystery of mitochondrial DNA replication in yeasts. *Mitochondrion* 38: 17–22.

Cho JH, Ha SJ, Kao LR, Megraw TL, Chae C-B. 1998. A Novel DNA-Binding Protein Bound to the Mitochondrial Inner Membrane Restores the Null Mutation of Mitochondrial Histone

- Abf2p in *Saccharomyces cerevisiae*. *Molecular and Cellular Biology* 18: 5712–5723.
- Claude K-L, Bureik D, Chatzitheodoridou D, Adarska P, Singh A, Schmoller KM. 2021. Transcription coordinates histone amounts and genome content. *Nature Communications* 12: 4202.
- Clay Montier LL, Deng JJ, Bai Y. 2009. Number matters: control of mammalian mitochondrial DNA copy number. *Journal of Genetics and Genomics* 36: 125–131.
- Collart MA, Oliviero S. 1993. Preparation of Yeast RNA. *Current Protocols in Molecular Biology* 23.
- Conrad MN, Newlon CS. 1982. The regulation of mitochondrial DNA levels in *Saccharomyces cerevisiae*. *Current Genetics* 6: 147–152.
- Contamine V, Picard M. 2000. Maintenance and Integrity of the Mitochondrial Genome: a Plethora of Nuclear Genes in the Budding Yeast. *Microbiology and Molecular Biology Reviews* 64: 281–315.
- Crider DG, García-Rodríguez LJ, Srivastava P, Peraza-Reyes L, Upadhyaya K, Boldogh IR, Pon LA. 2012. Rad53 is essential for a mitochondrial DNA inheritance checkpoint regulating G1 to S progression. *Journal of Cell Biology* 198: 793–798.
- Decker M, Jaensch S, Pozniakovsky A, Zinke A, O'Connell KF, Zachariae W, Myers E, Hyman AA. 2011. Limiting Amounts of Centrosome Material Set Centrosome Size in *C. elegans* Embryos. *Current Biology* 21: 1259–1267.
- D'Erchia AM, Atlante A, Gadaleta G, Pavesi G, Chiara M, De Virgilio C, Manzari C, Mastropasqua F, Prazzoli GM, Picardi E, Gissi C, Horner D, Reyes A, Sbisà E, Tullo A, Pesole G. 2015. Tissue-specific mtDNA abundance from exome data and its correlation with mitochondrial transcription, mass and respiratory activity. *Mitochondrion* 20: 13–21.
- Dickinson A, Yeung KY, Donoghue J, Baker MJ, Kelly RD, McKenzie M, Johns TG, St. John JC. 2013. The regulation of mitochondrial DNA copy number in glioblastoma cells. *Cell Death & Differentiation* 20: 1644–1653.
- Diffley JF, Stillman B. 1991. A close relative of the nuclear, chromosomal high-mobility group protein HMG1 in yeast mitochondria. *Proceedings of the National Academy of Sciences* 88: 7864–7868.
- Diffley JF, Stillman B. 1992. DNA binding properties of an HMG1-related protein from yeast mitochondria. *The Journal of Biological Chemistry* 267: 3368–3374.
- Divakaruni AS, Paradyse A, Ferrick DA, Murphy AN, Jastroch M. 2014. Analysis and Interpretation of Microplate-Based Oxygen Consumption and pH Data. Pages 309–354 in. *Methods in Enzymology*, vol. 547. Elsevier.

- Doudican NA, Song B, Shadel GS, Doetsch PW. 2005. Oxidative DNA Damage Causes Mitochondrial Genomic Instability in *Saccharomyces cerevisiae*. *Molecular and Cellular Biology* 25: 5196–5204.
- Egner A, Jakobs S, Hell SW. 2002. Fast 100-nm resolution three-dimensional microscope reveals structural plasticity of mitochondria in live yeast. *Proceedings of the National Academy of Sciences* 99: 3370–3375.
- Ekstrand MI, Falkenberg M, Rantanen A, Park CB, Gaspari M, Hultenby K, Rustin P, Gustafsson CM, Larsson N-G. 2004. Mitochondrial transcription factor A regulates mtDNA copy number in mammals. *Human Molecular Genetics* 13: 935–944.
- Ewald JC, Kuehne A, Zamboni N, Skotheim JM. 2016. The Yeast Cyclin-Dependent Kinase Routes Carbon Fluxes to Fuel Cell Cycle Progression. *Molecular Cell* 62: 532–545.
- Fangman WL, Henly JW, Brewer BJ. 1990. RPO41-independent maintenance of [rho-] mitochondrial DNA in *Saccharomyces cerevisiae*. *Molecular and Cellular Biology* 10: 10–15.
- Farge G, Falkenberg M. 2019. Organization of DNA in Mammalian Mitochondria. *International Journal of Molecular Sciences* 20: 2770.
- Filograna R, Koolmeister C, Upadhyay M, Pajak A, Clemente P, Wibom R, Simard ML, Wredenberg A, Freyer C, Stewart JB, Larsson NG. 2019. Modulation of mtDNA copy number ameliorates the pathological consequences of a heteroplasmic mtDNA mutation in the mouse. *Science Advances* 5: eaav9824.
- Foury F, Roganti T, Lecrenier N, Purnelle B. 1998. The complete sequence of the mitochondrial genome of *Saccharomyces cerevisiae*. *FEBS Letters* 440: 325–331.
- Foury F, Vanderstraeten S. 1992. Yeast mitochondrial DNA mutators with deficient proofreading exonucleolytic activity. *The EMBO Journal* 11: 2717–2726.
- Gabaldón T, Huynen MA. 2007. From Endosymbiont to Host-Controlled Organelle: The Hijacking of Mitochondrial Protein Synthesis and Metabolism. *PLOS Computational Biology* 3: e219.
- Gancedo JM. 1998. Yeast Carbon Catabolite Repression. *Microbiology and Molecular Biology Reviews* 62: 334–361.
- Genga A, Bianchi L, Foury F. 1986. A nuclear mutant of *Saccharomyces cerevisiae* deficient in mitochondrial DNA replication and polymerase activity. *The Journal of Biological Chemistry* 261: 9328–9332.
- Goehring NW, Hyman AA. 2012. Organelle Growth Control through Limiting Pools of Cytoplasmic Components. *Current Biology* 22: R330–R339.

- Göke A, Schrott S, Mizrak A, Belyy V, Osman C, Walter P. 2020. Mrx6 regulates mitochondrial DNA copy number in *Saccharomyces cerevisiae* by engaging the evolutionarily conserved Lon protease Pim1. *Molecular Biology of the Cell* 31: 527–545.
- Good MC, Vahey MD, Skandarajah A, Fletcher DA, Heald R. 2013. Cytoplasmic Volume Modulates Spindle Size During Embryogenesis. *Science* 342: 856–860.
- Grady JP, Pickett SJ, Ng YS, Alston CL, Blakely EL, Hardy SA, Feeney CL, Bright AA, Schaefer AM, Gorman GS, McNally RJ, Taylor RW, Turnbull DM, McFarland R. 2018. mt DNA heteroplasmy level and copy number indicate disease burden in m.3243A>G mitochondrial disease. *EMBO Molecular Medicine* 10.
- Gurdon JB, Partington GA, De Robertis EM. 1976. Injected nuclei in frog oocytes: RNA synthesis and protein exchange. *Journal of Embryology and Experimental Morphology* 36: 541–553.
- Hance N, Ekstrand MI, Trifunovic A. 2005. Mitochondrial DNA polymerase gamma is essential for mammalian embryogenesis. *Human Molecular Genetics* 14: 1775–1783.
- Hara Y, Kimura A. 2009. Cell-Size-Dependent Spindle Elongation in the *Caenorhabditis elegans* Early Embryo. *Current Biology* 19: 1549–1554.
- Harner M, Körner C, Walther D, Mokranjac D, Kaesmacher J, Welsch U, Griffith J, Mann M, Reggiori F, Neupert W. 2011. The mitochondrial contact site complex, a determinant of mitochondrial architecture: Molecular architecture of mitochondria. *The EMBO Journal* 30: 4356–4370.
- Hazel J, Krutkramelis K, Mooney P, Tomschik M, Gerow K, Oakey J, Gatlin JC. 2013. Changes in Cytoplasmic Volume Are Sufficient to Drive Spindle Scaling. *Science* 342: 853–856.
- Hori A, Yoshida M, Ling F. 2011. Mitochondrial fusion increases the mitochondrial DNA copy number in budding yeast: Mitochondrial fusion increases mtDNA copy number. *Genes to Cells* 16: 527–544.
- Hori A, Yoshida M, Shibata T, Ling F. 2009. Reactive oxygen species regulate DNA copy number in isolated yeast mitochondria by triggering recombination-mediated replication. *Nucleic Acids Research* 37: 749–761.
- Inoue H, Nojima H, Okayama H. 1990. High efficiency transformation of *Escherichia coli* with plasmids. *Gene* 96: 23–28.
- Jajoo R, Jung Y, Huh D, Viana MP, Rafelski SM, Springer M, Paulsson J. 2016. Accurate concentration control of mitochondria and nucleoids. *Science* 351: 169–172.
- Jakubke C, Roussou R, Maiser A, Schug C, Thoma F, Bunk D, Hörl D, Leonhardt H, Walter P, Klecker T, Osman C. 2021. Cristae-dependent quality control of the mitochondrial genome.

Science Advances 7: eabi8886.

Jemt E, Persson Ö, Shi Y, Mehmedovic M, Uhler JP, Dávila López M, Freyer C, Gustafsson CM, Samuelsson T, Falkenberg M. 2015. Regulation of DNA replication at the end of the mitochondrial D-loop involves the helicase TWINKLE and a conserved sequence element. *Nucleic Acids Research* 43: 9262–9275.

Jorgensen P, Edgington NP, Schneider BL, Rupeš I, Tyers M, Futcher B. 2007. The Size of the Nucleus Increases as Yeast Cells Grow. *Molecular Biology of the Cell* 18: 3523–3532.

Kitami T, Logan DJ, Negri J, Hasaka T, Tolliday NJ, Carpenter AE, Spiegelman BM, Mootha VK. 2012. A Chemical Screen Probing the Relationship between Mitochondrial Content and Cell Size. *PLOS ONE* 7: e33755.

Kühl I, Miranda M, Atanassov I, Kuznetsova I, Hinze Y, Mourier A, Filipovska A, Larsson N-G. 2017. Transcriptomic and proteomic landscape of mitochondrial dysfunction reveals secondary coenzyme Q deficiency in mammals. *eLife* 6: e30952.

Kukat C, Davies KM, Wurm CA, Spähr H, Bonekamp NA, Kühl I, Joos F, Polosa PL, Park CB, Posse V, Falkenberg M, Jakobs S, Kühlbrandt W, Larsson N-G. 2015. Cross-strand binding of TFAM to a single mtDNA molecule forms the mitochondrial nucleoid. *Proceedings of the National Academy of Sciences* 112: 11288–11293.

Kukat C, Wurm CA, Spahr H, Falkenberg M, Larsson N-G, Jakobs S. 2011. Super-resolution microscopy reveals that mammalian mitochondrial nucleoids have a uniform size and frequently contain a single copy of mtDNA. *Proceedings of the National Academy of Sciences* 108: 13534–13539.

Kukhtevich IV, Lohrberg N, Padovani F, Schneider R, Schmoller KM. 2020. Cell size sets the diameter of the budding yeast contractile ring. *Nature Communications* 11: 2952.

Lanz MC, Zatulovskiy E, Swaffer MP, Zhang L, Zhang S, You DS, Marinov G, McAlpine P, Elias JE, Skotheim JM. 2021. Increasing cell size remodels the proteome and promotes senescence. *bioRxiv*, DOI: 10.1101/2021.07.29.454227.

Larsson N-G, Wang J, Wilhelmsson H, Oldfors A, Rustin P, Lewandoski M, Barsh GS, Clayton DA. 1998. Mitochondrial transcription factor A is necessary for mtDNA maintenance and embryogenesis in mice. *Nature Genetics* 18: 231–236.

Lee S, Kim S, Sun X, Lee J-H, Cho H. 2007. Cell cycle-dependent mitochondrial biogenesis and dynamics in mammalian cells. *Biochemical and Biophysical Research Communications* 357: 111–117.

Lemasters JJ. 2007. Modulation of mitochondrial membrane permeability in pathogenesis, autophagy and control of metabolism. *Journal of Gastroenterology and Hepatology* 22: S31–

S37.

Lewis SC, Joers P, Willcox S, Griffith JD, Jacobs HT, Hyman BC. 2015. A Rolling Circle Replication Mechanism Produces Multimeric Lariats of Mitochondrial DNA in *Caenorhabditis elegans*. *PLOS Genetics* 11: e1004985.

Li CH, Tam PKS. 1998. An iterative algorithm for minimum cross entropy thresholding. *Pattern Recognition Letters* 19: 771–776.

Ling F. 2002. Recombination-dependent mtDNA partitioning: in vivo role of Mhr1p to promote pairing of homologous DNA. *The EMBO Journal* 21: 4730–4740.

Ling F, Hori A, Shibata T. 2007. DNA Recombination-Initiation Plays a Role in the Extremely Biased Inheritance of Yeast [*rho*⁻] Mitochondrial DNA That Contains the Replication Origin *ori5*. *Molecular and Cellular Biology* 27: 1133–1145.

Ling F, Hori A, Yoshitani A, Niu R, Yoshida M, Shibata T. 2013. Din7 and Mhr1 expression levels regulate double-strand-break–induced replication and recombination of mtDNA at *ori5* in yeast. *Nucleic Acids Research* 41: 5799–5816.

Ling F, Makishima F, Morishima N, Shibata T. 1995. A nuclear mutation defective in mitochondrial recombination in yeast. *The EMBO Journal* 14: 4090–4101.

Ling F, Yoshida M. 2020. Rolling-Circle Replication in Mitochondrial DNA Inheritance: Scientific Evidence and Significance from Yeast to Human Cells. *Genes* 11: 514.

Lisowsky T, Michaelis G. 1989. Mutations in the genes for mitochondrial RNA polymerase and a second mitochondrial transcription factor of *Saccharomyces cerevisiae*. *Molecular & general genetics: MGG* 219: 125–128.

Lucas P. 2004. Absence of accessory subunit in the DNA polymerase γ purified from yeast mitochondria. *Mitochondrion* 4: 13–20.

MacAlpine DM, Perlman PS, Butow RA. 1998. The high mobility group protein Abf2p influences the level of yeast mitochondrial DNA recombination intermediates in vivo. *Proceedings of the National Academy of Sciences* 95: 6739–6743.

Magnusson J. 2003. Replication of mitochondrial DNA occurs throughout the mitochondria of cultured human cells. *Experimental Cell Research* 289: 133–142.

Maleszka R, Skelly PJ, Clark-Walker GD. 1991. Rolling circle replication of DNA in yeast mitochondria. *The EMBO Journal* 10: 3923–3929.

Marguerat S, Bähler J. 2012. Coordinating genome expression with cell size. *Trends in Genetics* 28: 560–565.

Matsushima Y, Matsumura K, Ishii S, Inagaki H, Suzuki T, Matsuda Y, Beck K, Kitagawa Y.

2003. Functional Domains of Chicken Mitochondrial Transcription Factor A for the Maintenance of Mitochondrial DNA Copy Number in Lymphoma Cell Line DT40. *Journal of Biological Chemistry* 278: 31149–31158.
- Mbantenkhu M, Wang X, Nardozi JD, Wilkens S, Hoffman E, Patel A, Cosgrove MS, Chen XJ. 2011. Mgm101 is a Rad52-related protein required for mitochondrial DNA recombination. *The Journal of Biological Chemistry* 286: 42360–42370.
- Meeusen S, Nunnari J. 2003. Evidence for a two membrane-spanning autonomous mitochondrial DNA replisome. *The Journal of Cell Biology* 163: 503–510.
- Miettinen TP, Björklund M. 2016. Cellular Allometry of Mitochondrial Functionality Establishes the Optimal Cell Size. *Developmental Cell* 39: 370–382.
- Miyakawa I. 2017. Organization and dynamics of yeast mitochondrial nucleoids. *Proceedings of the Japan Academy, Series B* 93: 339–359.
- Miyakawa I, Miyamoto M, Kuroiwa T, Sando N. 2004. DNA Content of Individual Mitochondrial Nucleoids Varies Depending on the Culture Conditions of the Yeast *Saccharomyces cerevisiae*. *CYTOLOGIA* 69: 101–107.
- Morgenstern M, Stiller SB, Lübbert P, Peikert CD, Dannenmaier S, Drepper F, Weill U, Höß P, Feuerstein R, Gebert M, Bohnert M, van der Laan M, Schuldiner M, Schütze C, Oeljeklaus S, Pfanner N, Wiedemann N, Warscheid B. 2017. Definition of a High-Confidence Mitochondrial Proteome at Quantitative Scale. *Cell Reports* 19: 2836–2852.
- Muellner J, Schmidt KH. 2020. Yeast Genome Maintenance by the Multifunctional PIF1 DNA Helicase Family. *Genes* 11: 224.
- Nass S, Nass MMK. 1963. Intramitochondrial Fibres with DNA Characteristics. *Journal of Cell Biology* 19: 613–629.
- das Neves RP, Jones NS, Andreu L, Gupta R, Enver T, Iborra FJ. 2010. Connecting Variability in Global Transcription Rate to Mitochondrial Variability. *PLOS Biology* 8: e1000560.
- Newlon CS, Fangman WL. 1975. Mitochondrial DNA synthesis in cell cycle mutants of *Saccharomyces cerevisiae*. *Cell* 5: 423–428.
- Newman JRS, Ghaemmaghami S, Ihmels J, Breslow DK, Noble M, DeRisi JL, Weissman JS. 2006. Single-cell proteomic analysis of *S. cerevisiae* reveals the architecture of biological noise. *Nature* 441: 840–846.
- Newman S. 1996. Analysis of mitochondrial DNA nucleoids in wild-type and a mutant strain of *Saccharomyces cerevisiae* that lacks the mitochondrial HMG box protein Abf2p. *Nucleic Acids Research* 24: 386–393.

- Nicolson GL. 2014. Mitochondrial Dysfunction and Chronic Disease: Treatment With Natural Supplements. *Integrative Medicine (Encinitas, Calif.)* 13: 35–43.
- Nolfi-Donagan D, Braganza A, Shiva S. 2020. Mitochondrial electron transport chain: Oxidative phosphorylation, oxidant production, and methods of measurement. *Redox Biology* 37: 101674.
- Nunnari J, Marshall WF, Straight A, Murray A, Sedat JW, Walter P. 1997. Mitochondrial transmission during mating in *Saccharomyces cerevisiae* is determined by mitochondrial fusion and fission and the intramitochondrial segregation of mitochondrial DNA. *Molecular Biology of the Cell* 8: 1233–1242.
- Ono T, Isobe K, Nakada K, Hayashi J-I. 2001. Human cells are protected from mitochondrial dysfunction by complementation of DNA products in fused mitochondria. *Nature Genetics* 28: 272–275.
- Osman C, Noriega TR, Okreglak V, Fung JC, Walter P. 2015. Integrity of the yeast mitochondrial genome, but not its distribution and inheritance, relies on mitochondrial fission and fusion. *Proceedings of the National Academy of Sciences* 112: E947–E956.
- Ottoz DSM, Rudolf F, Stelling J. 2014. Inducible, tightly regulated and growth condition-independent transcription factor in *Saccharomyces cerevisiae*. *Nucleic Acids Research* 42: e130–e130.
- Padovani F, Mairhormann B, Falter-Braun P, Lengefeld J, Schmoller KM. 2021. Cell-ACDC: a user-friendly toolset embedding state-of-the-art neural networks for segmentation, tracking and cell cycle annotations of live-cell imaging data. *bioRxiv*, DOI: 10.1101/2021.09.28.462199.
- Padovan-Merhar O, Nair GP, Biaesch AG, Mayer A, Scarfone S, Foley SW, Wu AR, Churchman LS, Singh A, Raj A. 2015. Single mammalian cells compensate for differences in cellular volume and DNA copy number through independent global transcriptional mechanisms. *Molecular Cell* 58: 339–352.
- Parts L, Liu Y-C, Tekkedil MM, Steinmetz LM, Caudy AA, Fraser AG, Boone C, Andrews BJ, Rosebrock AP. 2014. Heritability and genetic basis of protein level variation in an outbred population. *Genome Research* 24: 1363–1370.
- Perkins EM, McCaffery JM. 2007. Conventional and Immunoelectron Microscopy of Mitochondria. Pages 467–483 in Leister D and Herrmann JM, eds. *Mitochondria*, vol. 372. Humana Press.
- Petes TD, Fangman WL. 1973. Preferential synthesis of yeast mitochondrial DNA in alpha factor-arrested cells. *Biochemical and Biophysical Research Communications* 55: 603–609.
- Pica-Mattoccia L, Attardi G. 1972. Expression of the mitochondrial genome in HeLa cells.

Journal of Molecular Biology 64: 465–484.

Posakony J, England J, Attardi G. 1977. Mitochondrial growth and division during the cell cycle in HeLa cells. *Journal of Cell Biology* 74: 468–491.

Rafelski SM, Viana MP, Zhang Y, Chan Y-HM, Thorn KS, Yam P, Fung JC, Li H, Costa L d. F, Marshall WF. 2012. Mitochondrial Network Size Scaling in Budding Yeast. *Science* 338: 822–824.

Ramanagoudr-Bhojappa R, Blair LP, Tackett AJ, Raney KD. 2013. Physical and functional interaction between yeast Pif1 helicase and Rim1 single-stranded DNA binding protein. *Nucleic Acids Research* 41: 1029–1046.

Ramos ES, Motori E, Brüser C, Kühl I, Yeroslaviz A, Ruzzenente B, Kauppila JHK, Busch JD, Hultenby K, Habermann BH, Jakobs S, Larsson N-G, Mourier A. 2019. Mitochondrial fusion is required for regulation of mitochondrial DNA replication. *PLOS Genetics* 15: e1008085.

Richardson HE, Wittenberg C, Cross F, Reed SI. 1989. An essential G1 function for cyclin-like proteins in yeast. *Cell* 59: 1127–1133.

Rickwood D, Chambers JAA, Barat M. 1981. Isolation and preliminary characterisation of DNA-protein complexes from the mitochondria of *Saccharomyces cerevisiae*. *Experimental Cell Research* 133: 1–13.

Roger AJ, Muñoz-Gómez SA, Kamikawa R. 2017. The Origin and Diversification of Mitochondria. *Current Biology* 27: R1177–R1192.

Sanchez-Sandoval E, Diaz-Quezada C, Velazquez G, Arroyo-Navarro LF, Almanza-Martinez N, Trasviña-Arenas CH, Brieba LG. 2015. Yeast mitochondrial RNA polymerase primes mitochondrial DNA polymerase at origins of replication and promoter sequences. *Mitochondrion* 24: 22–31.

Saraste M. 1999. Oxidative Phosphorylation at the *fin de siècle*. *Science* 283: 1488–1493.

Sasaki T, Sato Y, Higashiyama T, Sasaki N. 2017. Live imaging reveals the dynamics and regulation of mitochondrial nucleoids during the cell cycle in Fucci2-HeLa cells. *Scientific Reports* 7: 11257.

Sauer H, Wartenberg M, Hescheler J. 2001. Reactive Oxygen Species as Intracellular Messengers During Cell Growth and Differentiation. *Cellular Physiology and Biochemistry* 11: 173–186.

Scalettar BA, Abney JR, Hackenbrock CR. 1991. Dynamics, structure, and function are coupled in the mitochondrial matrix. *Proceedings of the National Academy of Sciences* 88: 8057–8061.

- Schindelin J, Arganda-Carreras I, Frise E, Kaynig V, Longair M, Pietzsch T, Preibisch S, Rueden C, Saalfeld S, Schmid B, Tinevez J-Y, White DJ, Hartenstein V, Eliceiri K, Tomancak P, Cardona A. 2012. Fiji: an open-source platform for biological-image analysis. *Nature Methods* 9: 676–682.
- Schmoller KM, Turner JJ, Kõivomägi M, Skotheim JM. 2015. Dilution of the cell cycle inhibitor Whi5 controls budding-yeast cell size. *Nature* 526: 268–272.
- Sedman T, Jöers P, Kuusk S, Sedman J. 2005. Helicase Hmi1 stimulates the synthesis of concatemeric mitochondrial DNA molecules in yeast *Saccharomyces cerevisiae*. *Current Genetics* 47: 213–222.
- Sedman T, Kuusk S, Kivi S, Sedman J. 2000. A DNA Helicase Required for Maintenance of the Functional Mitochondrial Genome in *Saccharomyces cerevisiae*. *Molecular and Cellular Biology* 20: 1816–1824.
- Shadel GS. 1999. Yeast as a Model for Human mtDNA Replication. *The American Journal of Human Genetics* 65: 1230–1237.
- Shapiro L, Grossman LI, Marmur J, Kleinschmidt AK. 1968. Physical studies on the structure of yeast mitochondrial DNA. *Journal of Molecular Biology* 33: 907–922.
- Sharma PK, Mittal N, Deswal S, Roy N. 2011. Calorie restriction up-regulates iron and copper transport genes in *Saccharomyces cerevisiae*. *Mol. BioSyst.* 7: 394–402.
- Springer M, Weissman JS, Kirschner MW. 2010. A general lack of compensation for gene dosage in yeast. *Molecular Systems Biology* 6: 368.
- Stodola JL, Burgers PM. 2017. Mechanism of Lagging-Strand DNA Replication in Eukaryotes. Pages 117–133 in Masai H and Foiani M, eds. *DNA Replication*, vol. 1042. Springer Singapore.
- Stringer C, Wang T, Michaelos M, Pachitariu M. 2021. Cellpose: a generalist algorithm for cellular segmentation. *Nature Methods* 18: 100–106.
- Stumpf JD, Bailey CM, Spell D, Stillwagon M, Anderson KS, Copeland WC. 2010. mip1 containing mutations associated with mitochondrial disease causes mutagenesis and depletion of mtDNA in *Saccharomyces cerevisiae*. *Human Molecular Genetics* 19: 2123–2133.
- Swaffer MP, Kim J, Chandler-Brown D, Langhinrichs M, Marinov GK, Greenleaf WJ, Kundaje A, Schmoller KM, Skotheim JM. 2021. Transcriptional and chromatin-based partitioning mechanisms uncouple protein scaling from cell size. *Molecular Cell* 1097-2765(21)00836–4.
- Torres EM, Springer M, Amon A. 2016. No current evidence for widespread dosage compensation in *S. cerevisiae*. *eLife* 5: e10996.
- Treitl MA, Carlson M. 1995. Repression by SSN6-TUP1 is directed by MIG1, a

- repressor/activator protein. *Proceedings of the National Academy of Sciences* 92: 3132–3136.
- Tyynismaa H, Sembongi H, Bokori-Brown M, Granycome C, Ashley N, Poulton J, Jalanko A, Spelbrink JN, Holt IJ, Suomalainen A. 2004. Twinkle helicase is essential for mtDNA maintenance and regulates mtDNA copy number. *Human Molecular Genetics* 13: 3219–3227.
- Tzagoloff A, Myers AM. 1986. GENETICS OF MITOCHONDRIAL BIOGENESIS. *Annual Review of Biochemistry* 55: 249–285.
- Ulery TL, Jang SH, Jaehning JA. 1994. Glucose repression of yeast mitochondrial transcription: kinetics of derepression and role of nuclear genes. *Molecular and Cellular Biology* 14: 1160–1170.
- Unger A-K, Geimer S, Harner M, Neupert W, Westermann B. 2017. Analysis of Yeast Mitochondria by Electron Microscopy. Pages 293–314 in Mokranjac D and Perocchi F, eds. *Mitochondria*, vol. 1567. Springer New York.
- Van Dyck E, Foury F, Stillman B, Brill SJ. 1992. A single-stranded DNA binding protein required for mitochondrial DNA replication in *S. cerevisiae* is homologous to *E. coli* SSB. *The EMBO Journal* 11: 3421–3430.
- Viana MP, Brown AI, Mueller IA, Goul C, Koslover EF, Rafelski SM. 2020. Mitochondrial Fission and Fusion Dynamics Generate Efficient, Robust, and Evenly Distributed Network Topologies in Budding Yeast Cells. *Cell Systems* 10: 287-297.e5.
- Viana MP, Lim S, Rafelski SM. 2015. Quantifying mitochondrial content in living cells. Pages 77–93 in. *Methods in Cell Biology*, vol. 125. Elsevier.
- Viikov K, Jasnovidova O, Tamm T, Sedman J. 2012. C-Terminal Extension of the Yeast Mitochondrial DNA Polymerase Determines the Balance between Synthesis and Degradation. *PLOS ONE* 7: e33482.
- Visser W, van Spronsen EA, Nanninga N, Pronk JT, Kuenen JG, van Dijken JP. 1995. Effects of growth conditions on mitochondrial morphology in *Saccharomyces cerevisiae*. *Antonie van Leeuwenhoek* 67: 243–253.
- de Vries S, Marres CAM. 1987. The mitochondrial respiratory chain of yeast. Structure and biosynthesis and the role in cellular metabolism. *Biochimica et Biophysica Acta (BBA) - Reviews on Bioenergetics* 895: 205–239.
- van der Walt S, Schönberger JL, Nunez-Iglesias J, Boulogne F, Warner JD, Yager N, Guillaud E, Yu T, scikit-image contributors. 2014. scikit-image: image processing in Python. *PeerJ* 2: e453.
- Wang Y, Wang X, Long Q, Liu Y, Yin T, Sirota I, Ren F, Gu Z, Luo J. 2021. Reducing embryonic mtDNA copy number alters epigenetic profile of key hepatic lipolytic genes and causes

abnormal lipid accumulation in adult mice. *The FEBS Journal* 288: 6828–6843.

Wang Z, Wu M. 2015. An integrated phylogenomic approach toward pinpointing the origin of mitochondria. *Scientific Reports* 5: 7949.

Weber SC, Brangwynne CP. 2015. Inverse Size Scaling of the Nucleolus by a Concentration-Dependent Phase Transition. *Current Biology* 25: 641–646.

West GB, Woodruff WH, Brown JH. 2002. Allometric scaling of metabolic rate from molecules and mitochondria to cells and mammals. *Proceedings of the National Academy of Sciences* 99: 2473–2478.

Williamson DH, Fennell DJ. 1975. Chapter 16: The Use of Fluorescent DNA-Binding Agent for Detecting and Separating Yeast Mitochondrial DNA. Pages 335–351 in. *Methods in Cell Biology*, vol. 12. Elsevier.

Wolters JF, Chiu K, Fiumera HL. 2015. Population structure of mitochondrial genomes in *Saccharomyces cerevisiae*. *BMC Genomics* 16: 451.

Wu C-Y, Rolfe PA, Gifford DK, Fink GR. 2010. Control of transcription by cell size. *PLOS biology* 8: e1000523.

Yang X, Chang HR, Yin YW. 2015. Yeast Mitochondrial Transcription Factor Mtf1 Determines the Precision of Promoter-Directed Initiation of RNA Polymerase Rpo41. *PLOS ONE* 10: e0136879.

Youle RJ, van der Bliek AM. 2012. Mitochondrial Fission, Fusion, and Stress. *Science* 337: 1062–1065.

de Zamaroczy M, Bernardi G. 1986. The GC clusters of the mitochondrial genome of yeast and their evolutionary origin. *Gene* 41: 1–22.

Zelenaya-Troitskaya O, Newman SM, Okamoto K, Perlman PS, Butow RA. 1998. Functions of the high mobility group protein, Abf2p, in mitochondrial DNA segregation, recombination and copy number in *Saccharomyces cerevisiae*. *Genetics* 148: 1763–1776.

Zelenaya-Troitskaya O, Perlman PS, Butow RA. 1995. An enzyme in yeast mitochondria that catalyzes a step in branched-chain amino acid biosynthesis also functions in mitochondrial DNA stability. *The EMBO journal* 14: 3268–3276.

Zheng F, Jia B, Dong F, Liu L, Rasul F, He J, Fu C. 2019. Glucose starvation induces mitochondrial fragmentation depending on the dynamin GTPase Dnm1/Drp1 in fission yeast. *Journal of Biological Chemistry* 294: 17725–17734.

Zhurinsky J, Leonhard K, Watt S, Marguerat S, Bähler J, Nurse P. 2010. A coordinated global control over cellular transcription. *Current biology: CB* 20: 2010–2015.

Bibliography

Zuo XM, Clark-Walker GD, Chen XJ. 2002. The mitochondrial nucleoid protein, Mgm101p, of *Saccharomyces cerevisiae* is involved in the maintenance of rho(+) and ori/rep-devoid petite genomes but is not required for hypersuppressive rho(-) mtDNA. *Genetics* 160: 1389–1400.

List of Abbreviations

General abbreviations	Description
ADP	Adenosine diphosphate
ATP	Adenosine triphosphate
cDNA	Complementary DNA
C _q	Quantification cycle
DNA	Deoxyribonucleic acid
DNA-qPCR	Deoxyribonucleic acid quantitative polymerase chain reaction
<i>E. coli</i>	<i>Escherichia coli</i>
EDTA	Ethylenediaminetetraacetic acid
ETC	Electron transport chain
FAD	Flavin adenine dinucleotide
FSC-A /-H	Forward-scatter area / height
gDNA	Genomic DNA
GFP	Green fluorescent protein
HI	Hormone inducible
LiOAc	Lithium acetate
MAT	Mating type
mRNA	Messenger RNA
mtDNA	Mitochondrial DNA
mtNetwork	Mitochondrial network
NAD	Nicotinamide adenine dinucleotide
NADH	Nicotinamide adenine dinucleotide Hydride
OD	Optical density
OXPHOS	Oxidative phosphorylation
PBS	Phosphate buffered saline
PCI	Phenol chloroform isoamyl alcohol
PCR	Polymerase chain reaction
PoIG	Polymerase gamma
RCR	Rolling-circle replication
RDR	Recombination-dependent rolling-circle replication
RNA	Ribonucleic acid
ROS	Reactive oxygen species
rRNA	Ribosomal RNA

List of Abbreviations

RT-qPCR	Reverse transcription quantitative PCR
SDS	Sodium dodecyl sulfate
SSC-A /-H	Side-scatter area / height
TAE	Tris-acetate-EDTA buffer
TBS	Tris-buffered saline
TE	Tris-EDTA buffer
TF	Transcription factor
tRNA	transfer RNA
UV	Ultraviolet
WT	Wild-type

Abbreviations of Units	Description
arb. u.	Arbitrary unit
bp	Base pairs
°C	Degree Celsius
Da	Dalton
g	Gram
k	Kilo
L	Litre
m	Milli
μ	Micro
m	Meter
M	Molar
min	Minutes
n	Nano
p	Pico
sec	Seconds
U	Units
V	Volt
v/v	Volume per volume
w/v	Weight per volume
x g	Times gravity

Acknowledgement - Danksagung

Ich möchte mich bei allen Personen ganz herzlich bedanken, die mich während meiner Doktorarbeit unterstützt haben. Allen voran möchte ich Dr. Kurt Schmoller danken, der mir die Möglichkeit gegeben hat, in seiner Arbeitsgruppe an einer spannenden Forschungsfrage zu arbeiten und mir dabei mit vielen hilfreichen fachlichen Diskussionen, aber auch seiner engen Betreuung zur Seite stand. Vielen Dank, dass du mich gefördert und mich mit deinem unerschütterlichen Optimismus motiviert hast!

Des Weiteren möchte ich den Mitgliedern meines *Thesis Advisory Committees* Prof. Dr. Christof Osman und Prof. Dr. Ralf Jungmann für die Begleitung meiner Doktorarbeit und ihre wertvollen Anmerkungen zum Projekt danken. Außerdem möchte ich Prof. Dr. Christof Osman als meinen universitären Betreuer für seinen wissenschaftlichen Ratschlag, seine Unterstützung und die Bereitstellung von Stämmen und Plasmiden danken. Ich danke auch herzlich Prof. Dr. Till Klecker und Moritz Mayer für die erfolgreiche Zusammenarbeit und die vielen hilfreichen Anmerkungen. Ein besonders großer Dank geht an Francesco Padovani, Alissa Finster und Daniela Bureik für die harmonische Zusammenarbeit am Projekt und die gegenseitige Unterstützung. Ohne euch wären meine Dissertation und das gesamte Projekt nicht da, wo sie heute sind!

Auch möchte ich mich ganz herzlich bei allen aktuellen und ehemaligen Mitgliedern des Instituts und der Arbeitsgruppe bedanken. Vielen Dank für alle kritischen Nachfragen, die das Thema geformt und mich zu einer besseren Wissenschaftlerin gemacht haben. Insbesondere möchte ich natürlich allen Mitgliedern des *Schmoller Labs* danken. Ich danke euch für alle wissenschaftlichen und auch nicht-wissenschaftlichen Unterhaltungen und Unternehmungen. Ich bin euch unglaublich dankbar für jede Unterstützung und das tolle Arbeitsklima. Ihr habt die Zeit im Labor noch besser gemacht! Ich möchte mich noch einmal bei den Menschen bedanken, mit denen ich die meiste Zeit verbracht habe. Dimitra Chatzitheodoridou, Daniela Bureik und Kora-Lee Claude, danke, dass ich jede Freude und jedes Leid mit euch teilen konnte und ihr mir immer mit hilfreichen Ratschlägen zur Seite standet.

Für das Korrekturlesen dieser Arbeit möchte ich mich bei Dr. Kurt Schmoller, Dimitra Chatzitheodoridou, Francesco Padovani, Sandra Nitsch und Benedikt Buchmann bedanken.

Abschließend möchte ich meinen Freunden und meiner gesamten Familie danken, insbesondere meinen Eltern und meinen Schwestern, auf die ich in jeder Lebenslage zählen kann. Ich bin dankbar, euch immer hinter mir zu wissen. Ihr seid die Besten! Zu guter Letzt geht auch sehr großer Dank an meinen Freund Ben. Danke, dass du mich motiviert und unterstützt hast und wirklich alles gegeben hast, um mich regelmäßig zum Lachen zu bringen. Ohne euch hätte ich das nicht geschafft! Vielen Dank!